# ตัวเร่งปฏิกิริยาโลหะออกไซด์ผสมที่ได้จากแหล่งธรรมชาติสำหรับการผลิตเมทิลเอสเทอร์ของกรดไขมัน

นายวายุ จินดาพล



วิทยานิพนธ์นี้เป็นส่วนหนึ่งของการศึกษาตามหลักสูตรปริญญาวิทยาศาสตรดุษฎีบัณฑิต
สาขาวิชาปิโตรเคมี
คณะวิทยาศาสตร์ จุฬาลงกรณ์มหาวิทยาลัย
ปีการศึกษา 2560

# MIXED METAL OXIDE CATALYSTS DERIVED FROM NATURAL SOURCES FOR PRODUCTION OF FATTY ACID METHYL ESTERS

Mr. Wayu Jindapon

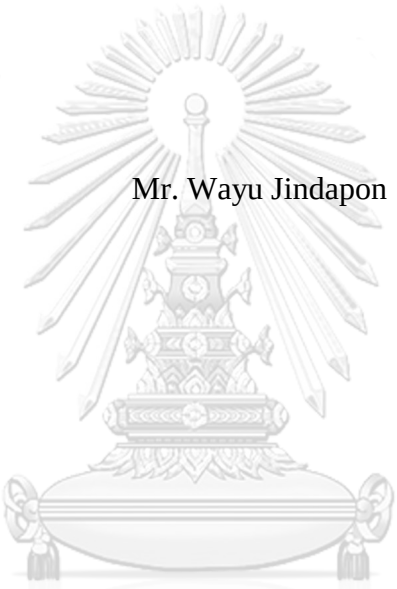



A Dissertation Submitted in Partial Fulfillment of the Requirements
for the Degree of Doctor of Philosophy Program in Petrochemistry
Faculty of Science
Chulalongkorn University
Academic Year 2017

| | |
|---|---|
| Thesis Title | MIXED METAL OXIDE CATALYSTS DERIVED FROM NATURAL SOURCES FOR PRODUCTION OF FATTY ACID METHYL ESTERS |
| By | Mr. Wayu Jindapon |
| Field of Study | Petrochemistry |
| Thesis Advisor | Associate Professor Chawalit Ngamcharussrivichai, Ph.D. |

Accepted by the Faculty of Science, Chulalongkorn University in Partial Fulfillment of the Requirements for the Doctoral Degree

.....Dean of the Faculty of Science
(Associate Professor Polkit Sangvanich, Ph.D.)

THESIS COMMITTEE

.....Chairman
(Professor Pattarapan Prasassarakich, Ph.D.)

.....Thesis Advisor
(Associate Professor Chawalit Ngamcharussrivichai, Ph.D.)

.....Examiner
(Duangamol Tungasmita, Ph.D.)

.....Examiner
(Assistant Professor Warinthorn Chavasiri, Ph.D.)

.....External Examiner
(Assistant Professor Bussarin Ksapabutr, Ph.D.)

วายุ จินดาพล : ตัวเร่งปฏิกิริยาโลหะออกไซด์ผสมที่ได้จากแหล่งธรรมชาติสำหรับการผลิตเมทิลเอสเทอร์ของกรดไขมัน (MIXED METAL OXIDE CATALYSTS DERIVED FROM NATURAL SOURCES FOR PRODUCTION OF FATTY ACID METHYL ESTERS) อ.ที่ปรึกษาวิทยานิพนธ์หลัก: รศ. ดร. ชวลิต งามจรัสศรีวิชัย, 109 หน้า.

วัตถุประสงค์ของการวิจัยนี้เพื่อศึกษาตำแหน่งกัมมันต์ในตัวเร่งปฏิกิริยาฐานแคลเซียม (Ca-based catalysts) ที่ได้จากแคลไซต์ ($CaCO_3$) และโดโลไมต์ ($CaMg(CO_3)_2$) และเพื่ออธิบายผลของแมกนีเซียมออกไซด์ (MgO) ในโดโลไมต์ที่ผ่านการเผาเพื่อใช้เป็นตัวเร่งปฏิกิริยาในทรานส์เอสเทอริฟิเคชันของน้ำมันปาล์มกับเมทานอล ส่วนแรกเป็นการศึกษาผลของอุณหภูมิการเผาต่อการเกิดวัฏภาค MgO ในโดโลไมต์และตำแหน่งกัมมันต์ของตัวเร่งปฏิกิริยา MgO ที่อยู่ในโดโลไมต์ที่ผ่านการเผาจะไม่แสดงกัมมันตภาพ ขณะที่ตำแหน่งกัมมันต์หลักคือแคลเซียมออกไซด์ (CaO) อย่างไรก็ตามแมกนีเซียมผสมแคลเซียมออกไซด์ผสมที่ได้จากโดโลไมต์มีกัมมันตภาพสูงกว่าแมกนีเซียมและแคลเซียมออกไซด์ผสมที่เตรียมด้วยการผสมทางกายภาพระหว่างแคลไซต์กับแมกนีไซต์ ($MgCO_3$) ตามสัดส่วนองค์ประกอบเดียวกับโดโลไมต์ ผลการทดลองชี้ว่า MgO ในโดโลไมต์ที่ผ่านการเผาช่วยลดขนาดผลึกของ CaO และเพิ่มเสถียรภาพในการเร่งเร่งปฏิกิริยา การทำปฏิกิริยาโดยตรงของออกไซด์ฐานแคลเซียม (Ca-based oxides) กับเมทานอลชี้ว่าโดโลไมต์ที่ผ่านการเผาซึ่งมีผลึก CaO ที่เล็กกว่า ทำให้อัตราการเกิดแคลเซียมเมทอกไซด์ ($Ca(OCH_3)_2$) สูงกว่า CaO บริสุทธิ์ กรณีการทำปฏิกิริยาโดยตรงกับกลีเซอรอลเพื่อศึกษาการเกิดแคลเซียมกลีเซอรอกไซด์ ($Ca(C_3H_7O_3)_2$)) ซึ่งเป็นวัฏภาคที่เกี่ยวข้องกับการชะละลายของตำแหน่งกัมมันต์พบว่าการเกิดวัฏภาคนี้ถูกชะลอในตัวเร่งปฏิกิริยาออกไซด์ผสม การนั้นทำการเตรียมตัวเร่งปฏิกิริยาออกไซด์ฐานแคลเซียม (Ca-based oxides) เมทอกไซด์ฐานแคลเซียม (Ca-based methoxides) และกลีเซอรอกไซด์ฐานแคลเซียม (Ca-based glyceroxides) เพื่อทดสอบในปฏิกิริยาทรานส์เอสเทอริฟิเคชัน ตัวเร่งปฏิกิริยาออกไซด์ฐานแคลเซียมมีอัตราการเกิดปฏิกิริยาเริ่มต้นสูงกว่าตัวเร่งปฏิกิริยาชนิดอื่นทำให้ถูกเปลี่ยนเป็นสารประกอบอื่นได้ง่ายในระหว่างปฏิกิริยา เช่นแคลเซียมไฮดรอกไซด์ ($Ca(OH)_2$) แคลเซียมคาร์บอเนตและ $Ca(C_3H_7O_3)_2$ เมทอกไซด์ฐานแคลเซียมมีเสถียรภาพสูงกว่าออกไซด์ฐานแคลเซียมแม้ว่ามันมีกัมมันตภาพน้อยที่สุด ขณะที่กลีเซอรอกไซด์ฐานแคลเซียมส่งเสริมปฏิกิริยาผ่านระบบการเร่งแบบเอกพันธุ์ เสถียรภาพเชิงโครงสร้างของตัวเร่งปฏิกิริยาในบรรยากาศมีความสำคัญเนื่องจากแก๊สคาร์บอนไดออกไซด์และความชื้นสามารถดูดซับเชิงเคมีบนตำแหน่งกัมมันต์ได้อย่างแข็งแรงส่งผลให้ตัวเร่งปฏิกิริยาเสื่อมสภาพ ออกไซด์ฐานแคลเซียมเป็นตัวเร่งปฏิกิริยาที่มีเสถียรภาพสูงในการเร่งปฏิกิริยาที่สุดเนื่องจาก $Ca(OH)_2$ที่เกิดขึ้นยังมีกัมมันตภาพ ส่วนสุดท้ายเป็นการศึกษาการเตรียมตัวเร่งปฏิกิริยาฐานแคลเซียมในลักษณะแบบเส้น (extrudate) เพื่อใช้ในการผลิตไบโอดีเซลในเครื่องปฏิกรณ์เบดนิ่งแบบต่อเนื่อง ศึกษาผลของการเติมไฮดรอกซีเอทิลเซลลูโลส (hydroxyethyl cellulose) ต่อการขึ้นรูปและลักษณะของตัวเร่งปฏิกิริยาแบบเส้นที่เตรียมได้ การผสมตัวเร่งปฏิกิริยาแบบเส้นกับเมทิลเอสเทอร์เชิงพาณิชย์ (commercial methyl esters, CMEs) ชนิดต่างๆ ส่งผลให้ผลได้ของเมทิลเอสเทอร์ (96.5 %) คงที่ตลอดการดำเนินการ เนื่องจากความสามารถในการละลายของสารตั้งต้นทั้งสองชนิดในชั้น CME ที่ปกคลุมตัวเร่งปฏิกิริยาแบบเส้น

สาขาวิชา ปิโตรเคมี ลายมือชื่อนิสิต .....

ปีการศึกษา 2560 ลายมือชื่อ อ.ที่ปรึกษาหลัก .....

# # 5672913823 : MAJOR PETROCHEMISTRY
KEYWORDS: CA-BASED CATALYST / TRANSESTERIFICATION / DOLOMITE / STABILITY / CATALYST EXTRUDATE

WAYU JINDAPON: MIXED METAL OXIDE CATALYSTS DERIVED FROM NATURAL SOURCES FOR PRODUCTION OF FATTY ACID METHYL ESTERS. ADVISOR: ASSOC. PROF. CHAWALIT NGAMCHARUSSRIVICHAI, Ph.D., 109 pp.

The objectives of this research are to study active sites of Ca-based catalysts derived from calcite ($CaCO_3$) and dolomite ($CaMg(CO_3)_2$), and to clarify catalytic effect of MgO in the calcined dolomite as catalyst in transesterification of palm oil with methanol. Firstly, the effects of calcination temperature on evolution of MgO in dolomite and its catalytic activity were studied. The MgO containing in the calcined dolomite was not active, while the main active site was CaO. However, Ca and Mg mixed oxides obtained from calcined dolomite had higher activity than that prepared by physical mixing in which calcite and magnesite ($MgCO_3$) were mixed at the same metal composition as dolomite. The results indicated that the presence of MgO in the calcined dolomite reduced the CaO crystallite size, and stabilized the catalytic activity. The direct reaction of Ca-based oxides with methanol indicated that the calcined dolomite with smaller CaO crystallites gave higher formation rate of calcium methoxide ($Ca(OCH_3)_2$) than the pure CaO. In the case of direct reaction with glycerol, the formation of calcium glyceroxide ($Ca(C_3H_7O_3)_2$), related with leaching of calcium active phase, was delayed over the mixed oxide catalysts. Subsequently, the Ca-based oxides were prepared in form of Ca-based methoxides and glyceroxides and tested in the transesterification. Since the Ca-based oxides had a higher initial rate than the others, they were easily changed to other calcium compounds, such as $Ca(OH)_2$, $CaCO_3$ and $Ca(C_3H_7O_2)_2$ during the transesterification. The Ca-based methoxides were more stable than the Ca-based oxides although their activity was the least. On the other hand, the Ca-based glyceroxides promoted the reaction *via* homogenous catalysis routes. The structural stability of catalysts exposed to ambient air was investigated since $CO_2$ and moisture were strongly chemisorbed onto the basic sites, leading to catalyst deactivation. The Ca-based oxides were the most stable catalysts because the $Ca(OH)_2$ generated was somewhat active. Finally, the Ca-based catalysts in extrudate form were used in biodiesel production using continuous-flow fixed-bed reactor. The effects of hydroxyethyl cellulose addition on the extrusion and the characteristics of the extrudates obtained were studied. Premixing the catalyst extrudates with different types of commercial methyl esters (CMEs) resulted in a stable FAME yield of ≈96.5% throughout the operation. This beneficial effect arises from high solubilities of both reactants in the CME layer covering the catalyst extrudates.



Field of Study: Petrochemistry Student's Signature .....

Academic Year: 2017 Advisor's Signature .....

# ACKNOWLEDGEMENTS

Firstly, I would like to express my sincere gratitude to my advisor Prof. Assoc. Prof. Dr. Chawalit Ngamcharussrivichai for the continuous support of my Ph.D study and related works, for his patience, motivation, and immense knowledge. His guidance helped me in all the time of research and writing of this thesis. I could not have imagined having a better advisor and mentor for my Ph.D study.

Besides my advisor, I would like to thank the rest of my dissertation committee: Prof. Dr. Pattarapan Prasassarakich, Dr. Duangamol Tungasmita, Asst. Prof. Dr. Warinthorn Chavasiri and Asst. Prof. Dr. Bussarin Ksapabutr, for their insightful comments and encouragement, but also for the hard question which incented me to widen my research from various perspectives.

I am also grateful to Prof. Dr. Tharapong Vitidsant and Assoc. Prof. Dr. Prapan Kuchonthara, who assisted, advised and supported me. Without they precious support, it would not be possible to conduct this research.

I also acknowledge department of chemical technology for providing the support and equipment and the scholarships for Ph.D student from the Graduate school, Chulalongkorn University and from Renewable Energy Plan (biodiesel), Energy Policy and Planning Office (EPPO), Ministry of Energy for helping and providing the funding for the work.

I would like to thank to my co-workers Dr. Sivashunmugam Sankaranarayanan, Atikun Chotirattanachote and Supapan Ruengyoo and my research group members Dr. Sakdinun Nuntang, Dr. Boontawee Lertpanyapornchai, Mr. Niti Nitiwattanalert and etc. for suggestion, kindly support about my Ph.D study and related works.

Finally, I would like to thank my parents and my sister for supporting me spiritually throughout my Ph.D study, related works and my life in general.

Thanks for all your encouragement!

**CONTENTS**

Page

Page

Page

# LIST OF TABLE

# LIST OF FIGURE

# CHAPTER I
# Introduction

## 1.1 Motivation

Fatty acid methyl esters (FAMEs) and glycerol are major basic oleochemicals, which can be used as intermediates for manufacturing of various bio-based chemicals and specialties [1]. Biodiesel is one of the most successful applications of FAME due to its several advantages in terms of exhaust gas cleanliness, non-toxicity, lubricity, biodegradability, and petroleum diesel-like fuel properties. FAME is industrially produced *via* transesterification of triglycerides, as major components in vegetable oil and fats, with methanol in the presence of either homogeneous or heterogeneous base catalysts. The homogeneous process using alkaline catalysts provides a fast reaction rate under mild conditions. However, this process requires extensive conditioning and purifying of the products to ensure the standard specification. The heterogeneous base catalysis is a promising route for FAME production due to expediency of catalyst recovery, catalyst reusability, process simplicity, and higher purity of FAME and crude glycerol [2]. Moreover, transesterification process in fixed-bed reactors is of industrial interest because both biodiesel and glycerol can be continuously produced at a high throughput [3]. However, powder catalysts cannot be used in fixed-bed reactors because of product contamination with fine particles and a large pressure drop. To overcome these problems, powder catalysts are formulated as larger particles with various shapes, such as extrudates, pellets, spheres, and monoliths [4, 5].

Calcium-based oxides are a class of potential heterogeneous catalysts for the transesterification of triglycerides with methanol. The sources for CaO catalyst preparation are available in abundance, for example natural calcium compounds found in limestone, dolostone, cuttlebone and seashell. Limestone, cuttlebone and seashell are consisted of calcium carbonate ($CaCO_3$) as main phase, while dolomite, as a primary component in dolostone found in nature, is composed of a mixed carbonate of calcium and magnesium ($CaMg(CO_3)_2$). Dolomite has attracted considerable attention because the mixed oxides obtained from the dolomite exhibited a superior catalytic activity, stability and reusability to the pure CaO [6]. The MgO nanocrystallites dispersed in the mixed oxides was suspected to be a key to stabilize the CaO phase [6]. It is interesting to study role of MgO presenting in the dolomite-derived mixed metal oxides in promoting the catalytic reaction. Moreover, the active sites responsible for the transesterification over the mixed oxide catalysts are a matter of debate.

The real active species of Ca-based oxides using as catalysts for the transesterification of triglycerides with methanol were recently studied because CaO was easily transformed after exposure to atmosphere air and/or during the reaction [7-9]. In some process, CaO was stirred with methanol before mixing with oil in order to generate calcium methoxide ($Ca(OCH_3)_2$) as active phase [10, 11]. A small amount of water was directly added to the reaction because the active OH–species formed on the CaO surface improved the FAME yield [12, 13]. Moreover, the calcium glyceroxide ($Ca(C_3H_7O_3)_2$) generated from CaO reacted with glycerol as a by-product was believed to be the active phase of pure CaO catalyst [14]. However, the Ca compounds formed during the reaction have higher solubility in methanol than CaO: the solubility of CaO, $Ca(OH)_2$, $Ca(CH_3O)_2$ and $Ca(C_3H_7O_3)_2$ is 28 mg $L^{-1}$ [15], 100 mg $L^{-1}$ [16], 200 mg $L^{-1}$ [16], 6216 mg $L^{-1}$ [14], respectively, which resulted in leaching of calcium ion into biodiesel product [15]. The metals, such as sodium [17], potassium [18], lithium [19] and zinc [20] were prepared in the corresponding glyceroxide forms in order to catalyze in the transesterification. In stability Ca-based oxide catalysts were easily deactivated *via* chemisorption of atmospheric carbon dioxide ($CO_2$) and moisture upon exposure to ambient air [14, 21].

Previously, the Ca-based oxides, hard but brittle materials, were formulated in extrudates, which used as catalysts in the FAME production using fixed-bed reactor [3, 22-24]. Their formulation required the addition of binders to enhance powder contact and the mechanical strength of the shaped particles obtained after calcination [22-24], and the addition of plasticizers to adjust the viscosity and lubricity of the catalyst paste to facilitate processing [22, 24]. When a catalyst powder is mixed with binders and/or plasticizers and then pressed to give a specific shape, its textural properties and active site content are usually adversely affected, resulting in a decrease in catalytic performance [5]. The formulation conditions should therefore be carefully adjusted to optimize the mechanical, physical, and chemical properties of the resulting shaped catalysts. Due to a mass transfer limitation related to immiscibility of the reactants and the number of accessible active sites, tetrahydrofuran [16] and FAME [22] were added as co-solvents in the reaction system to improve mass transfer. Premixing CaO with FAME further increased the reaction rate [25]. Moreover, the FAME coating on the catalyst surface prevented deactivation caused by adsorption of atmospheric moisture and $CO_2$ on the active sites [25].

In this dissertation, the effects of MgO presenting in the dolomite-derived mixed oxide catalysts on the transesterification of palm oil, as model triglyceride, with methanol were investigated. To clarify the real active species of the mixed oxide catalysts, different Ca and Mg mixed compounds in form of oxide, methoxide or glyceroxide were synthesized and comparatively studied in the reaction. The effects

of crystalline structure of the catalysts obtained on their structural and catalytic stability after exposure to ambient air were investigated. The catalysts obtained were tested in the reusability and deactivation study. Finally, the catalyst extrudates were prepared *via* a dissolution–precipitation method, using waste enamel venus shell as a renewable Ca source, zinc nitrate and alumina as a binder precursors, and HEC as a plasticizer. The catalyst paste was formulated using either manual extruder or single-screw extruder. The effects of HEC addition on extrusion and the characteristics of the resulting extrudates were studied. The catalyst extrudates obtained under the suitable conditions, designated as ZSAH catalysts, were applied to a continuous production of FAME in fixed-bed reactor. The effect of premixing the ZSAH extrudates with methanol, vegetable oil or commercial methyl esters (CMEs) with different fatty acid chain lengths on the catalytic transesterification was also investigated.

## 1.2 Objectives

1.2.1 To study active sites presenting in metal oxides derived from calcite and dolomite for synthesis of fatty acid methyl esters

1.2.2 To study Ca-based oxides, methoxides and glyceroxides as a catalyst in transesterification of palm oil with methanol and their stability in ambient air

1.2.3 To produce FAME in continuous-flow fixed-bed reactor using the Ca-based catalysts in extrudate form

1.2.4 To study catalyst formulation in extrudate form and effect of premixing the catalyst extrudates with methanol, vegetable oil or commercial methyl esters (CMEs) with different fatty acid chain lengths on the transesterification in fixed-bed reactors



## 1.3 Scope of this dissertation

Part I: The active sites presenting in metal oxides derived from calcite ($CaCO_3$), magnesite ($MgCO_3$) and dolomite ($CaMg(CO_3)_2$) for synthesis of fatty acid methyl esters were investigated. The calcite, magnesite and dolomite were used as raw materials to prepared CaO, MgO and mixed oxide of CaO and MgO (CaMgO), respectively. Moreover, calcite and magnesite at the same $CaCO_3$: $MgCO_3$ mass ratio as the raw dolomite was used to prepare a physically mixed CaO and MgO catalyst (CaO+MgO). The effects of calcination temperatures and heating rates of the catalysts on physicochemical properties were investigated. The catalysts obtained were evaluated for its catalytic properties in the transesterification of palm oil with methanol at a catalyst loading, 10 wt%, 60 °C, ambient pressure and methanol: oil

molar ratio, 30:1. To understand the reactivity of active phases presenting on the catalysts towards phase transformation during the reaction, direct reaction of the catalysts with methanol or glycerol as a by-product was also studied.

Paper II: The active phases of Ca-based catalysts used in during initial state and repeated use in transesterification of palm oil with methanol were studied. The raw materials of calcite and dolomite were calcined at 800 °C for 3 h in order to prepare Ca-based oxide catalysts. Ca-based methoxide and glyceroxide catalysts were synthesized *via* direct reaction with methanol and glycerol solution, respectively. The physicochemical properties of the catalysts obtained were investigated. Moreover, the Ca-based oxide, Ca-based methoxide and Ca-based glyceroxide catalysts were exposed to ambient air (RH ≈ 73%) to reveal the structural stability of the catalysts resisted the chemisorption of atmospheric moisture and $CO_2$. The catalysts and catalysts exposed to ambient air were used to catalyze in the transesterification of palm oil with methanol at a catalyst loading, 10 wt%, 60 °C, ambient pressure and methanol: oil molar ratio, 30:1.

Paper III: The Ca-based catalysts in extrudate form were used to produce FAME in continuous-flow fixed-bed reactor. Heterogeneous base catalysts in the form of extrudates prepared *via* a dissolution–precipitation method, using waste seashells as a renewable Ca source, zinc nitrate and alumina as binder precursors and hydroxyethylcellulose (HEC) as a plasticizer were synthesized. The catalyst paste were formulated by using manual and single extruder and followed by calcination at 400 °C (ZSAH-400). The effects of HEC addition on extrusion and the characteristics of were studied. To reveal promoting of FAME product in methanol–oil miscibility, the effect of premixing the ZSAH-400 extrudates with methanol, vegetable oil or commercial methyl esters (CMEs) with different fatty acid chain lengths on the catalytic transesterification was also investigated.

# CHAPTER II
# Theory and literature reviews

## 2.1 Fatty acid methyl esters as basic oleochemicals produced *via* transesterification

In principle, oleochemicals are products obtained from various types of oils and fats derived from vegetable or animals sources, respectively. The production of oleochemicals is widely developed in Asia due to an abundance of raw materials. Nowadays, the products formulated from oleochemicals are more interesting than those from petroleum-based chemicals due to several advantages, such as biodegradability and low toxicity of oleochemicals themselves. Fatty acids, fatty acid methyl esters (FAMEs) and glycerol are basic oleochemicals, which can be subsequently used to produce various bio-based chemicals and specialties (Figure 2.1). The FAME can be directly used as renewable fuel in diesel engine, so-called biodiesel, which has several advantages in terms of exhaust gas cleanliness, non-toxicity, lubricity, biodegradability, and petroleum-diesel-like fuel properties [1, 2, 26, 27]. Moreover, glycerol can be used in many applications.

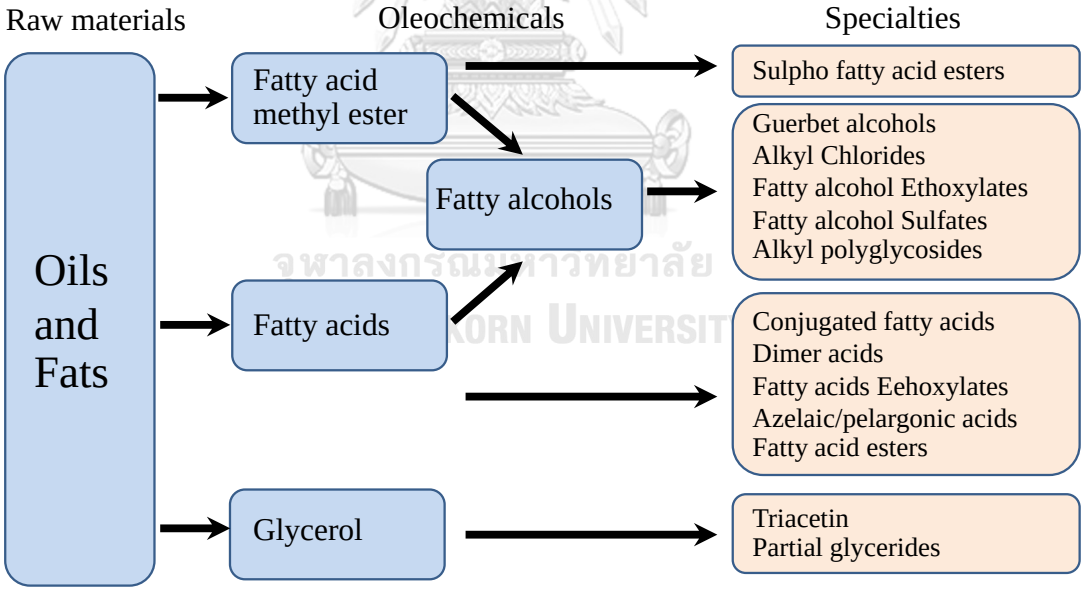


**Figure 2.1** Basic oleochemicals and their derivatives.

Figure 2.2 shows the basic equation of transesterification of a triglyceride molecule with methanol to produce three molecules of FAME and one molecule of glycerol. Generally, an excess amount of methanol is used, at a methanol: oil molar ratio ranging from 6: 1 to 12: 1, in order to shift the reaction equilibrium to the

products side. Moreover, using a catalyst increases the reaction rate and the triglyceride conversion [2].

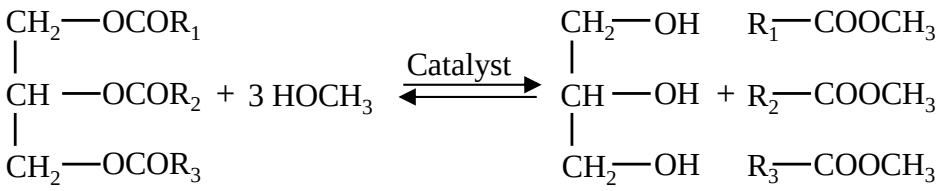


**Figure 2.2** Basic equation of transesterification of triglycerides with methanol.
Heterogeneous based catalysts are a more promising route in order to produce high purity of FAME and glycerol.

## 2.2 Ca-based catalysts used in transesterification

CaO is one of alkaline earth metal oxides composed of ionic crystal and Lewis acidity of the metal cation that is very weak due to its low electronegativity. Therefore, the conjugated oxygen anion displays the strong basic property. The advantages of CaO are low cost, high basicity and low solubility in methanol. Commercially, CaO is produced *via* a thermal decomposition of calcium carbonate ($CaCO_3$) at high temperatures (Eq. (2.1)). There are various $CaCO_3$ sources, such as limestone, dolomite, seashells and egg shell [9, 23, 28-30]. The Ca-based catalysts used in the transesterification can be classified into five groups: (1) pure CaO, (2) metal oxide-supported CaO, (2) metal oxide-supported CaO, (4) mixed oxides of Ca and other metals, and (5) other Ca compounds**.**

$$CaCO_3 \xrightarrow[\Delta]{} CaO + CO_2 \qquad (2.1)$$



### 2.2.1 Pure CaO catalysts

In order to use as catalytic materials in the base-catalyzed reactions, CaO can be prepared from various types of calcium sources, which depend on decomposition temperatures used to convert them into oxide form. To screen for potentials sources, $CaCO_3$, $Ca(OH)_2$, $Ca(CH_3COO)_2$, $Ca(NO_3)_2$ and $CaC_2O_2$ were used as precursors for the preparation of CaO [31]. The calcination temperatures required for maximizing the catalytic activity of the CaO prepared from $Ca(NO_3)_2$, $Ca(OH)_2$, $CaC_2O_2$, $Ca(CH_3COO)_2$ and $CaCO_3$ precursors were 600, 700, 800, 800 and 900 °C, respectively. The CaO obtained from $Ca(NO_3)_2$ was the least active because the CaO formed had the largest particles, whereas The CaO obtained from $Ca(OH)_2$ showed the highest activity due to its high surface area. Among $CaCO_3$, $Ca(CH_3COO)_2$ and $CaC_2O_2$, there was no significant difference in the catalytic activity.

Towards more environmentally friendly preparation of Ca-based catalysts, a number of natural sources as calcium rocks, such as calcite [29], and waste calcium materials, such as abalone [32], duck eggs [33], golden apple snail, and *meretrix venus* shell [30], were investigated. The CaO obtained from eggshells gave higher catalytic activity than golden apple snail shell and *meretrix venus* shell in the transesterification of palm olein oil with methanol [30]. The results indicate that high Ca content, high surface area and small particle size are required properties for a good CaO catalyst. According to Yoosuk *et al.* [34], limestone was calcined and refluxed with water to prepare the hydroxide precursor, followed by its dehydration to nano-sized CaO form. The surface area of CaO nanoparticles (25 $m^2$ $g^{-1}$) was higher than that of dense CaO catalyst (12 $m^2$ $g^{-1}$). As a result, the total basicity was improved.

### 2.2.2 Metal-doped CaO catalysts

CaO was modified by doping with alkali metal to improve the basic and catalytic properties [35, 36]. According to Watkins *et al.* [35], an aqueous solution of lithium nitrate ($Li_2NO_3$) was impregnated onto the CaO surface, followed by calcination at high temperatures. The results showed that the resulting Li/CaO had an enhanced catalytic activity when compared to the pristine CaO. The $Ca^{2+}$ ions in the CaO lattice were exchanged with $Li^+$ ions, generating the vacancies of oxygen anions. Moreover, it caused the isolated hydroxyl groups ($OH^-$) formed at the defect sites. The basic properties of Li/CaO were increased because of the oxygen anion vacancies and the isolated OH groups generated. Moreover, doping other alkali metals (sodium and potassium nitrates) onto CaO by incipient wetness method was studied [36]. However, the resulting metal-doped CaO catalysts had a leaching problem by which the leached alkali species catalyzed the reaction *via* homogeneous process.



### 2.2.3 Metal oxide-supported CaO catalysts

Since classical supported alkali metal catalysts experienced a severe leaching in methanol, the using of CaO with much lower solubility in methanol was more attractive. A number of studies based on the catalysts prepared by loading CaO onto supports, such as γ-$Al_2O_3$ [37], $Al_2O_3$ [38], mesoporous silica [39], SBA-15 [40], MgO, $SiO_2$ [41], and $SnO_2$ [42], have been reported. The metal oxide-supported CaO catalysts showed a superior performance to the pure CaO due to a high dispersion of CaO crystallites on the supports, which resulted in positive effects on their textural and chemical properties. Moreover, the CaO loaded onto supports exhibited an improved stability against leaching and tolerance to water and free fatty acids (FFA), as contaminants in oil feedstock, due to a strong interaction between CaO and the

support surface. The CaO was an active phase of the solid catalysts, whereas the support stabilized the active sites on its surface. The basic amount and strength of the catalysts can be varied in accord with coordination of $Ca^{2+}$ and $O^{2-}$ ions on the surface. The supported CaO catalysts retained their particles and shapes after being spent in the reaction.

### 2.2.4 Ca-based mixed metal oxides

Mixed oxides of Ca and different metals have been applied in the transesterification of vegetable oils with methanol to produce biodiesel [27, 43, 44]. The mixed oxide catalysts had stronger basicity than the pure CaO [27]. The mixed oxide of Ca and Mg (CaMgO) is easily prepared from dolomite by calcination at high temperatures as shown in Eq. (2.2). The dolomite is a common natural rock-forming mineral, which is composed of mixed calcium and magnesium carbonate ($CaMg(CO_3)_2$). Its use as catalytic precursor has several advantages in terms of low cost, low toxicity and abundance in many regions of Thailand. Different models as intermediate steps in the dolomite decomposition have been proposed [43]. $CaMg(CO_3)_2$ was dissociated into two carbonates, followed by decarbonation of $MgCO_3$ to MgO as shown in Eq. (2.3). A mixed form of calcite and magnesite is showed in Eq. (2.4). According to the reaction in Eq. (2.5), a metastable solid-solution precursor is formed. The CaO derived from $CaMg(CO_3)_2$ was immediately recarbonized by the released $CO_2$ to yield $CaCO_3$ (Eq. (2.6)). The direct formation of calcite and periclase (MgO) is showed in Eq. (2.7). Finally, MgO and CaO are simultaneously produced when the decomposition temperature is higher than of the decarbonation temperature of calcite. During the transition from the mixed carbonates to mixed oxides, the growth of MgO occurred on the external surface simultaneously with an internal growth of $CaCO_3$ (Figure 2.3) [43, 44]. As a result, the calcined dolomite possessed magnesium-rich surface when compared to its bulk composition.

Main reaction:

$$CaMg(CO_3)_2 \rightarrow CaO + MgO + 2CO_2 \quad (2.2)$$

Intermediate step:

Model I: $$CaMg(CO_3)_2 \rightarrow CaCO_3 + MgCO_3 \rightarrow CaCO_3 + MgO + CO_2 \quad (2.3)$$

Model II: $$CaMg(CO_3)_2 \rightarrow CaCO_3(1 - n)MgCO_3 + nMgO + nCO_2 \quad (2.4)$$

Model III: $$CaMg(CO_3)_2 \rightarrow (1 - x)CaCO_3(1 - y)MgCO_3 + xCaCO_3 + yMgO + yCO_2 \quad (2.5)$$

Model IV: $$CaMg(CO_3)_2 \rightarrow CaO + MgO + 2CO_2 \rightarrow CaCO_3 + MgO + CO_2 \quad (2.6)$$

Model V: $$CaMg(CO_3)_2 \rightarrow CaCO_3 + MgO + CO_2 \quad (2.7)$$

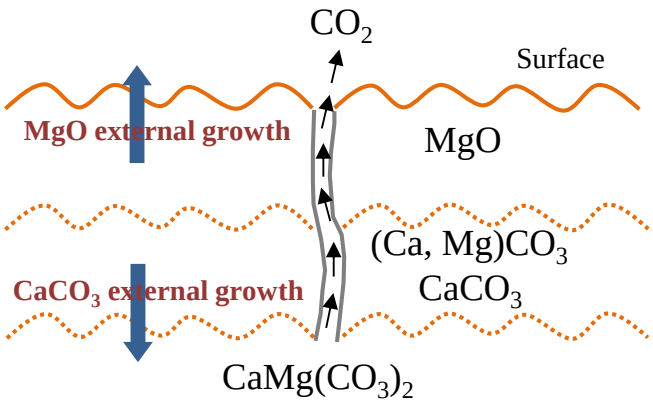


**Figure 2.3** Schematic illustration of surface of dolomite during calcination in air.

The CaMgO can be used as a heterogeneous base catalyst in transesterification of vegetable oil with methanol to produce FAMEs and glycerol. The highly basic of CaO gives a high reaction rate in the transesterification under mild conditions. On the other hand, the pure MgO has been reported to be an effective catalyst under conditions operated at high temperature and high methanol: oil molar ratio [45]. CaO has higher basic strength than MgO due to a lower electronegativity of Ca than Mg [14]. However, MgO prepared in nanocrystalline form *via* sol-gel process showed a higher FAME yield than microcrystalline MgO under mild conditions [46]. The MgO nanoparticles dispersed on CaO, obtained from the calcined dolomite, was reported to be the active sites responsible for the transesterification [47], while other works reported that MgO acted as a support [48] or retarded the growth of CaO crystallites [6]. The CaMgO from the calcined dolomite exhibited higher surface area than the pure CaO [48]. The crystal size of CaO found in the mixed oxide was smaller than that of the pure CaO [6]. Although CaO had a higher Ca content than CaMgO, the mixed metal oxide catalyst exhibited a superior basicity [6, 49]. Therefore, the MgO presenting in the mixed oxides significantly affects the physicochemical and catalytic properties of the dolomite-derived CaMgO.

A series of supported mixed oxide catalysts was investigated by Jindapon and co-workers [28]. The Ca and Zn mixed oxides supported on $Al_2O_3$ (ZSA) were prepared by dissolution-precipitation method and tested in the transesterification of palm oil with methanol. Waste mixed seashells (*Perna viridis, Anadara granosa, Amusium pleuronectes,* and *Meretrix meretrix)* as abundant, low-cost, and nontoxic were used as calcium sources. After calcination at 500 °C (ZSA-500), the surface area, metal oxide dispersion and total basicity were improved when compared to the parent calcined seashells. The $Ca_{12}Al_{14}O_{33}$ generated from solid-state reaction of CaO and $Al_2O_3$ also improved the mechanical strength [50]. Moreover, the solid-state reaction of ZnO and $Al_2O_3$ generated a spinel $ZnAl_2O_4$ used as heterogeneous base

catalyst in the first commercialized biodiesel plant [3]. In term of catalyst reusability, the ZSA-500 had a high stability against the glycerol adsorption as well as the phase transformation.

Furthermore, CaO was combined with various metal oxides, such as lanthanum oxide ($La_2O_3$) [51], cesium oxide ($CeO_2$) [52] zinc oxide (ZnO) [53], and zirconium oxide ($ZrO_2$) [54]. The obtained results confirmed that this strategy is an effective route to increase the specific surface area, basicity and catalytic performance. A series of three-component mixed oxides of Ca, Mg and Zn was reported to be highly active catalysts in the transesterification of palm kernel oil with methanol [55]. Moreover, calcium aluminate compound ($Ca_{12}Al_{14}O_{33}$) as a new phase obtained from CaO and $Al_2O_3$ *via* solid-state reaction at high temperatures stabilized the CaO active phase and enhanced the mechanical strength of resulting catalysts [50].

### 2.2.5 Other Ca compounds

According to previous studies, several calcium phases, such as calcium hydroxide ($Ca(OH)_2$), calcium glyceroxides ($Ca(C_3H_7O_3)_2$) and calcium methoxide ($Ca(OCH_3)_2$), were formed in the reaction medium when CaO was used as the catalyst in the transesterification of vegetable oil with methanol. These Ca compounds contributed the catalytic process, more or less depending on their basicity and solubility in the reaction media. Raafat *et al.* [10] reported that the catalytic activity of different Ca compounds was ranked in the ascending order: $Ca(OH)_2$ < CaO < $Ca(OCH_3)_2$, which agree with the Lewis basic theory. The CaO can react with methanol at room temperature to produce $Ca(OCH_3)_2$. Other researchers directly used $Ca(OCH_3)_2$ as a transesterification catalyst [11]. This phase was also prepared by premixing of CaO with methanol before oil addition [9, 28]. $Ca(OH)_2$ was mentioned to be active in the transesterification due to the basicity derived from the surface hydroxide ions ($OH^-$) [10]. Some authors added a small amount of water into the reaction in order to generate surface hydroxide on the CaO surface [12, 13]. Moreover, $Ca(C_3H_7O_3)_2$ [15, 56, 57] and calcium glycerolate ($Ca(C_3H_6O_3)$) [58], which generated by reaction of CaO with glycerol as a by-product, were used as new catalytic materials in the transesterification of vegetable oil with methanol. According to Kouzu *et al.* [26], the S-shape kinetics curves were explained by changing of the activity phases during the reaction (Figure 2.4). At the initial state, the surface of CaO was transformed to $Ca(OCH_3)_2$ and $Ca(OH)_2$, which could be used to catalyze the reaction. Dias *et al.* [59] demonstrated that CaO was fully converted to $Ca(OH)_2$ at the early state of reaction. However, when $Ca(OH)_2$ was directly used as a catalyst, the induction period was not observed. Other explanation was the presence of mass

transfer limitation [60]. At the final state, the $Ca(C_3H_7O_3)_2$ generated from the reaction between CaO and glycerol as a by-product was the main contribution to the catalysis in this region [26]. Table 2.1 summarizes the reaction conditions and the FAME yield obtained over different Ca compounds [7, 11, 58, 61-63].

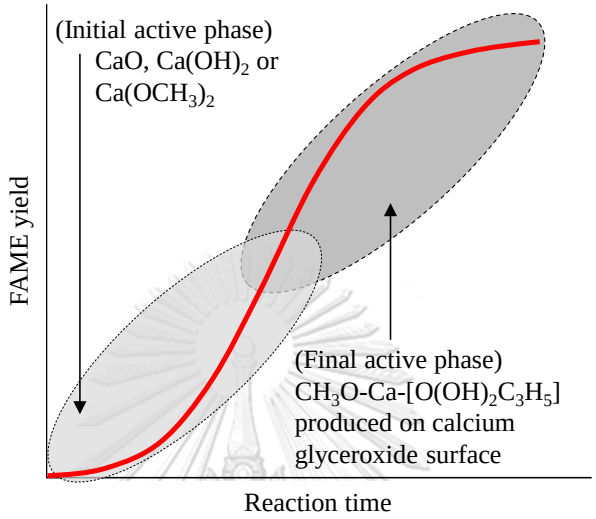


**Figure 2.4** Transformation of CaO to different Ca compounds during the transesterification of vegetable oil with methanol.

**Table 2.1** Catalytic activity of different Ca compounds in the transesterification of vegetable oils with methanol

| Ca compound | Catalyst loading (wt%) | Transesterification | | | | FAME yield (wt%) | Ref. |
|---|---|---|---|---|---|---|---|
| | | Stirred rate (rpm) | Ratio[a] | Temp. (°C) | Time (h) | | |
| $Ca(OH)_2$ | 5 | 900 | 6: 1 | 60 | 2 | 97 | [61] |
| $Ca(OCH_3)_2$ | 4 | 900 | 7.5: 1 | 65 | 2 | 98 | [11] |
| $Ca(OCH_3)_2$ | 1 | 1000 | 9: 1 | 65 | 1.5 | 90 | [62] |
| $Ca(C_3H_7O_3)_2$ | 3.5 | 500 | 12: 1 | 65 | 2 | 88 | [7] |
| $Ca(C_3H_7O_3)_2$/ $Al_2O_3$ | 3 | 500 | 12: 1 | 150 | 6 | 82 | [63] |
| $Ca(C_3H_7O_3)$ | 2 | Stirred | 12: 1 | 60 | 8 | ~95 | [58] |

[a] Methanol:oil molar ratio.

### 2.3 Reaction mechanism of Ca-based catalyst in transesterification

The transesterification of triglycerides with methanol to produce three molecules of methyl ester and one molecule of glycerol is shown in Figure 2.5. The reaction consists of a number of consecutive and reversible reactions. Firstly,

diglyceride and one molecules of methyl ester are produced as shown in Eq. (2.8). Subsequently, the diglyceride generated is converted to monoglyceride (Eq. (2.9)), and glycerol (Eq. (2.10)). Totally, one molecule of triglycerides is requested with three molecules of methanol. The monoglyceride conversion produced the methyl ester is believed to be the rate determining step due to the most stable intermediate compound. Moreover, the mechanism of Ca-based catalysts in transesterification was presented in many types, such as mechanism of CaO in Eley–Rideal (ER) and Langmuir–Hinshel-wood–Hougen–Watson (LHHW), CaO in the presence of a small water amount, calcium methoxide, and calcium glyceroxide as a heterogeneous and homogeneous form.

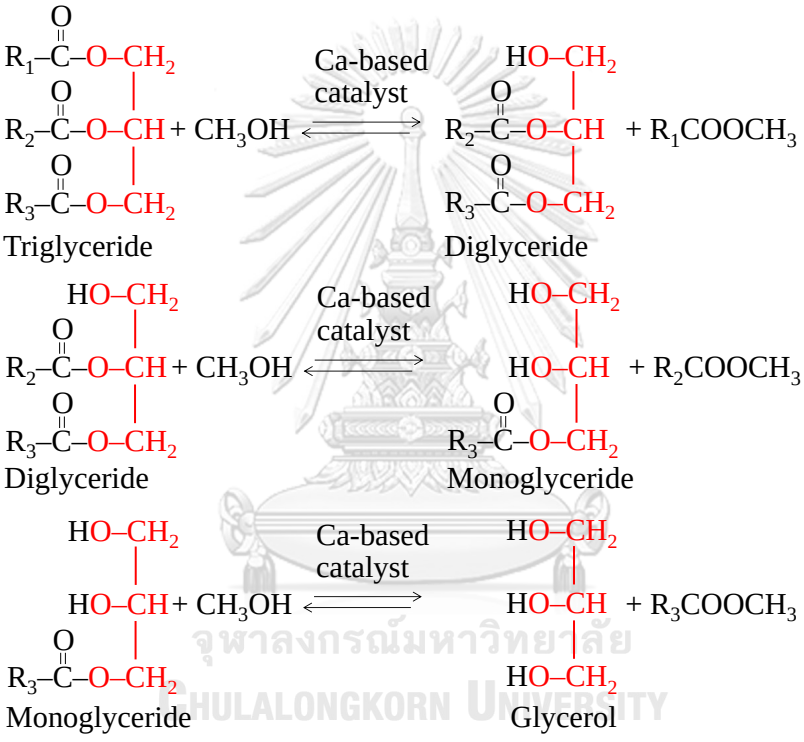


(2.8)

(2.9)

(2.10)

**Figure 2.5** Three consecutive transesterification of triglycerides.

### 2.3.1 Mechanism of CaO in transesterification

The mechanisms of CaO as a heterogeneous catalyst in transesterification of triglycerides with methanol were purposed in two basics including Eley–Rideal (ER) and Langmuir–Hinshel-wood–Hougen–Watson (LHHW). According to the ER mechanism (Figure 2.6) [14], the CaO surface is preliminary covered by methanol and then formed methoxide species (Eq. (2.11)). The carbonyl carbon of the triglycerides is attacked by the methoxide species, following by the formation of a tetrahedral intermediate. The intermediate is then readjusted to a diglyceride anion form stabilized by a proton from the catalyst surface and one molecule of methyl ester (Eq. (2.12)). Finally, the diglyceride anion is stabilized by a proton from the catalyst

surface to produce the regenerated surface of catalyst (Eq. (2.13)). The remaining of two carbonyl carbons of the diglyceride is continuously attacked by the methoxide species to give three molecules of methyl esters and one molecule of glycerol.

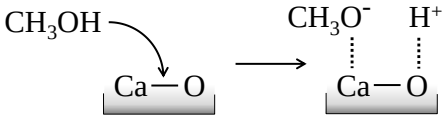


(2.11)

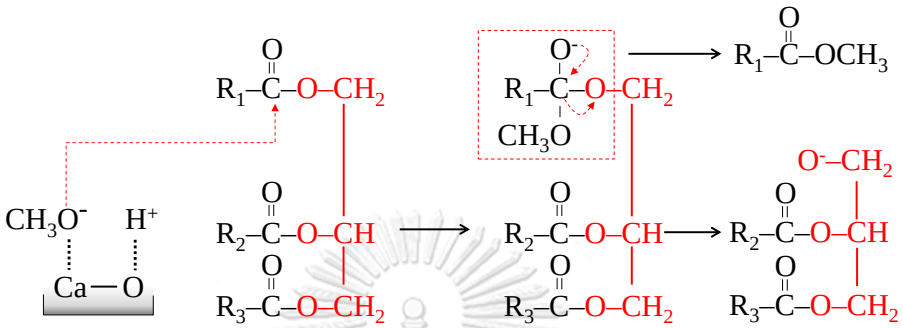


(2.12)

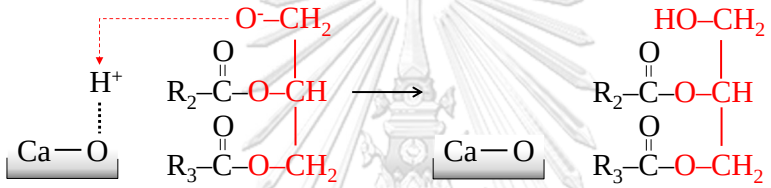


(2.13)

**Figure 2.6** The mechanism *via* ER for the transesterification of triglycerides with methanol.

Based on the transesterification of ethyl acetate with alcohol catalyzed by solid base catalyst [64], the LHHW mechanism of the transesterification of triglycerides with methanol is proposed in Figure 2.7. Both reactants are preliminary adsorbed on the catalyst surface (Eq. (2.14)). The methoxide species generated attack on neighboring carbonyl cation to produce a tetrahedral intermediate (Eq. (2.15)). One molecule of methyl ester is desorbed, and then the diglyceride adsorbed is stabilized by a proton from the catalyst surface to produce the regenerated surface of catalyst (Eq. (2.16)). Finally, the cycle reaction is continuously attacked to produce the methyl eater and glycerol.

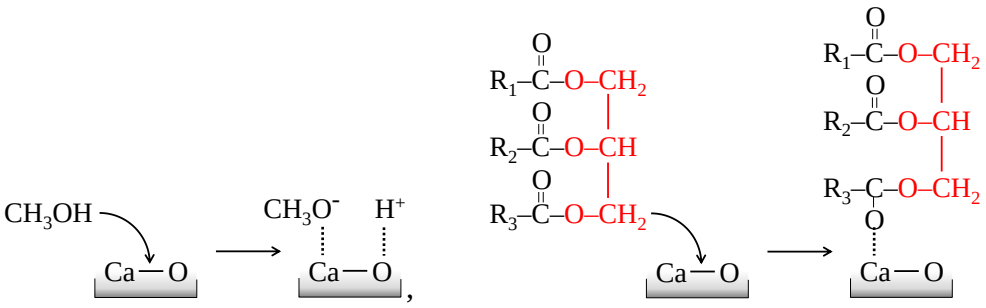


(2.14)

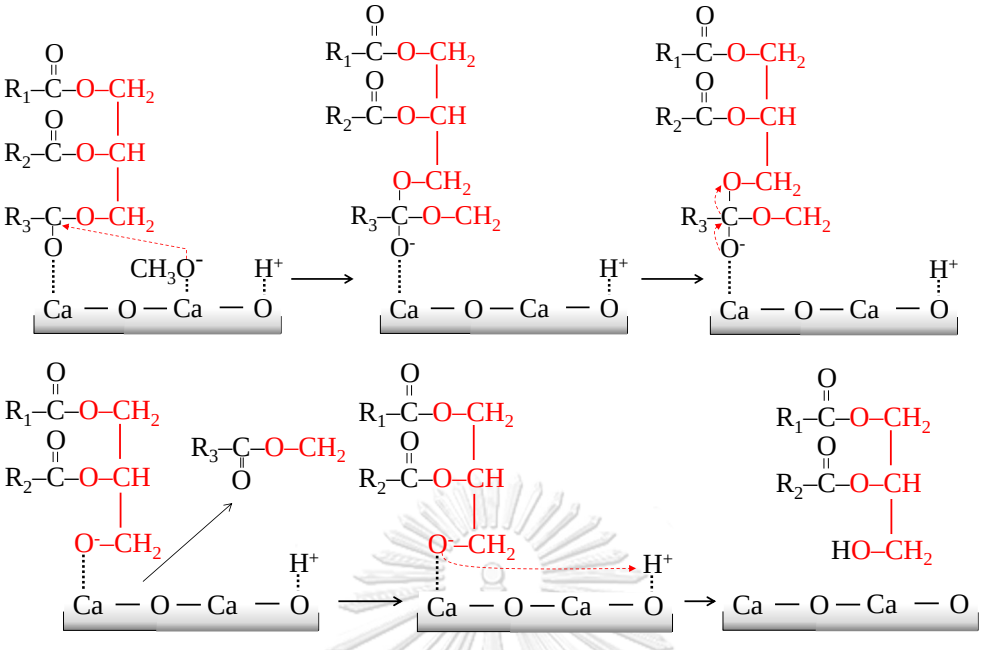

(2.15)

(2.16)

**Figure 2.7** The mechanism *via* LHHW for the transesterification of triglycerides with methanol.

### 2.3.2 Mechanism of CaO in the presence of a small water amount in transesterification

According to Liu *et al.* [13], the CaO activity in the transesterification of soybean oil with methanol was improved by the mixing of a small amount of water with methanol. Figure 2.8 shows the mechanism presented by CaO surface developed by adding of a small amount of water. Due to higher electron donor capacity of the oxygen in the water molecule than in methanol molecule [65], CaO is preliminary reacted with water to from $OH^-$ group that continuously attacked with $H^+$ from methanol to generate methoxide anion and water (Eq. (2.17)). Moreover, the CaO is directly reacted by methanol and form methoxide species on surface (Eq. (2.18)). Both methoxide anion and surface methoxide generated attach to a carbonyl carbon of the triglyceride molecule to form the tetrahedral intermediate to next produce the methyl ester.

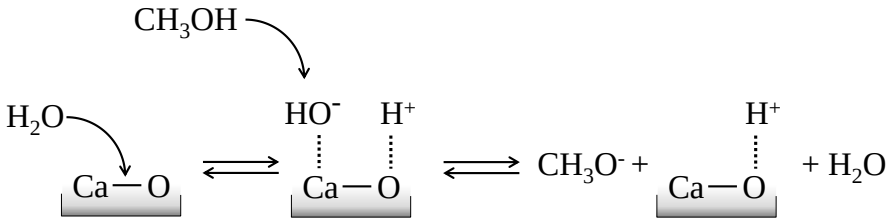

(2.17)

Methoxide anion

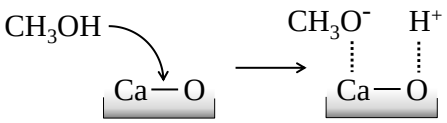


(2.18)

Methoxide anion on the surface

**Figure 2.8** The mechanism of CaO initiated by using of a small amount of water.

### 2.3.3 Mechanism of calcium methoxide in transesterification

Based on mechanism of trimethylolpropane (TMP) and palm oil methyl esters (POME) over calcium methoxide as a catalyst [66], the behavior in transesterification of triglycerides with methanol is probably similar. Figure 2.9 shows the possible mechanism of using calcium methoxide as a catalyst. The methanol and triglycerides are adsorbed with Ca and O on surface followed by (Eq. (2.19)) and (Eq. (2.20)), respectively. The reaction between adsorbed neighboring species of both intermediate produces a diglyceride and ester molecules (Eq. (2.21)). Finally, the cycle reaction is continuously performed to produce the methyl eater and glycerol.

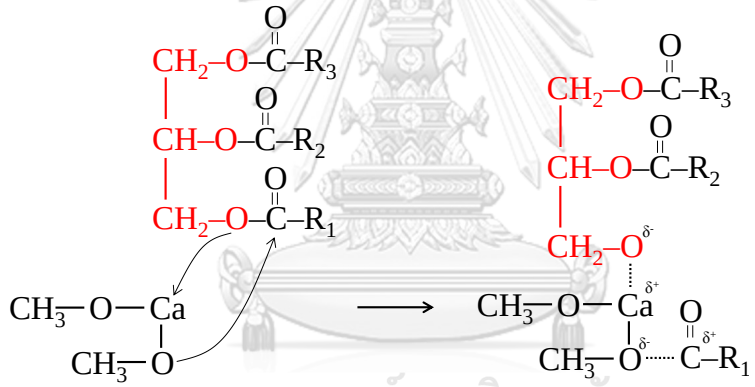

(2.19)

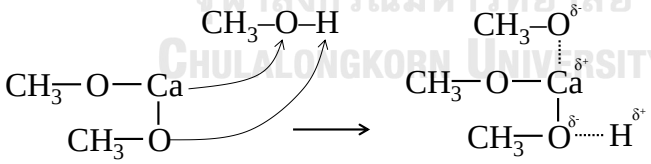

(2.20)

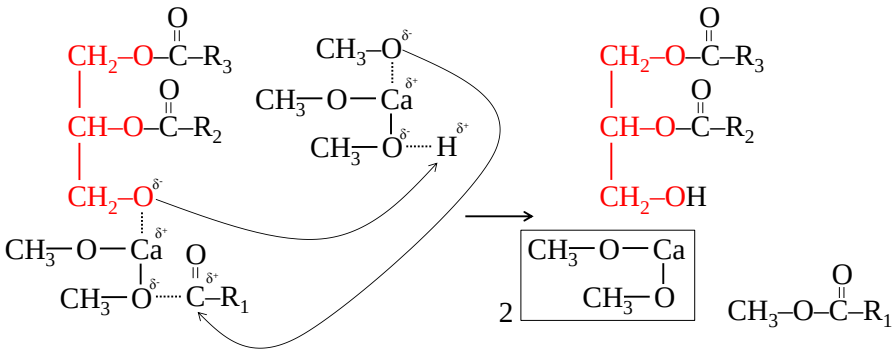

(2.21)

**Figure 2.9** The mechanism of transesterification of triglycerides with methanol catalyzed by calcium methoxide.

### 2.3.4 Mechanism of calcium glyceroxide as a heterogeneous catalyst in transesterification

According to Kouzu *et al.* [7], the proposed mechanism of transesterification of triglycerides with methanol over calcium glyceroxide is shown in Figure 2.10. Two neighboring OH groups from calcium glyceroxide are used to the adsorption of methanol molecule using hydrogen bond interaction (Eq. (2.22)). Moreover, it was possible that the abstraction of protons was enhanced by the neighboring location of the OH groups. The proton of the methanol is abstracted by the basic sites, generating of methoxide species (Eq. (2.23)). The carbonyl carbon is attracted by the methoxide species, following by stabilization of the anion by proton (Eq. (2.24)).

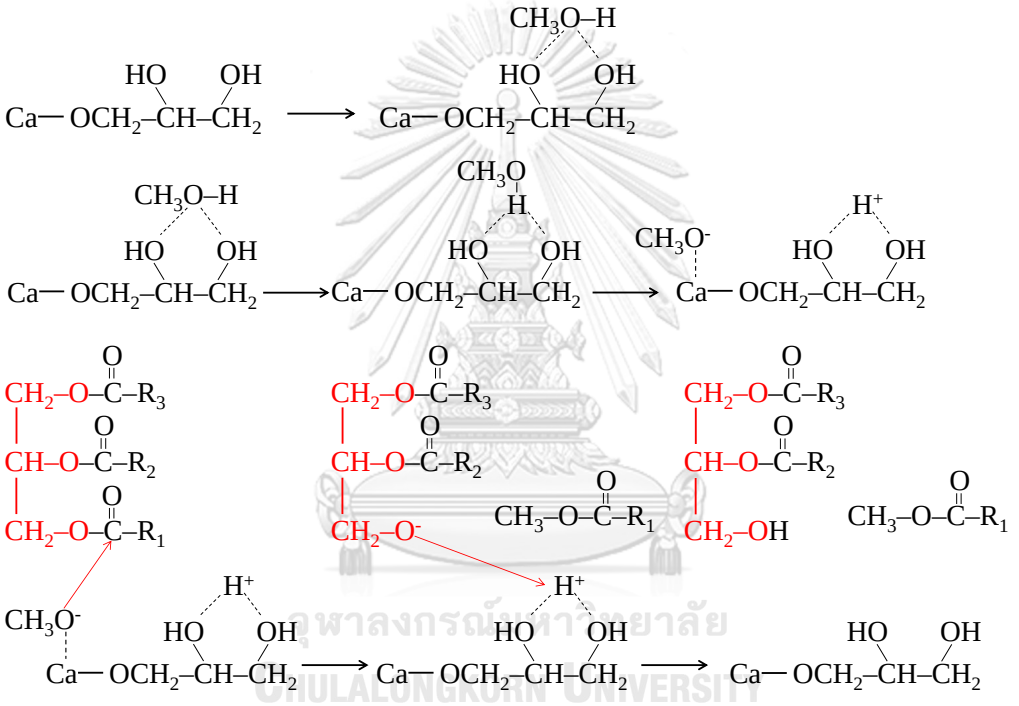


**Figure 2.10** The mechanism of transesterification of vegetable oil with methanol catalyzed by calcium glyceroxide on surface.

### 2.3.5 Mechanism of calcium glyceroxide as a homogeneous catalyst in transesterification

CaO is successively transformed to calcium methoxide and calcium glyceroxides ($Ca(C_3H_7O_3)_2$) during use [8]. Although the $Ca(C_3H_7O_3)_2$ was believed to be the active phase of the pure CaO catalyst [14], their formation contributed to homogeneous catalysis [8, 14]. It is worth noting that the solubility in methanol of $Ca(C_3H_7O_3)_2$, at 6216 mg $L^{-1}$ [14], is about 200-fold higher than that of CaO, at 28 mg $L^{-1}$ [8]. Based on using homogeneous catalysts mechanism [67], the possible mechanism over $Ca(C_3H_7O_3)_2$ catalyzed in transesterification of vegetable oil with

methanol is shown in Figure 2.11. The $Ca(C_3H_7O_3)_2$ is leached in methanol and then create calcium cation and glyceroxide anion (Eq. (2.25)). The methoxide anion is produced and generate of glycerol (Eq. (2.26)). The nucleophile from methoxide anion attacks on carbonyl carbon, generating a tetrahedral intermediate (Eq. (2.27)). After the intermediate readjusted, the diglyceride anion is stabilized by a proton from the glycerol caused in formation of glyceroxide anion (Eq. (2.28)).

$$Ca(C_3H_7O_3)_{2\,(s)} \rightleftharpoons Ca^{2+}{}_{(l)} + 2C_3H_7O_3^-{}_{(l)} \quad (2.25)$$

$$C_3H_7O_3^- + CH_3O{-}H \rightleftharpoons CH_3O^- + C_3H_7O_3H \quad (2.26)$$

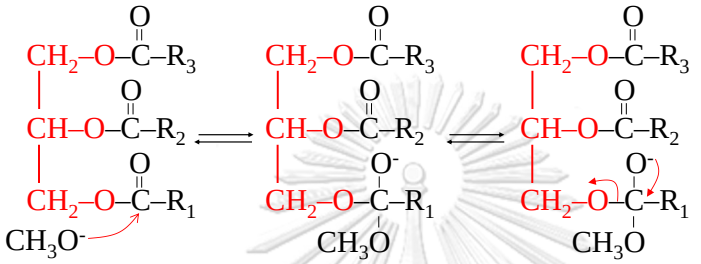

(2.27)

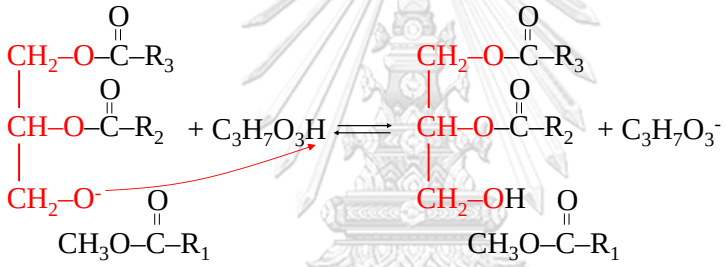

(2.28)

**Figure 2.11** The mechanism of transesterification of vegetable oil with methanol catalyzed by calcium glyceroxide as a homogeneous route.

### 2.3 Deactivation of Ca-based catalyst in transesterification

According to the many researchers [7-9, 14-16], the causes for deactivation of Ca-based catalysts can be classified into three groups: (1) the basic sites is adsorbed by ambient $CO_2$ and $H_2O$, (2) the basic sites come into contact with $H_2O$ and free fatty acids (FFA) contaminated in reactants, and (3) the basic sites is transformed into other phases during the reaction. According to Kouzu *et al.* [7], explained that CaO catalyst was rapidly deactivated by the ambient $CO_2$ and $H_2O$ when CaO catalyst was exposed to ambient air for 3 min. The catalytic activity obtained from the CaO exposed was significantly decreased. Granados *et al.* confirmed that the ambient $CO_2$ and $H_2O$ can chemisorb on the CaO surface in a few minute [8].

Our previous research paper [9] tested the stability of the series ZSA catalysts exposed to ambient air (RH ≈ 73%) for 3 days. The chemisorption of $CO_2$ and $H_2O$ onto CaO produced $CaCO_3$ and $Ca(OH)_2$, respectively. The structure changes analyzed by XRD of series ZSA catalysts revealed that the degree of carbonation

strongly depended on crystallite size of $Ca(OH)_2$ because $CaCO_3$ (36.9 $cm^3$ $g^{-1}$) has larger volume than $Ca(OH)_2$ (33.6 $cm^3$ $g^{-1}$) and CaO (16.9 $cm^3$ $g^{-1}$). The $CaCO_3$ formation from direct carbonation of $Ca(OH)_2$ prefered on large crystals.

The FFA (5.1 mg-KOH $g^{-1}$) and $H_2O$ (0.05 wt%) contained in the waste cooking oil were tested in transesterification over CaO catalyst [14]. The complete FAME yield (99 wt%) was obtained at 2 h of reaction time, but the formation of calcium soap was received at initial stage of the transesterification. The calcium soap generated resulted in leaching of calcium species contained in biodiesel (3065 ppm). According to European standard (EN 14538), the calcium content of biodiesel is limited to 5 ppm. However, when edible grade of soybean oil, which less acid valve (<0.1 mg-KOH $g^{-1}$) and $H_2O$ (<0.01 wt%), was used as a reactant, the high calcium leaching of 187 ppm was also found. This result indicated that Ca-based catalysts can be leached itself. Table 2.2 shows the solubility of calcium in many compounds into alcoholic liquid phase. The $Ca(C_3H_7O_3)_2$ shows the highest solubility of calcium in methanol.

**Table 2.2** Solubility of Ca-based compounds into alcoholic liquid phase.

| Entry | Ca-based compounds | Solubility in methanol ($mg\ L^{-1}$) | Ref |
|---|---|---|---|
| 1[a] | CaO | 28 | [15] |
| 2[b] | $Ca(OH)_2$ | 100 | [16] |
| | $Ca(OCH_3)_2$ | 200 | [16] |
| 3 | $Ca(C_3H_7O_3)_2$ | 6216 | [14] |

[a] Based on conductivity measured at 60 °C.
[b] The measurement procedure was not appreciable.

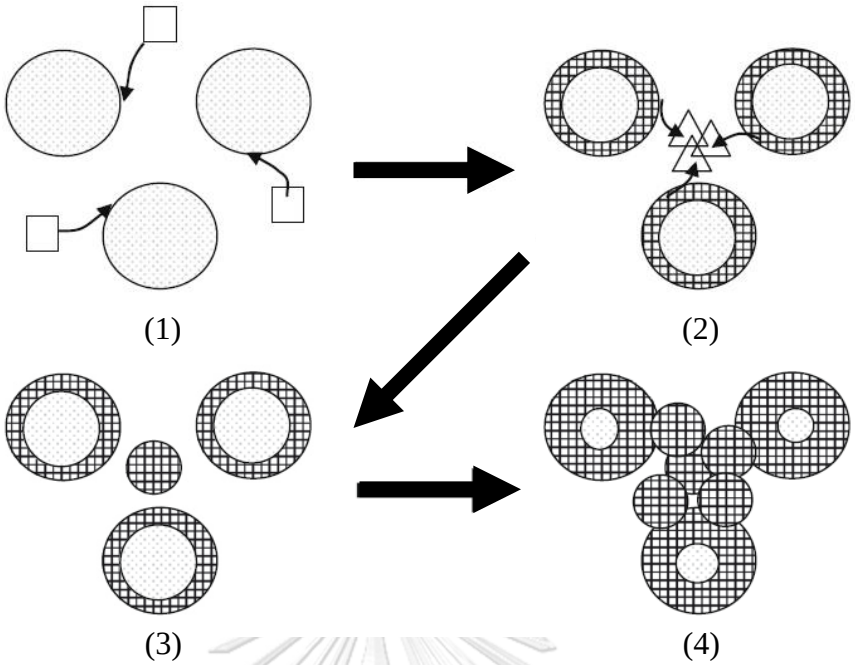


**Figure 2.12** Deactivation of CaO catalyst *via* $Ca(C_3H_7O_3)_2$. (Symbols: ○ = CaO, □ = Glycerol, ◍ = Calcium glyceroxide of solid phase and △ = dissolved calcium glyceroxide).

The deactivation of CaO used in the transesterification was reported to occur *via* the formation of $Ca(C_3H_7O_3)_2$ [68], which can be explained in the following four steps: (1) chemical reaction of CaO and glycerol; (2) formation of $Ca(C_3H_7O_3)_2$, followed by its partial dissolution; (3) recrystallization of the dissolved $Ca(C_3H_7O_3)_2$; and (4) agglomeration of CaO catalyst by the crystallized fine particles (Figure 2.12).



## 2.4 Literature reviews

Ngamcharussrivichai *et al.* [29] studied the transesterification of palm kernel oil (PKO) with methanol over different natural calcium sources, including calcite, cuttlebone, dolomite, hydroxyapatite, and dicalcium phosphate. The transesterification conditions were performed at 60 °C, 1 atm, catalyst amount of 6 wt%, reaction time of 3 h and methanol: oil molar ratio of 30: 1. Mixed oxide of CaO and MgO (CaMgO) obtained from dolomite calcined at 800 °C was the most active catalyst. The FAME yield obtained from using the CaMgO was achieved of 98.0 wt%. After 10 repetition test, the calcined dolomite can be reused with the retention of the ME content higher than 90 wt%.

Verziu *et al.* [46] demonstrated that nanocrystalline MgO catalyst synthesized *via* sol-gel process using $Mg(OCH_3)_2$ as a magnesium precursor, followed by calcination in air at 500 °C. The catalyst obtained exhibited an active for

transesterification of sunflower and rapeseed oils with methanol under mild condition. Furthermore, the nanocrystalline MgO form showed a higher FAME yield than the microcrystalline MgO form prepared by a conventional process. In addition, the transesterification using microwave irradiation can provide a rapid and convenient method for transesterification of triglycerides. From reusability study, the nanocrystalline MgO was stable during FAME synthesis at least seven cycles under microwave irradiation at 70 °C, methanol: oil molar ratio of 4:1 and the reaction time of 40 min. However, a leaching of magnesium was evidenced as a direct consequence of a saponification reaction.

Kouzu *et al.* [69] reported the mechanism and leaching behavior of CaO used as a heterogeneous catalyst in the transesterification of soybean oil with refluxed methanol. The calcium contents of biodiesel and glycerol were 139 and 4602 ppm, respectively. Moreover, a high leaching of CaO was only found at the first run. When CaO was used in the transesterification, the reaction was catalyzed *via* two heterogeneous and homogeneous routes. The homogeneous catalysis was mainly originated from $Ca(C_3H_7O_3)_2$, which was hydrolyzed to produce hydroxide ion coupled with calcium ion according to Eq. (2.29). The hydroxide abstracted proton from methanol, (Eq. (2.30)), and then the methoxide generated reacted with triglyceride molecule to produce FAME as a product. In minor case, CaO was dissolved in methanol to calcium ion and methoxide ion according to Eq. (2.31), which was active in the transesterification.

$$Ca(C_3H_7O_3)_2 + 2H_2O \rightleftharpoons Ca^{2+} + 2OH^- + 2C_3H_8O_3 \quad (2.29)$$

$$2OH^- + CH_3OH \rightleftharpoons H_2O + CH_3O^- \quad (2.30)$$

$$CaO + CH_3OH \rightarrow Ca^{2+} + CH_3O^- + H_2O \quad (2.31)$$

Lukić *et al.* [57] prepared $Ca(C_3H_7O_3)_2$ as a catalyst for transesterification of palm oil with methanol. The $Ca(C_3H_7O_3)_2$ catalyst was prepared by mechanochemical treatment. The CaO obtained by calcining limestone was mixed with glycerol (CaO: glycerol molar ratio of 1:5) in a planetary ball mill for 5 h. The $Ca(C_3H_7O_3)_2$ obtained was very active in transesterification of sunflower oil with methanol under different reaction conditions. The FAME yield was enhanced by mitigating the mass transfer resistance at the initial process. $Ca(C_3H_7O_3)_2$ acted as an emulsifier to stabilize the interface between vegetable oil and methanol, resulting in a reduction of mass transfer limitation.

Taufiq-Yap *et al.* [70] prepared the mixed calcium and magnesium oxides with different Ca: Mg atomic ratios (0.5–10.0 mol%) using co-precipitation method. A slight MgO loading (0.5 mol%) improved the FAME yield, but when Mg loading was increased, a drop in the FAME yield from 90 to 75 wt% was found. When compared the catalytic activity between CaO and CaMgO, CaO had better

transesterification activity than the mixed oxide catalyst due to its higher Ca content. However, the catalytic activity of CaO was decreased more severe than that of CaMgO after five runs.

Jaiyen *et al.* [6] compared the catalytic activity and stability of the CaMgO derived from dolomite and the CaO obtained from waste mixed seashells in transesterification of palm oil with methanol. The CaMgO possessed smaller CaO crystallites and higher basicity than the pure CaO, which was probably due to the presence of MgO dispersed in the CaO lattice, retarding the crystal growth of CaO. The FAME yield of >98 wt% was found for both catalysts at the first run. However, using of CaO revealed a severe drop of the FAME yield to 42 wt% after ten repetitive uses. In case of the CaMgO catalyst, the FAME yield was stable over seven repetitive uses (90 wt%) and gradually dropped to 82 wt% at the ten cycle. The deactivation of CaO was more severe than that of CaMgO due to an extensive formation of $Ca(C_3H_7O_3)_2$ *via* the reaction of CaO with glycerol. Thus, the presence of MgO dispersed in the CaO matrix may be important to stabilize the CaO phase.

Bournay *et al*. [3] reported about new heterogeneous process for biodiesel production that had been developed by French Institute of Petroleum (IFP). The Zn–Al mixed oxide is used as the heterogeneous catalyst. It is packed into two fixed-bed reactor located in a stream of the continuous-flow transesterifying system. However, the reaction condition is operated at high temperature ranging from 210 °C to 250 °C and high pressure between 3 and 5 MPa. Excess of methanol is evaporated after each reactor by partial evaporation. Subsequently, the esters and glycerol is separated in settlers. In this procedure, biodiesel and glycerol has high purity without any salt contaminants. The process was first used in an industrial context in 2006, by Sofiproteol in Sete.

Ngamcharussrivichai *et al*. [23] investigated the effects of binder addition on the preparation of catalyst extrudates from limestone. The extrudates from heterogeneous catalysts from limestone using manual extruder can be conducted as followed: (1) add calcined limestone and/or metals oxide, hydroxide and carbonates (Ca, Mg and Al), (2) add an $NH^{4+}$ based ($NH_4OH$ and $(NH_4)_2CO_3$) caustic solvent or deionized water, (3) change a powdery mixture into a uniform paste, (4) shape into a continuous rod with a cross-sectional diameter of 2 mm by using a manual extruder, (5) dry at 100 °C and calcined in a muffle furnace at 800 °C. As the result, the addition of $NaAlO_2$ was a key to attain the dense and hard extrudates by inducing the formation of the mixed Ca and Al phases. The catalyst can be regenerated and used repeatedly. The catalytic test of the catalyst extrudates in the continuous-flow using fixed-bed reactor suggested the good activity and stability in the transesterification.

# CHAPTER III
# Experimental and analytical method

## 3.1 Materials and chemical reagents

### 3.1.1 Chemicals for catalyst preparation

- Calcite ($CaCO_3$, 98%) (Commercial grade, Union Chemical 1986 CO., Ltd.)
- Dolomite ($CaMg(CO_3)_2$, 99.4%) (Commercial grade, P&S DOLO-LIME Co., Ltd.)
- Magnesite ($MgCO_3$, 98%) (Commercial grade, PPM Chemical CO., Ltd.)
- Calcite ($CaCO_3$, 98%) (Commercial grade, ucs1986 Chemical)
- Dolomite ($CaMg(CO_3)_2$, 99.4%) (Commercial grade, P&S DOLO-LIME Co., Ltd.)
- Glycerol ($C_3H_8O_3$) (99.0%, Sigma-Aldrich)
- Methanol ($CH_3OH$, 99.5%) (Commercial grade, 99.8%, Zen Point)
- Aluminum oxide ($Al_2O_3$, 99.6%) (Commercial grade, Fuji Kasei)
- Enamel venus shells (*Meretrix meretrix*)
- Hydroxyethyl cellulose (2,960 cP at 1 wt%) (Commercial grade, Thai Specialty Chemical Company)
- Nitric acid ($HNO_3$, 50-70 %) (JT. Baker)
- Zinc nitrate ($Zn(NO_3)_2 \cdot 6H_2O$, 98%) (Commercial grade, PPM Chemical CO., Ltd.)



### 3.1.2 Chemicals for miscibility test of methanol–oil–CME system

- $C_{12}$–$C_{14}$ commercial methyl esters (CMEs) (Thai Oleochemicals (TOL) Co., Ltd.)
- Methanol ($CH_3OH$, 99.5%) (Commercial grade, 99.8%, Zen Point)
- Refined bleached deodorized (RBD) palm kernel oil (Chumporn Palm Oil Industry Co.,Ltd., Thailand)

### 3.1.3 Chemicals for transesterification reaction

- Methanol ($CH_3OH$, 99.5%) (Commercial grade, 99.8%, Zen point)
- Refined bleached deodorized (RBD) palm oil (Oleen Co.,Ltd., Thailand)
- Refined bleached deodorized (RBD) palm oil (Chumporn Palm Oil Industry Co.,Ltd., Thailand)

- Sodium sulfate anhydrous ($Na_2SO_4$, 99%) (AR grade, Ajax Finechem)

### 3.1.4 Chemicals for reaction product analysis

- 1,4-Dioxane (99.99%, Fisher)
- Methyl heptadecanoate ($C_{18}H_{36}O_2$, 99.5%) (Standard grade, Fluka)
- *N*-Methyl-*N*-(trimethylsilyl)trifluoroacetamide (MSTFA, 99%) (Synthesis grade, Fluka)

## 3.2 Equipment and apparatus

- Centrifuge
- Desiccator
- Electric oven
- Glass column reactor equipped with a heating band, insulator jacket and a thermocouple connected to a temperature controller
- Hot plate stirrer equipped with thermocouples (model: ETS-D5)
- Micro pipettes
- Muffle furnace
- Overhead stirrer
- pH meter
- Rotary evaporator
- Round bottom flask (50 mL) equipped with a water-cooled condenser and a magnetic stirrer.
- Manual extruder (Figure 3.1)
- Single screw extruder (Figure 3.2) (The Bonnot Company, Catalyst Extruders)



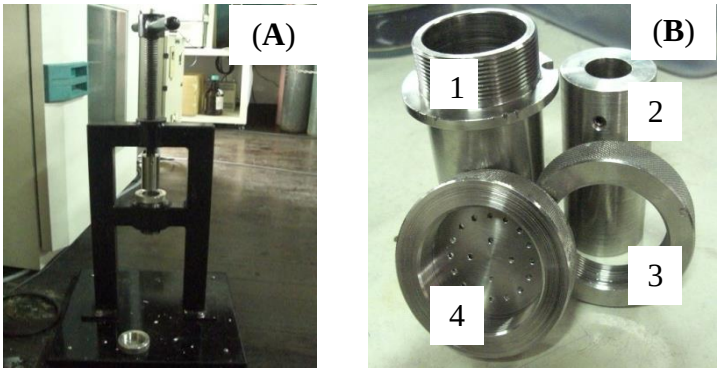


**Figure 3.1** Manual extruder used for catalyst formulation: (A) extruder and (B) extruder components (1= barrel, 2 = pressing rod, 3= ring for locking the receptacle and 4 = 2-mm hole die).

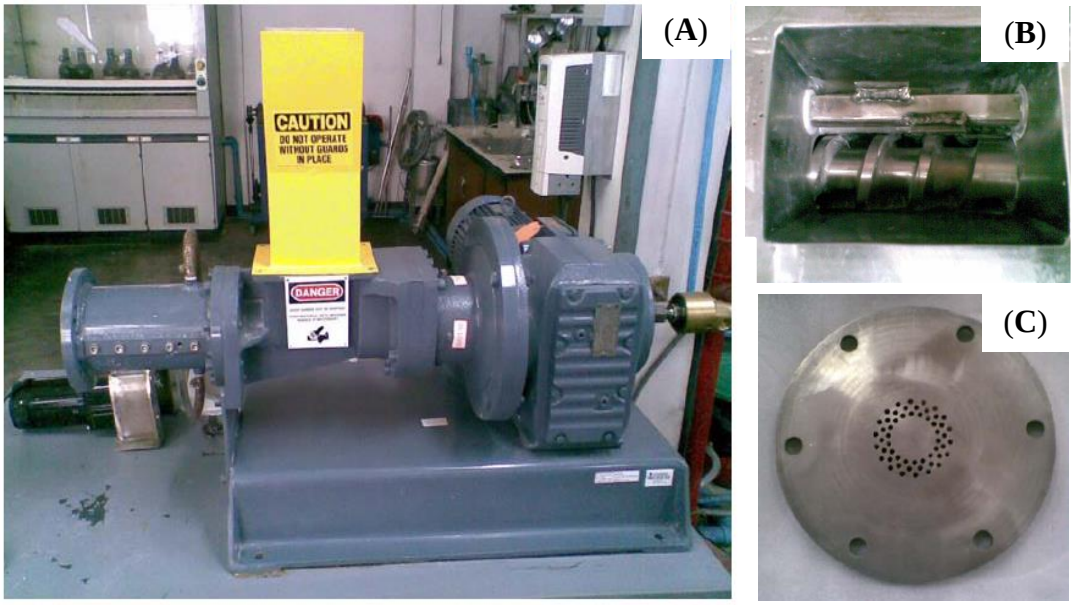


**Figure 3.2** Single screw extruder used for catalyst formulation: (A) extruder, (B) screw feeder and (C) 3.5-mm hole die**.**

### 3.3 Catalyst preparation

#### 3.3.1 Preparation of metal oxides catalyst derived from calcite, dolomite and magnesite

The raw materials of dolomite ($CaMg(CO_3)_2$), calcite ($CaCO_3$) and magnesite ($MgCO_3$) were sieved to reduce the particle sizes to less than 38 μm before being used. Then, the powder materials were calcined in a muffle furnace at different temperatures (700–1000 °C) for 3 h using a heating rate of 3 °C $min^{-1}$. In case of raw dolomite, the heating rate and calcination time were also varied to obtain different types of mixed Ca and Mg compounds. After the process completed, the furnace temperature was decreased to 500 °C in order to avoid moisture contamination, and the calcined samples were kept in a desiccator at room temperature before being used. The obtained catalysts were designated as CaO-*x*, CaMgO-*x* and MgO-*x*, where *x* represents the calcination temperatures used. In addition, a mixed CaO and MgO catalyst was prepared by a physical mixing of calcite and magnesite at the same $CaCO_3$: $MgCO_3$ mass ratio as the raw dolomite, followed by calcination in a muffle furnace at 800 °C for 3 h using a heating rate of 3 °C $min^{-1}$. The resulting catalyst was denoted as (CaO+MgO)-800.

### 3.3.2 Preparation of Ca-based methoxide and glyceroxide catalysts from CaO-800 and CaMgO-800

Various Ca-based methoxides and glyceroxides were prepared *via* direct reaction of CaO-800 and CaMgO-800 with methanol and glycerol, respectively. The CaO-800 and CaMgO-800 were prepared according to previous section (*see* section 3.3.1). The direct reaction of Ca-based oxides with methanol or glycerol was performed in a 100-mL round bottom flask equipped with a water-cooled condenser and a magnetic stirrer. The reaction temperature was controlled at 60±0.5 °C using a water bath equipped with a PID controlled electronic thermometer. For the Ca-based methoxides preparation, the CaO-800 or CaMgO-800 (1.5 g) was vigorously stirred in methanol (17.1 g) for 120 min. The mass ratio of the amount of metal oxide: methanol was similar to the ratio used in transesterification of reactants. In the case of Ca-based glyceroxided, glycerol (5.0 g) was dissolved in methanol (22.0 g), followed by adding CaO-800 or CaMgO-800 (1.5 g) and continuously stirring for 120 min. The resulting solid products were recovered by centrifugation at 7000 rpm. The catalysts obtained were used to analyze by other techniques without washing step, and were kept in a desiccator in order to avoid moisture contamination. The Ca-based methoxides obtained from CaO-800 and CaMgO-800 were denoted as CaMet and MgO·CaMet, respectively. On the other hand, Ca-based glyceroxides obtained were designated as CaGly (from CaO-800) and MgO·CaGly (from CaMgO-800).

### 3.3.3 Preparation of extrudate catalysts *via* dissolution-precipitation method

In order to apply the Ca-based catalyst in the biodiesel production using a fixed-bed reactor, the natural Ca powder was formulated as extrudate catalyst. Enamel venus shells (*Meretrix meretrix*) were used as a calcium source in this study. The $Zn(NO_3)_2{\cdot}6H_2O$ and $Al_2O_3$ added was a binder component in the extrudate catalysts [9, 28]. The seashells were washed, ground, and sieved to reduce the particle sizes to less than 10 μm before being used. The powdery seashell obtained was calcined in a muffle furnace at 800 °C for 2 h. An solution pH of aqueous solution of $Zn(NO_3)_2{\cdot}6H_2O$ was adjusted to 1 by adding 1 M HNO. The calcined seashell was added into the acidified $Zn(NO_3)_2$ solution, and then vigorously stirred using an overhead stirrer for 2 h. Subsequently, $Al_2O_3$ was then added and continually stirred for 1 h. The mass ratio of calcined seashell: $Zn(NO_3)_2{\cdot}6H_2O$: $Al_2O_3$ was fixed at 1: 0.6: 0.4. HEC as a plasticizer was finally added to the white slurry. The amount of HEC added was varied between 0 and 5 wt% based on the total solid mass. The resulting mixture was continuously stirred and heated to remove water until a paste

was formed. The catalyst paste was formulated as extruded rods with cross-sectional diameter of 2 mm by using a manual extruder or cross-sectional diameter of 3.5 mm by using a Bonnot single-screw extruder. In the case of using the single-screw extruder, screw speed and frequency were set at 40 rpm and 40 Hz, respectively. The length of extruded rods dried at 100 °C for 2 h were equally cut into 5 mm. The as-prepared extrudate were calcined in a muffle furnace at 400 °C for 2 h using a heating rate of 3 °C $min^{-1}$. The as-prepared extrudate was denoted as ZSAH, and ZSAH-400 represents in the calcined form of extrudate catalyst.

### 3.4 Transesterification reaction

#### 3.4.1 Batch conditions

The transesterification of RBD palm oil (purchased from Oleen Co.,Ltd., Thailand) with methanol was performed in a 50-mL round bottom flask equipped with a water-cooled condenser and a magnetic stirrer. The reaction temperature was controlled at 60±0.5 °C using a water bath equipped with a PID controlled electronic thermometer (Figure 3.3). Typically, 10 g of palm oil was pre-heated in the reactor at 60 °C for 20 min, and then methanol (11.40 g) and catalyst powder (1.00 g) were added under vigorous stirring. After the course of reaction, the solid phase was recovered by centrifugation at 7000 rpm for 10 min. The excess methanol was removed from the products using a rotary evaporator at 60 °C and 0.1 bar. The remaining liquid was separated in two-phase product including top layer of FAME and glyceride derivatives and bottom layer of crude glycerol.

**Figure 3.3** Experimental setup for the transesterification of RBD palm oil with methanol under batch conditions.

#### 3.4.2 Continuous conditions

The transesterification of RBD palm oil (Chumporn Palm Oil Industry Co.,Ltd., Thailand) with methanol to FAME was performed in a fixed-bed reactor. The experimental setup was performed by a glass column reactor (height of 300 mm

and diameter of 30 mm) equipped with a heating band, insulator jacket and a thermocouple, which connected to a temperature controller. A simplified diagram of the fixed-bed reactor system is shown in Figure 3.4. The catalyst extrudate (135 mL) was packed into the column, which glass beads (average diameter 3 mm) were added between top and bottom of the catalyst bed and finally terminated with quartz wool. During the start-up period, the reactor column was filled with methanol in order to stabilize the column temperature. After the temperature was attained at 65±1 °C, the methanol filled was drained once. Fresh RBD palm oil and methanol were separately fed by using peristaltic pumps (Longer, BQ50-1J) into the bottom of the column at constant flow rates. The liquid hourly space velocity (LHSV) was kept constant at 1.43 $h^{-1}$, and the methanol: oil molar ratio was fixed at 30:1. The effluent overflowing from the top of the glass column was collected in a 50 mL screw-cap glass bottle at different time intervals.

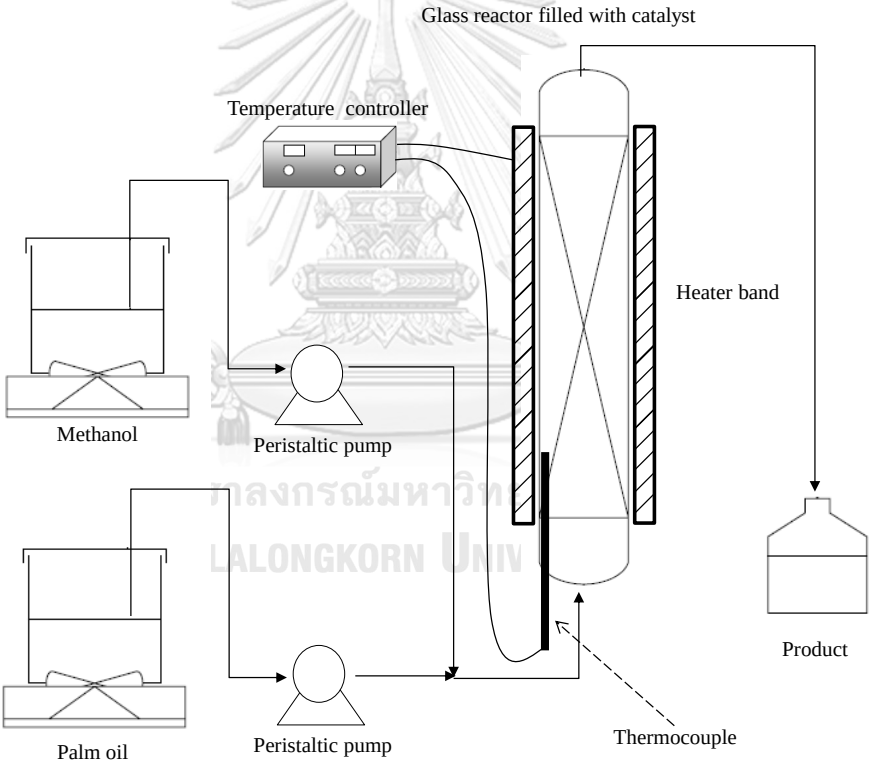


**Figure 3.4** Schematic diagram of experimental setup for the transesterification of palm oil with methanol under continuous condition.

### 3.5 Product analysis

For batch reaction, the FAME and glyceride derivative phases were recovered without any washing and diluted 10 times with 1,4-dioxane. 0.1 g of the resulting solution was derivatized with MSTFA to convert the mono- and di-glycerides remaining to more volatile derivatives. To this solution, methyl heptadecanoate, as a

reference standard, was added, and the sample volume was adjusted by an additional amount of 1,4-dioxane. The composition of FAME and glycerides was analyzed using an Agilent 7890A gas chromatograph (Figure 3.5) equipped with a flame ionization detector, a 15-m DB-5ht capillary column and an auto-injector. The column temperature was started at 50 °C, which was initially increased to 200 °C at a ramp rate of 10 °C $min^{-1}$ and then elevated to 350 °C for 5 min at a ramp rate of 15 °C $min^{-1}$. The FAME yield and triglyceride derivative was calculated using by a calibration curve. The conditions of gas chromatography (GC), representative chromatogram and calibration curve of $C_{16}$ FAME, $C_{18}$ FAME, monoglyceride, diglyceride and triglyceride are summarized in APPENDIX A.

**Figure 3.5** Agilent 7890A gas chromatograph for reaction product analysis.

In the case of continuous process, the FAME phase (0.03 g) was added into sample vial (2.0 mL). To this solution, 0.03 g of methyl heptadecanoate, as a reference standard, was added, and the sample volume was adjusted to 1.5 mL by using hexane. The FAME composition was determined by GC, using a Shimadzu 14B gas chromatograph (Figure 3.6) equipped with a 30-m DB-Wax capillary column and a flame ionization detector. The column temperature was started at 50 °C for 4 min and increased to 200 °C for 5 min at a ramp rate of 10 °C $min^{-1}$. The FAME yield (wt%) was calculated according to an external standardization method (EN 14103). The FAME yield was defined as follows:

$$\text{FAME yield (wt\%)} = \frac{\text{Weight of FAME attained by GC}}{\text{Theoretical weight of FAME}} \times 100 \qquad (3.1)$$

The GC conditions and example chromatogram of product obtained from Agilent 7890A gas chromatograph are shown in APPENDIX B.

**Figure 3.6** Shimadzu 14B gas chromatograph for reaction product analysis.

### 3.6 Direct reaction of CaO-800 and CaMgO-800 with methanol or glycerol

To understand the reactivity of active phases presenting on the Ca-based oxide catalysts towards phase transformation *via* a strong chemisorption of methanol and glycerol by-product, direct reaction of CaO-800 and CaMgO-800 with methanol or glycerol was studied. The reaction was performed in a 100-mL round bottom flask equipped with a water-cooled condenser and a magnetic stirrer. The reaction temperature was controlled at 60±0.5 °C using a water bath equipped with a PID controlled electronic thermometer. The calcined catalysts (1.50 g) were vigorously stirred with methanol (17.1 g) or a glycerol solution, prepared by dissolving 5.0 g of glycerol in 22.0 g of methanol, for different reaction periods (10–120 min). The resulting solid products were recovered by centrifugation at 7000 rpm. The samples obtained were analyzed for their structural properties without prior washing.



### 3.7 Reusability of Ca-based oxide, Ca-based methoxide and Ca-based glyceroxide catalysts

The reusability of the Ca-based methoxide and glyceroxide catalysts in the transesterification of RBD palm oil with methanol was investigated to reveal their catalytic stability. After a 2-h transesterification reaction, the catalysts were recovered by centrifugation at 7000 rpm. The spent catalysts were subsequently used in the next run without washing step. The reusability of the catalysts was tested for five repetitions under the suitable conditions at 60 °C, catalyst loading of 10 wt% and methanol: oil molar ratio of 30: 1 and reaction time of 2 h. The composition of FAME and glycerides was analyzed using an Agilent 7890A gas chromatograph (*See* Section 3.5). Moreover, the structural change of the spent catalysts was investigated using the XRD technique.

### 3.8 Structural stability of the catalysts in ambient air

Moisture and carbon dioxide ($CO_2$) preventing in ambient air are harmful to basic catalysts due to a strong chemisorption ion on the basic sites. To reveal the structural stability of the Ca-based oxide, Ca-based methoxide and Ca-based glyceroxide catalysts against the chemisorption of atmospheric moisture and $CO_2$, the freshly prepared catalysts were exposed to ambient air (RH ≈ 73%) at different exposure conditions at (i) 60 °C for 2 h, and (ii) room temperature for 2 h, 10 d and 42 d. After that, the resulting catalysts were analyzed for their structure change by XRD technique.

### 3.9 Miscibility test of methanol–oil–CME system

The miscibility test was carried out to verify effect of CME addition on solubility of methanol–triglycerides mixture. Methanol, RBD palm kernel oil, and $C_{12}$–$C_{14}$ CMEs were used in the miscibility test. All three components were mixed at different volume ratios, while the total volume was maintained at 10 mL. After vigorously stirring at room temperature for 1 h, the mixture was left for 1 h, and the phase formed was recorded as a miscible phase, an emulsion, or separate phases. The results obtained were presented as a three-phase diagram.

### 3.10 Premixing of ZSAH-400 extrudate with methanol, palm kernel oil, or CMEs

Methanol, RBD palm kernel oil, and CMEs with different fatty acid compositions were premixed with the catalyst extrudate to study the effects of adsorption of these substances by the extrudate on the transesterification of RBD palm oil with methanol. After calcination and cooling to room temperature in a desiccator, the ZSAH-400 extrudate was immersed in methanol, palm kernel oil, or CMEs at a solid: liquid mass ratio of 70:30 and stored at room temperature overnight. The saturated ZSAH-400 extrudates were then packed into the glass reactor, and transesterification was performed using the procedure described in Section 3.4.2, but without filling the reactor with methanol during the start-up period. When $C_8$–$C_{10}$ and $C_{12}$–$C_{14}$ CMEs were used in the premixing, the yields of FAMEs obtained from the reaction were unambiguously determined because the palm oil mainly consisted of $C_{16}$ and $C_{18}$ fatty acids. However, for premixing with $C_{16}$–$C_{18}$ CMEs, the total amount of FAME determined by GC was directly subtracted by the amount of CME used prior to calculation of the FAME yield.

## 3.11 Material characterization procedure

### 3.11.1 X-ray diffraction (XRD)

The crystalline structure of the raw materials and the resulting catalysts was determined by powder X-ray diffraction (XRD) using a Bruker D8 Discover X-ray diffractometer equipped with a Cu Kα radiation (λ = 1.54 Å), which was operated at 40 V and 40 mA (Figure 3.7). The XRD patterns were recorded in a 2$\theta$ range of 5–80 degree with a 0.02 degree step size range and a count time of 1 sec at room temperature. The results are shown in term of XRD pattern that plot between the angle 2$\theta$ and signal count (count per second, cps). The diffraction peaks were assigned after consulting the Joint Committee on Powder Diffraction Standards (JCPDS) powder diffraction files (PDFs). The resulting catalysts were crushed to fine powders before analysis.

**Figure 3.7** Bruker D8 Discover X-ray diffractometer.



Moreover, the data from XRD pattern can be used to calculate a cluster size by using Scherrer's equation, as showed in Eq. (3.3). The examples and main peak used to calculate of cluster size were demonstrated in Appendix C.

$$\Gamma = \frac{K\lambda}{\beta\cos\theta} \tag{3.3}$$

where
$\Gamma$ = Crystallite size, Å
$\lambda$ = X-ray wavelength, Å
K = Shape factor (in case of cubic, K = 0.94)
$\beta$ = Full width at half maximum (FHHM), radian
$\theta$ = Angle between X-ray beam and crystal planes (degree)

### 3.11.2 X-ray fluorescence spectroscopy (XRF)

The elemental composition of the raw materials and the resulting catalysts was determined by X-ray fluorescence spectroscopy (XRF) using an Oxford ED-2000 X-ray fluorescence spectrometer at the Scientific and Technological Research Equipment Centre of Chulalongkorn University (Figure 3.8).

**Figure 3.8** Oxford ED-2000 X-ray fluorescence spectrometer**.**

### 3.11.3 X-ray photoelectron spectroscopy (XPS)

The raw materials and the resulting catalysts were analyzed for their surface elemental composition using X-ray photoelectron spectroscopy (XPS). The XPS spectra were recorded on a Kratos Axis Ultra DLD X-ray photoelectron spectrometer with a monochromatic Al Kα X-ray source (1486.6 eV) operated at 15 kV and 10 mA (Figure 3.9). Binding energy (B.E.) scale was calibrated by using the C 1s peak energy of adventitious carbon at 284.6 eV. The OriginPro 8.5 program was applied to the deconvolution of XPS spectra obtained.

**Figure 3.9** Kratos Axis Ultra DLD X-ray photoelectron spectrometer.

### 3.11.4 Thermo gravimetric/ differential thermal analysis (TG/DTA)

The weight loss (TG) and derivative thermogravimetric (DTG) curves of the raw materials and the resulting catalysts were determined by a PerkinElmer Diamond thermogravimeter (Figure 3.10). The sample weight (≈10 mg) was loaded into alumina pan and put on the microbalance and followed by heating from room temperature to 900 °C at a ramp rate of 8 °C $min^{-1}$ under a dry nitrogen ($N_2$) flow (50 mL $min^{-1}$). When the temperature of the sample is increased, the transition of the weight of a sample compared with the referent pan is continuously recorded. Moreover, the OriginPro 8.5 program was applied to the deconvolution of DTG peaks obtained in order to separate the range of decomposition temperature of the samples.


**Figure 3.10** Perkin Elmer Pyris Diamond thermogravimetric/differential thermal analyzer.

### 3.11.5 $N_2$ physisorption measurement

The textural properties of materials and the resulting catalysts were measured by $N_2$ physisorption using a Micromeritics ASAP 2020 surface area and porosity analyzer (Figure 3.11). The adsorption and desorption were performed at -196 °C using liquid $N_2$. The samples (≈80 mg) were pretreated in vacuum at 300 °C for 2 h, then accurately weighed before being analyzed. In the case of samples composed of methoxide or glyceroxide, the pretreat temperature was reduced to 120 °C for 2 h. The specific surface area ($S_{BET}$) was calculated by the Brunauer-Emmett-Teller (BET) equation using the adsorption data in the relative pressure ($P/P_0$) range of 0.02–0.2. The total pore volume ($V_t$) was obtained from the accumulative volume of $N_2$ adsorbed at a $P/P_0$ of about 0.990. The total pore volume ($V_p$) was calculated from the slope of linear portion of the t-plot in the relative pressure range above which $N_2$ was condensed inside the primary mesopores.


**Figure 3.11** Micromeritic ASAP 2020 surface area and porosity analyzer.

### 3.11.6 Optical microscopy (OM)

The morphology of raw material and resulting catalysts was preliminary measured by optical microscopy (OM) using an Olympus light microscope (Figure 3.12). The snap-shot images were analyzed using the S-viewer program.

**Figure 3.12** Olympus light microscope.

### 3.11.7 Scanning electron microscopy (SEM)

Scanning electron microscopy (SEM) is used to study the morphology of raw material and resulting catalysts. The SEM images were recorded on a JEOL JSM-5410 LV scanning electron microscope using a 15 kV electron beam with a magnification of 15–35000× at the Scientific and Technological Research Equipment Centre of Chulalongkorn University (Figure 3.13). The sample was sputter-coated with gold before the observation in order to improve the signal/noise ratio for samples of low atomic number.

**Figure 3.13** JEOL JSM-5410 LV scanning electron microscope.

### 3.11.7 Temperature-programmed desorption of $CO_2$ ($CO_2$-TPD)

To determine the basic amount and basic strength of the catalysts, temperature-programmed desorption of $CO_2$ ($CO_2$-TPD) was applied using a Micromeritics AutoChemII 2920 chemisorption analyzer. The calcined catalysts (≈0.06 g) were added into U-tube terminated with a layer of quartz wool. The catalysts were again pretreated at 800 °C for 1 h under helium (He) flow (50 mL $min^{-1}$). After the temperature was reduced to 100 °C, the $CO_2$ (10 vol% in He) was performed at 100 °C. The $CO_2$ physisorbed on the catalyst surface was purged with He flow (20 mL $min^{-1}$) at the same temperature for 30 min. The temperature was then increased to 900 °C at 10 °C $min^{-1}$ for desorbing $CO_2$.

### 3.11.8 $CO_2$ pulse chemisorption ($CO_2$-pulse)

The basic amount of the catalysts was investigated by the $CO_2$- pulse chemisorption measurement using a Micromeritics AutoChem II 2920 chemisorption analyzer (Figure 3.14). The samples were pretreated *in situ* at 200 °C for 1 h under an He flow (50 mL $min^{-1}$), after which the temperature was reduced to 120 °C. Then, the $CO_2$ (10 vol% in He) were released and injected on catalyst surface. The volume of the pulse injector is 0.04135 $cm^3$. The injection was repeated until $CO_2$ adsorption reached saturation. The amount of basic sites was determined from the accumulated amount of $CO_2$ that disappeared in each step, measured using a thermal conductivity detector (TCD).


**Figure 3.14** Micromeritics AutoChemII 2920 Chemisorption analyzer.

### 3.11.9 Crushing strengths

The catalyst extrudates in a fixed-bed reactor were used to solve of reactor blockage and pressure drop. However, the catalyst extrudates necessarily had enough strength during the reaction procedure. Therefore, mechanical properties of the extrudates were used to determine the strength of catalyst extrudates by crushing strength method by using an ASTM International-Standards (ASTM D-4179-82, 1988). The standards were determined by simply crushing a several particles or single particle representative of the lot between parallel plates of a device capable of exerting compressive stress, while recording the force mandatory to crush the material. In the procedure, the extrudate sample (≈15 g) was placed in a sample holder in order to compress by mobile piston at an initial force of 100 N. The applied force was increased stepwise to 200, 400, and 1000 N until the extrudates obtained force transform to powder. The powder was sieved and recorded the weight loss, which 0.5 wt% catalyst was determined quantitatively as a limit for the sieving.

# CHAPTER IV
# Nature of active sites presenting in metal oxides derived from calcite and dolomite for synthesis of fatty acid methyl esters

In this chapter, heterogeneous base catalysts obtained from calcite and dolomite were used in the transesterification of palm oil with methanol at 60 °C and ambient pressure. As described in Section 3.3.1, calcite and dolomite were calcined at different temperatures and heating rates. Moreover, calcite and magnesite at the same $CaCO_3$: $MgCO_3$ mass ratio as the raw dolomite was used to prepare a physically mixed CaO and MgO catalyst (CaO+MgO). Moreover, the direct reaction of the catalysts with methanol or glycerol was studied to reveal the reactivity of active phases *via* a strong chemisorption of methanol and glycerol.

## 4.1 Evolution of MgO in the calcined dolomite

**Table 4.1** Elemental composition of natural calcite and dolomite as analyzed by XRF spectroscopy

| Material | Composition (wt%) | | | | | |
|---|---|---|---|---|---|---|
| | CaO | MgO | $Al_2O_3$ | $SiO_2$ | $CO_2$ balance | Total[a] |
| Calcite | 54.6 | 2.0 | 0.3 | 5.7 | 36.3 | 99.1 |
| Dolomite | 31.7 | 21.6 | 0.2 | 0.1 | 40.9 | 99.7 |

[a] The rest was other metals such as $P_2O_5$, $SO_3$, $K_2O$, $MnO_2$, SrO and $ZrO_2$ etc.

From the XRF analysis, the as-received calcite was composed of CaO (54.6 wt%) as the main oxide phase, whilst CaO (31.7 wt%) and MgO (21.6 wt%) were present in the raw dolomite, as summarized in the Table 4.1. The XRD patterns of the calcium-based catalysts obtained at different calcination temperatures are compared in Figure 4.1. The raw calcite and dolomite were characterized as high purity calcitic and dolomitic phases, corresponding to $CaCO_3$ (PDF: 01-083-1762) and $CaMg(CO_3)_2$ (PDF: 00-005-0622), respectively. The complete conversion of the carbonate phases to the metal oxides required the temperatures above 800 °C.

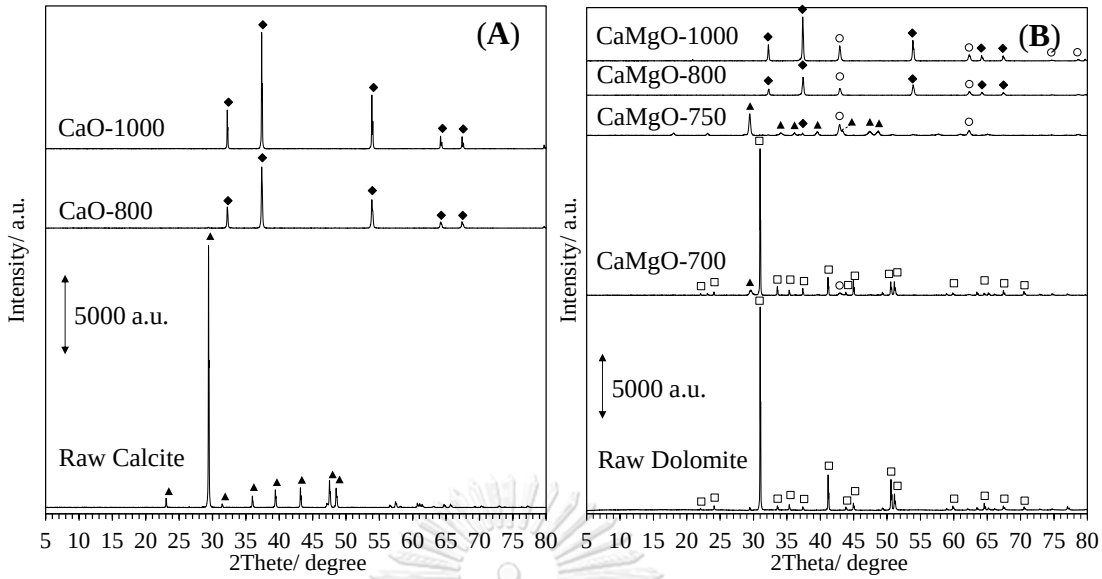


**Figure 4.1** XRD patterns of (A) calcite and (B) dolomite before and after calcination at different temperatures for 3 h using a heating rate of 3 °C $min^{-1}$. (Symbol: ▲ = $CaCO_3$, ◆ = CaO, □ = $CaMg(CO_3)_2$ and ○ = MgO).

**Table 4.2** Effect of the calcination temperatures of calcite and dolomite on the cluster size and transesterification activity of the resulting catalysts

| Catalyst[a] | Cluster size[b] (nm) | | | | Initial rate[c] | FAME yield[d] |
|---|---|---|---|---|---|---|
| | $CaCO_3$ | $CaMg(CO_3)_2$ | CaO | MgO | | |
| Calcite | 103.4 | - | - | - | *n.d.*[e] | *n.d.* |
| CaO-800 | - | - | 45.2 | - | 61.4 | 99.9 |
| CaO-1000 | - | - | 108.2 | - | 52.4 | 82.6 |
| Dolomite | - | 118.0 | - | - | *n.d.*[e] | *n.d.*[e] |
| CaMgO-650[f] | 44.6 | 25.7 | - | 18.2 | 0.2 | 0.6 |
| CaMgO-700 | 22.6 | 113.2 | - | 14.5 | 11.2 | 18.5 |
| CaMgO-750 | 32.9 | - | 18.6 | 22.4 | 22.1 | 99.5 |
| CaMgO-800 | - | - | 38.1 | 29.1 | 32.9 | 99.9 |
| CaMgO-1000 | - | - | 50.1 | 35.8 | 31.7 | 99.7 |

[a] Catalysts were calcined in muffle furnace using a heating rate of 3 °C $min^{-1}$ for 3 h.
[b] Calculated from the XRD results using Sherrer's equation.
[c] Determined at 5 min of the reaction. ($g_{FAME}$ $g^{-1}_{cat}$. $h^{-1}$)
[d] Reaction conditions: catalyst amount, 10 wt%; palm oil amount, 10 g; methanol: oil molar ratio, 30: 1; temperature, 60 °C; time, 60 min. (wt%)
[e] *n.d.* means not determined.
[f] Calcined using a heating rate of 1 °C $min^{-1}$ for 3 h.

As shown in Table 4.2, the cluster size of CaO in the calcite series was increased by 139 % from 45.2 nm to 108 nm when increasing the calcination temperature from 800 to 1000 °C. A similar trend was also observed for the dolomite series. However, the difference in the crystal size only 31.5% CaMgO-800 and CaMgO-1000 exhibited respectively 15.7% and 53.7% smaller CaO clusters than the calcites calcined at the same temperatures. The result confirmed that the MgO presenting in the calcined dolomite retarded the agglomeration of CaO phase to larger crystallites [6].

Figure 4.2 shows weight loss and DTG curve of raw calcite and dolomite. The decomposition of dolomitic $CaMg(CO_3)_2$ phase to the corresponding mixed oxides is a multi-stage decarbonation process, and several models for the dolomite decomposition were proposed [43, 44]. The OriginPro 8.5 program was applied to the deconvolution of DTG peaks obtained from the dolomite (insets in Figure 4.2 (B)). The decomposition of dolomite at 673 °C was ascribed the decarbonation of $MgCO_3$ to MgO as reported by Demir *et al.* [71]. From this result, it was possible to obtain the calcined dolomites with different metal phases *via* controlled calcination conditions. Then, the three-step decomposition obtained from deconvoluted peaks of dolomite at temperatures between 650 and 800 °C were similar to those of calcite explained by term of shrinking process and recarbonation rate [72]. The weight loss at 743 °C was related to the decarbonation on particle surface concomitantly with the formation of $CaCO_3$ shrinking core. The decomposition at 763 °C was related to the decarbonation on $CaCO_3$ core. The final weight loss at 782 °C was due to decarbonation of recarbonated CaO with $CO_2$. Due to large particle site of dolomite, the decomposition temperatures observed from dolomite were slightly more than that from calcite.

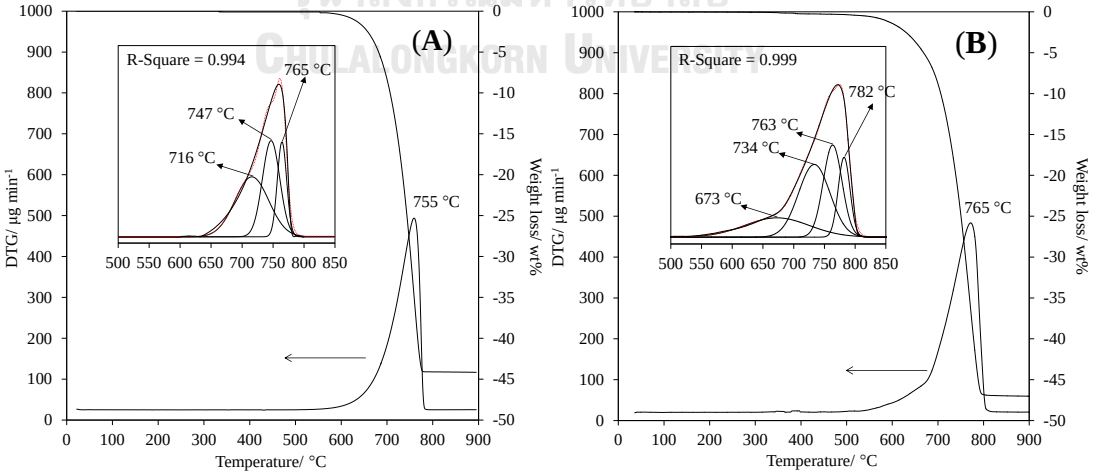


**Figure 4.2** Weight loss and DTG curves of (A) calcite and (B) dolomite.

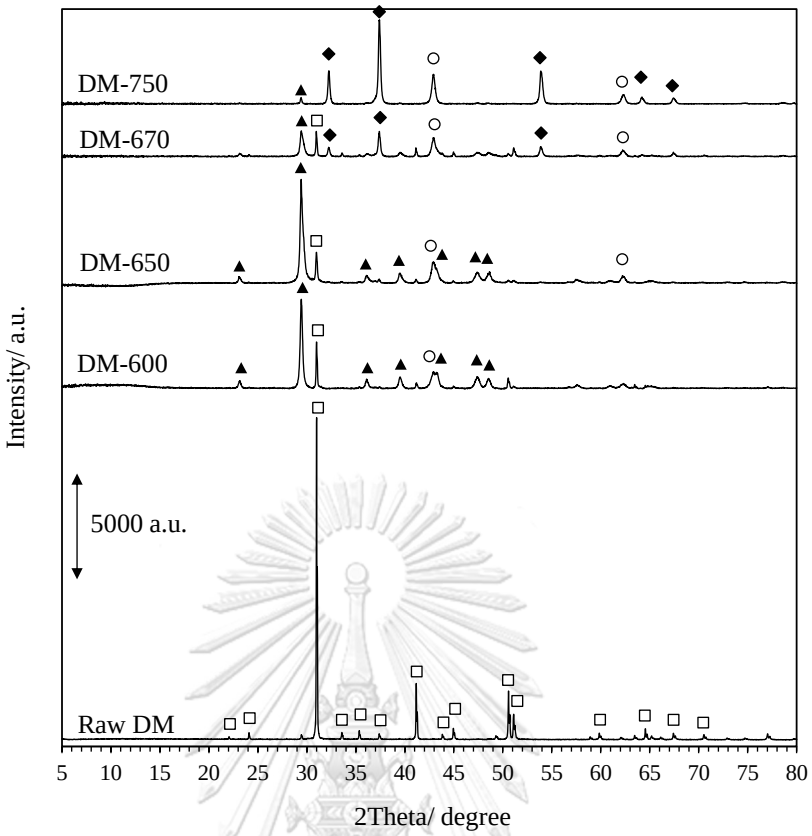


**Figure 4.3** XRD patterns of dolomite calcined at different calcination temperatures using heating rate of 1 °C $min^{-1}$ for 5 h. (Symbol: ▲ = $CaCO_3$, ◆ = CaO, □ = $CaMg(CO_3)_2$ and ○ = MgO)).

Effect of calcination condition (temperature and heating rate) on the evolution of metal oxides derived from dolomite was invested by XRD. At 600–650 °C and 1 °C $min^{-1}$, $CaMg(CO_3)_2$ were substantially decomposed to $CaCO_3$ and MgO (Figure 4.3), while CaMgO-700 (3 °C $min^{-1}$) was consisted of $CaMg(CO_3)_2$ as a main phase (Figure 4.1 (B)). It was related to the time required for heat transfer from the external surface into interior particles, whereas $CO_2$ was released and diffused in the opposite direction. A majority of CaO was generated from $CaCO_3$ at higher temperatures. Milodowski and Morgan proposed that $CaMg(CO_3)_2$ was dissociated into two carbonates, followed by decarbonation of $MgCO_3$ to MgO according to Eq. (4.1) [73]. Since $MgCO_3$ was not observed by XRD even at low heating rate, a direct conversion of dolomite to $CaCO_3$ and MgO was described our result (Eq. (4.2)). Finally, MgO and CaO are simultaneously produced when the decomposition temperature was higher than of decarbonation of calcite according to Eq. (4.3). Calcining dolomite at 750 °C and 3 °C $min^{-1}$ (CaMgO-750) produced a new catalyst, probably in form of $CaCO_3$-supported MgO with a trace amount of CaO (Figure 4.1).

$$CaMg(CO_3)_2 \rightarrow CaCO_3 + MgCO_3 \rightarrow CaCO_3 + MgO + CO_2 \quad (4.1)$$

$$CaMg(CO_3)_2 \rightarrow CaCO_3 + MgO + CO_2 \quad (4.2)$$

$$CaMg(CO_3)_2 \rightarrow CaO + MgO + 2CO_2 \quad (4.3)$$

**4.2 Effect of MgO in the calcined dolomite on the catalytic activity**

The calcite and dolomite catalysts obtained at different calcination temperatures were investigated for their activity in the transesterification of palm oil with methanol (Table 4.2). The reactions catalyzed by CaMgO-650 (rate 1 °C $min^{-1}$) and CaMgO-700 (rate 3 °C $min^{-1}$), both of which had the MgO nanocrystallites as the main oxide phase, gave very low FAME yield. The catalytic activity of dolomite was insignificantly affected by high calcination temperatures: CaMgO-800 and CaMgO-1000 exhibited a comparable initial rate and FAME yield. CaO-800 had the highest initial rate of the FAME production (61.4 $g_{FAME}$ $g^{-1}_{cat.}$ $h^{-1}$) and promoted the FAME yield to 99.9% within 60 min. The initial rate and the FAME yield were decreased by 14.6% and 17.3%, respectively, when the calcination was performed at 1,000 °C (CaO-1000). It was attributed to an enlarged cluster size of CaO, which essentially reduced the specific surface area and the total amount of basic sites. The evolution of small crystallize CaO (CaMgO-750 rate 3) enhanced the reaction. The results indicated that CaO was the catalytically active sites responsible for the transesterification over the calcined dolomite, and the presence of MgO as mixed Ca and Mg oxides maintained not only the crystallite size but also the activity of CaO phase.

To confirm this conclusion, the catalytic activity of (CaO+MgO)-800 and MgO-800 was comparatively studied with that of CaO-800 and CaMgO-800 (Figure 4.4). It can be seen that the MgO-800 derived from magnesite was not active under this condition. When the reaction was used in severe conditions, such as, high temperature, high methanol: oil molar ratio or assisting with microwave or ultrasound, the MgO can provide a high FAME conversion [46]. However, nanocrystalline MgO prepared *via* sol-gel process can be active under mild condition, which it possessed high surface area and basic site obtained from isolate $O^{2-}$ generated by (111) plane as a defect of MgO nano-sheets edge [46]. Although (CaO+MgO)-800 gave 99.9 wt% FAME yield within 30 min, the initial rate of reaction was ranked in this descending order: CaO-800 (61.4 $g_{FAME}$ $g^{-1}_{cat.}$ $h^{-1}$) > CaMgO-800 (32.9 $g_{FAME}$ $g^{-1}_{cat.}$ $h^{-1}$) > (CaO+MgO)-800 (11.4 $g_{FAME}$ $g^{-1}_{cat.}$ $h^{-1}$). The result indicated that the reaction rate was primarily determined by the content of CaO in the catalysts, which was in accord with our previous work [6]. Nevertheless, both CaMgO-800 and (CaO+MgO)-800 had a similar metal composition. The difference in their activities should be accounted for

by the smaller crystallite sizes of CaO in the calcined dolomite, as well as the chemical nature of CaO phase presenting in different environments.

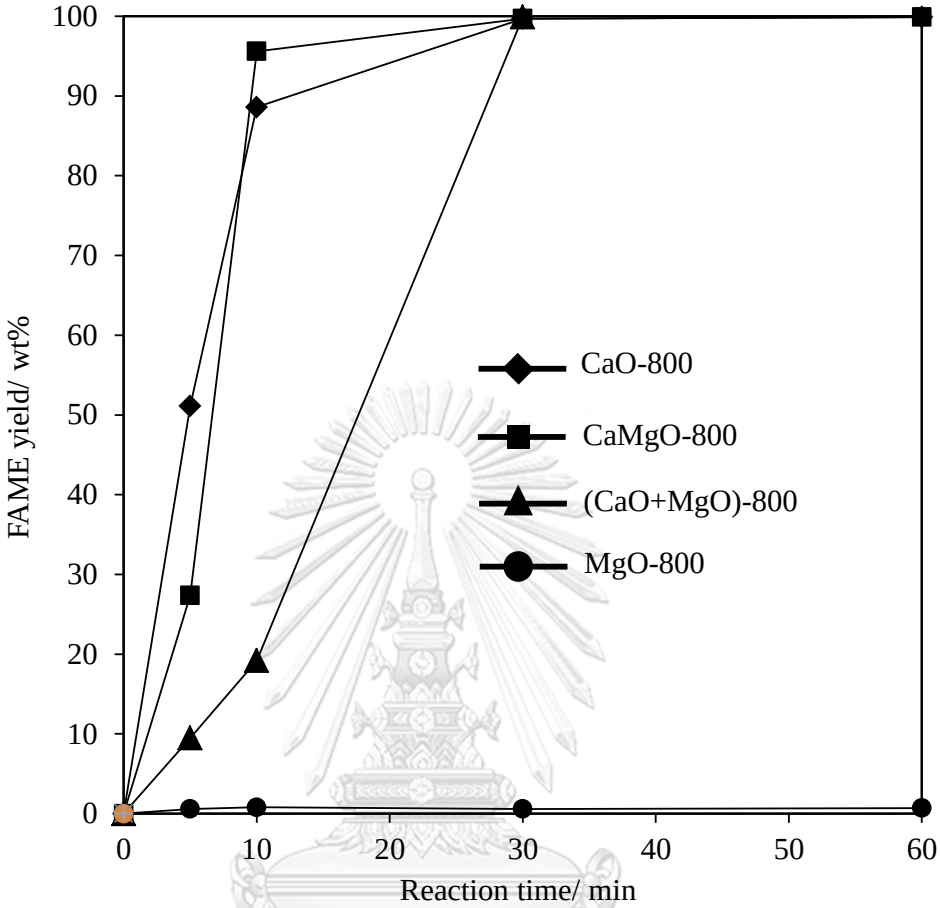


**Figure 4.4** Dependence of FAME yield on time over (◆) CaO-800, (■) CaMgO-800, (▲) (CaO+MgO)-800 and (●) MgO-800 in the transesterification of RBD palm oil with methanol. Reaction conditions: catalyst amount, 10 wt%; methanol: oil molar ratio, 30: 1; temperature, 60 °C.



### 4.3 Morphological and chemical properties of CaO-800 and CaMgO-800

The SEM images of the CaO-800 (Figure 4.5 (A–B)) exhibited agglomerates of particles with sizes (≈68 μm) bigger than those in the CaMgO-800 (≈67 nm) (Figure 4.5 (D)). The MgO presenting in the CaMgO-800 prevented the sintering of CaO crystallites since the melting point of MgO (2852 °C) is higher than that for CaO (2613 °C) [6]. A similar morphology was previously observed in mixed metal oxide of CaO and ZnO [53]. These results suggested that CaO and MgO particles should be very close or MgO was inserted into CaO cluster.

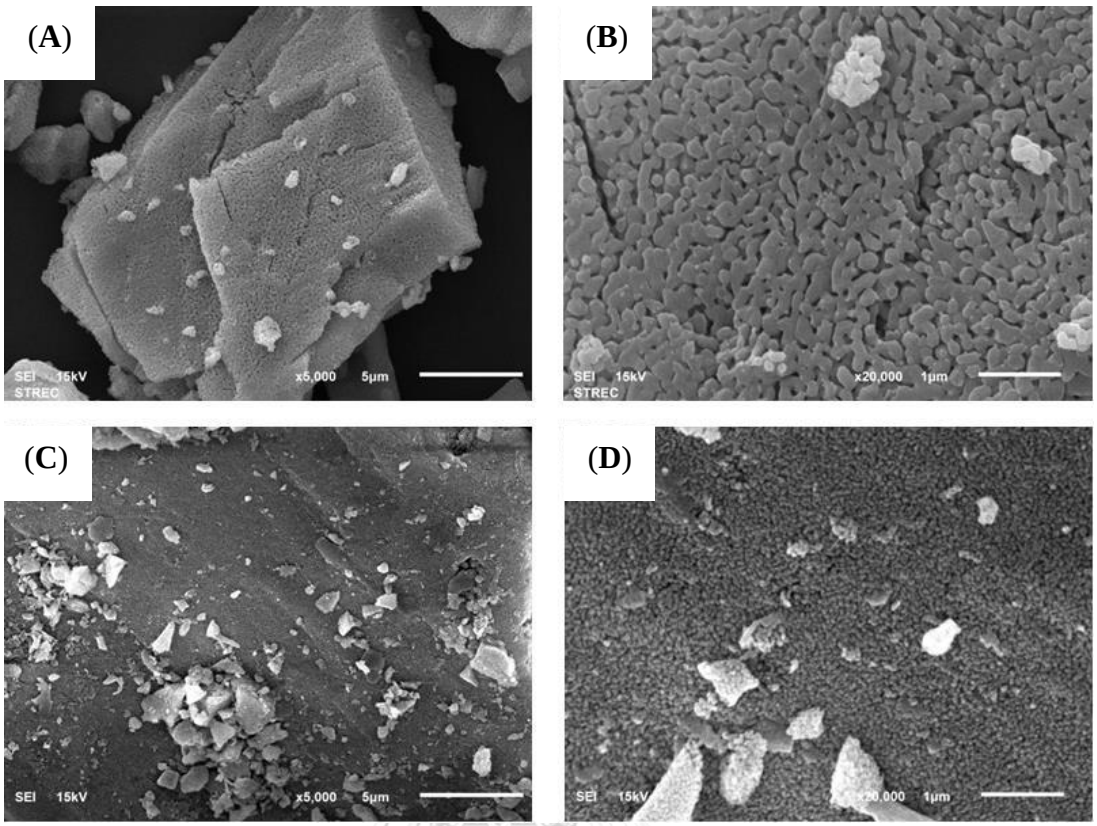


**Figure 4.5** SEM images of (A and B) CaO-800 and (C and D) CaMgO-800 at magnifications of (A and C) 5000× and (B and C) 20000×.

The textural properties and elemental composition of each sample are summarized in Table 4.3. Although the particle of CaMgO-800 was very smaller than that of the CaO-800, the surface area of CaMgO-800 (15.0 $m^2$ $g^{-1}$) was not significantly different with CaO-800 (17.5 $m^2$ $g^{-1}$). It should be due to initial surface area of raw calcite (7.2 $m^2$ $g^{-1}$) higher than that of raw dolomite (3.4 $m^2$ $g^{-1}$). When calcite was calcined at 800 °C, calcium content of CaO-800 in bulk and surface was increased due to decomposition of $CO_2$. When compared the bulk and surface composition of CaMgO-800, the Mg: Ca ratios in bulk (0.45) is about 2-fold lower than that in surface (1.00). During the transition from the mixed carbonates to mixed oxides, the growth of MgO was formed on external surface on internal growth of $CaCO_3$ [43, 44, 73]. The calcined dolomite possessed magnesium-rich surface when compared to its bulk composition.

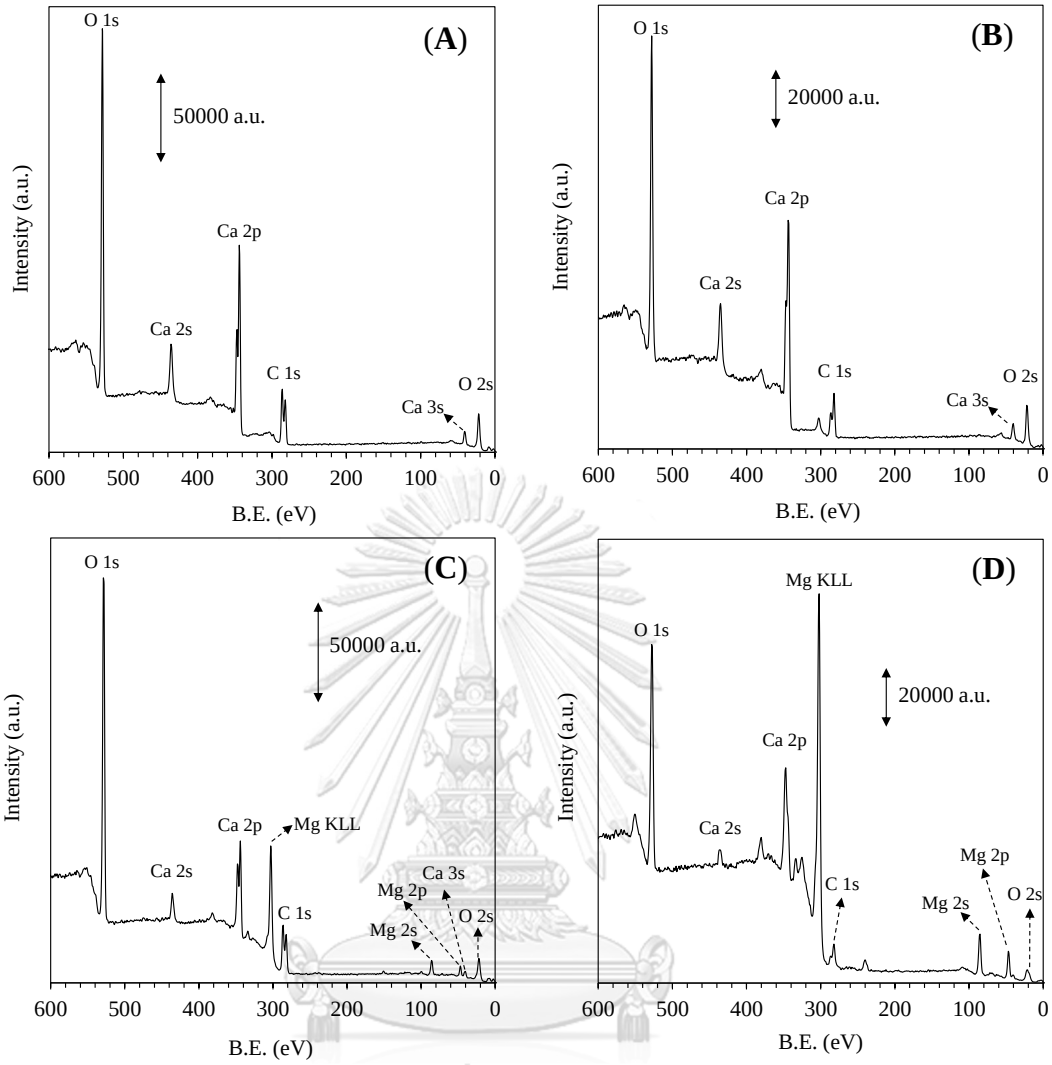


**Figure 4.6** Wide scans XPS spectra of (A) calcite, (B) CaO-800, (C) dolomite, and (D) CaMgO-800.

**Table 4.3** Elemental composition and textural properties of calcite and dolomite before and after calcination at 800 °C

| Catalyst | Bulk composition[a] (wt%) | | | Surface composition[b] (wt%) | | | $S_{BET}$[c] ($m^2$ $g^{-1}$) | $V_p$[d] ($cm^3$ $g^{-1}$) | $D_p$[e] (Å) | Basic properties[f] | |
|---|---|---|---|---|---|---|---|---|---|---|---|
| | | | | | | | | | | Temp. desorbed (°C) | Amount (μmol $g^{-1}$) |
| | Ca | Mg | Mg: Ca | Ca | Mg | Mg: Ca | | | | | |
| Calcite | 39.2 | - | - | 17.5 | - | - | 7.2 | 0.0065 | 37.6 | *n.d.*[g] | *n.d.* |
| CaO-800 | 70.0 | - | - | 25.2 | - | - | 17.5 | 0.0293 | 75.0 | 558.1 | 470 |
| Dolomite | 18.0 | 1.9 | 0.43 | 24.8 | 4.6 | 0.30 | 3.4 | 0.0009 | 23.8 | *n.d.* | *n.d.* |
| CaMgO-800 | 39.9 | 4.6 | 0.45 | 24.9 | 14.8 | 1.00 | 15.0 | 0.0242 | 116.4 | 563.1 | 370 |

[a] Determined by XRF technique.
[b] Determined by XPS (Figure 4.6).
[c] BET surface area
[d] Total pore volume
[e] Average pore size
[f] Determined by $CO_2$-TPD (*see* Figure 4.7)
[g] *n.d.* means not determined.

The $CO_2$-TPD profiles obtained from the CaO-800 and CaMgO-800 exhibited multiple peaks deconvoluted by using an Origin 8.5 program (Figure 4.7), and the total basic amounts are summarized in Table 4.3. The deconvoluted peaks of $CO_2$ desorbed from CaO-800 and CaMgO-800 consist of three peaks. This result suggested that the active phase of both catalysts was CaO. The basic amount of CaO-800 (470 μmol $g^{-1}$) is about 21.2% higher than that of CaMgO-800 (370 μmol $g^{-1}$). It wrote to note that calcium content of CaO-800 is about 41.9% higher than that of CaMgO-800 (Table 4.1).

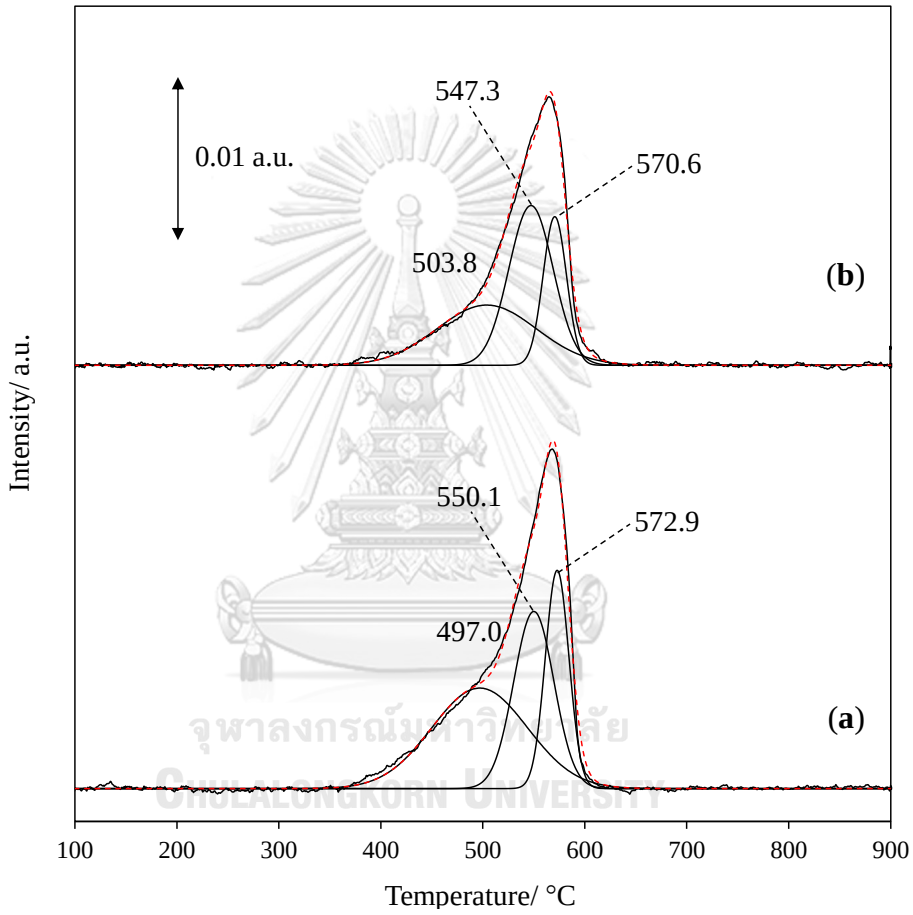


**Figure 4.7** $CO_2$-TPD profiles for (a) CaO-800 and (b) CaMgO-800.

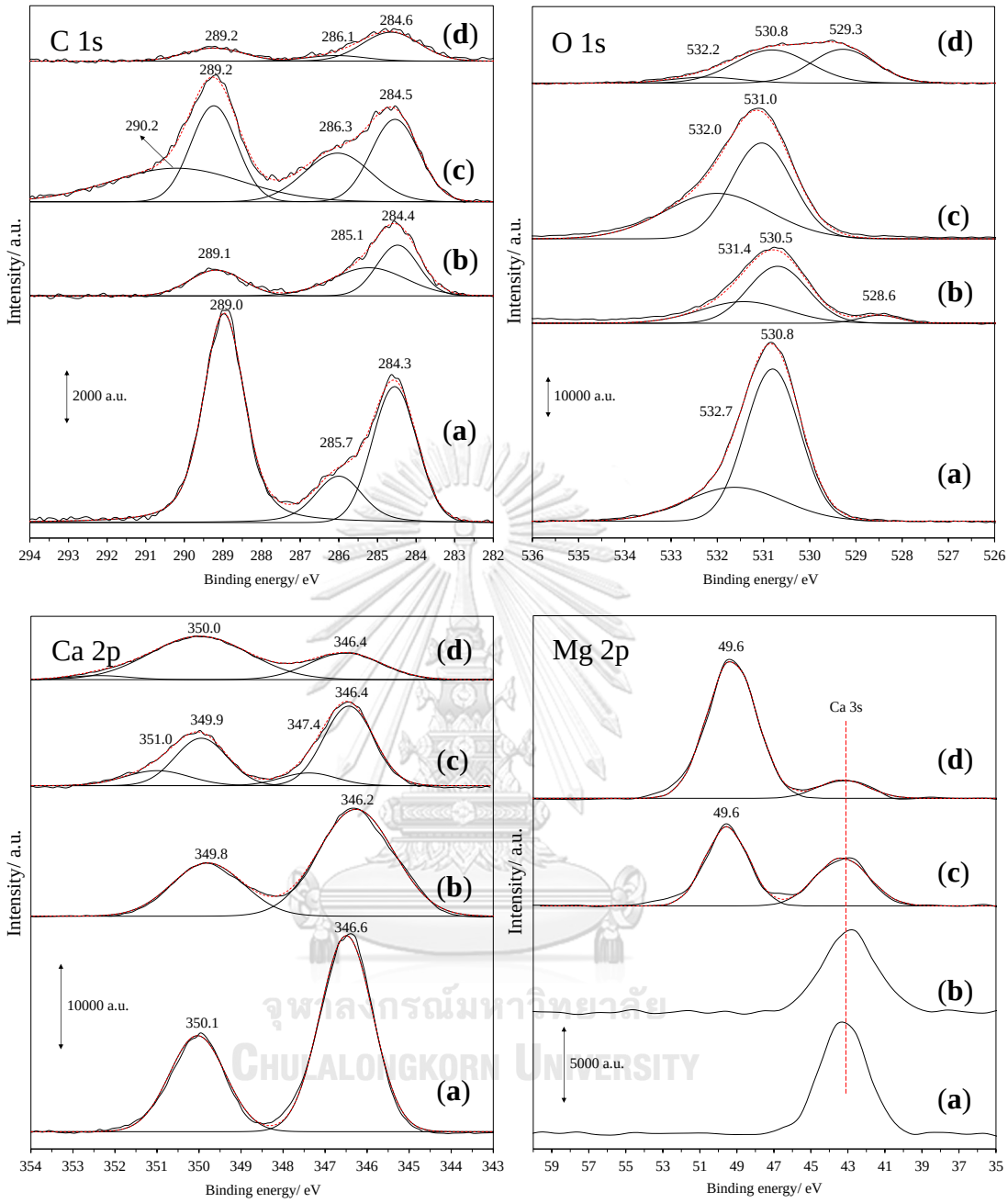


**Figure 4.8** HR-XPS spectra of (a) calcite, (b) CaO-800, (c) dolomite and (d) CaMgO-800 in different binding energy regions.

Figure 4.8 shows the high resolution XPS (HR-XPS) spectrum in the C1s, O1s and Ca2p regions. The peak of surface carbonate from calcite was found at 289.0 eV corresponded to the oxygen from the carbonate (Figure 4.8 (C 1s) (a)), while the dolomite had two peaks deconvoluted at 289.2 eV and 290.2 eV (Figure 4.8 (C 1s) (b)). It should be because the dolomite composed of mixed $CaCO_3$ and $MgCO_3$. After calcination, the C 1s carbonate of CaO-800 (289.1 eV) and CaMgO-800 (289.2 eV) were slightly found (Figure 4.8 (C 1s) (c) and (d)). The results suggested that the

oxide active sites of the both catalysts were rapidly reacted with $CO_2$ during air exposure during XPS analysis.

The O 1s spectrums were assigned to be into four step of the $O^{2-}$ bonds from metal oxide (≈528.5 eV), the signals overlapped between $OH^-$ and $CO_3^{2-}$ (≈530.5 eV) and the signals overlapped between $O^-$ and $H_2O$ (≈532.0 eV) [74-76] as shown in Figure 4.8 (O 1s). According to Wilson et al., the binding energy of $CO_3^{2-}$ was slightly higher than that of $OH^-$ (ΔE = 0.2 eV) [47]. The spectrums of calcite and dolomite were assigned to be $CO_3^{2-}$ and $H_2O$ obtained from moisture on surface. After calcination, the signals assigned as $O_2^{2-}$ was slightly shifted to low binding energy assigned to be $OH^-$ (ΔE = 0.3 eV for CaO-800, and ΔE = 0.2 eV for CaMgO-800). The small signal of $O^{2-}$ (at 528.6 eV) was obtained from CaO-800, while CaMgO-800 had large signal in the range from 527 to 350 eV. Compared with MgO result (Figure 4.9), the deconvolute peaks between CaMgO-800 and MgO were completely matched. This result indicated that MgO was less active than CaO. Other explanation is the $O_2^{2-}$ was protected by MgO particles.

The Ca 2p spectrum consists of spin orbital doublet of Ca $2p^{3/2}$ around ≈346.4 eV and Ca $2p^{1/2}$ around ≈350.0 eV, respectively (Figure 4.8 (Ca 2p)). From previous reports, the energy difference (ΔE) between the Ca $2p^{3/2}$ and Ca $2p^{1/2}$ peak positions is around 3.5 eV [77, 78] The Ca $2p^{3/2}$ (350.1 eV) and Ca $2p^{1/2}$ (346.6 eV) peak from the calcite had ΔE of 3.4 eV, corresponded to structure of $CaCO_3$. The ΔE from the CaO-800 was 3.6 eV, assigned to oxygen bonded with calcium. The dolomite gave peak deconvuluted at 346.4 eV (Ca $2p^{1/2}$) and 349.9 eV (Ca $2p^{3/2}$), assigned to calcium bonded with carbonate (ΔE = 3.5 eV). Moreover, both small peak deconvuluted at 347.4 eV (Ca $2p^{1/2}$) and 351.0 eV (Ca $2p^{3/2}$) should be assigned to calcium bonded with magnesium (ΔE = 3.6 eV). It worth to note that peak area of Ca $2p^{3/2}$ was larger than that of Ca $2p^{1/2}$ after calcination at 800 °C (CaMgO-800). It should be due to disturbing of spin orbital doublet of Ca by MgO diffused on surface [79]. In the case of Mg 2p spectrum, dolomite and CaMgO-800 were similarly appeared at 49.6 eV (Figure 4.8 (Mg 2p)), which was matched from pure MgO found at 49.6 eV (Figure 4.9). Thus, Mg 2p spectrum in MgO was stable than Ca 2p spectrum, which calcium conjugated with oxygen could be caused to surface interaction.

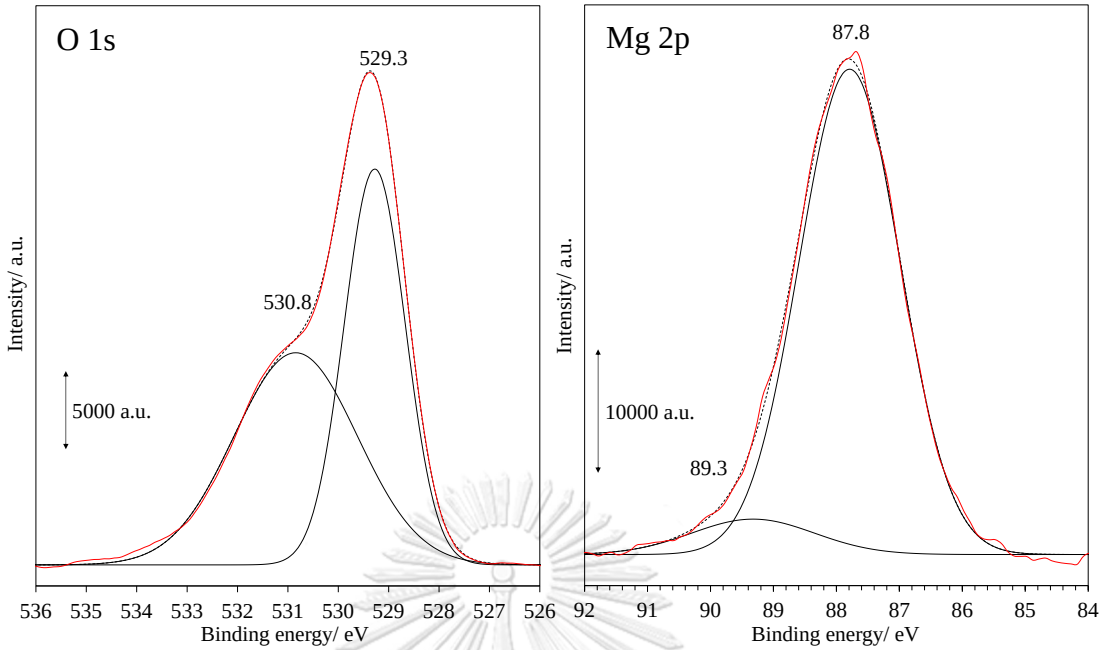


**Figure 4.9** HR-XPS spectra of MgO in different regions.

### 4.4 Direct reaction of CaO-800 and CaMgO-800 catalysts

The reaction between triglycerides and methanol on the catalyst surface occurred *via* the Eley–Rideal mechanism. The methanol molecules are activated on the basic sites of the catalyst to form methoxide species [80]. Therefore, surface methoxide generated can be used to represent the activity of catalyst in transterification of palm oil with methanol. The structural change of CaO-800 and CaMgO-800 directly reacted with methanol at different reaction time was analyzed by the XRD technique (Figure 4.10). The $Ca(OCH_3)_2$ was also referred to give higher basic strength and higher catalytic activity when compared to CaO and $Ca(OH)_2$ [10]. The growth of $Ca(OCH_3)_2$ from CaO-800 was gradually increased concomitantly with a decrease in the of intensity of CaO ($2\theta$ = 37.5 degree) (Figure 4.10 (A)), according to Eq. (4.4). Moreover, the small main peak of $Ca(OH)_2$ ($2\theta$ = 18.1 degree) was slightly found, which was generated by reaction between CaO and $H_2O$ as a by-product and/or moisture in methanol, oil and atmosphere (Eq. (4.5)).

$$CaO + 2CH_3OH \longleftrightarrow Ca(OCH_3)_2 + H_2O \quad (4.4)$$

$$CaO + H_2O \longrightarrow Ca(OH)_2 \quad (4.5)$$

The CaO phase was completely transformed at 120 min of reaction. Due to high cluster size of CaO in CaO-800, the methanol gradually diffused and gradually generated of $Ca(OCH_3)_2$. The CaO in CaMgO-800 was rapidly changed to $Ca(OCH_3)_2$

due to small cluster size and high dispersion (Figure 4.10 (B)). MgO was immediately agglomerated to high cluster size when CaO phase was transformed to $Ca(OCH_3)_2$ after 10 min of direct reaction. The MgO cluster was not reacted with methanol over 120 min of direct reaction. This result confirmed that small cluster size of CaO affects on phase change, resulted in its transesterification activity.

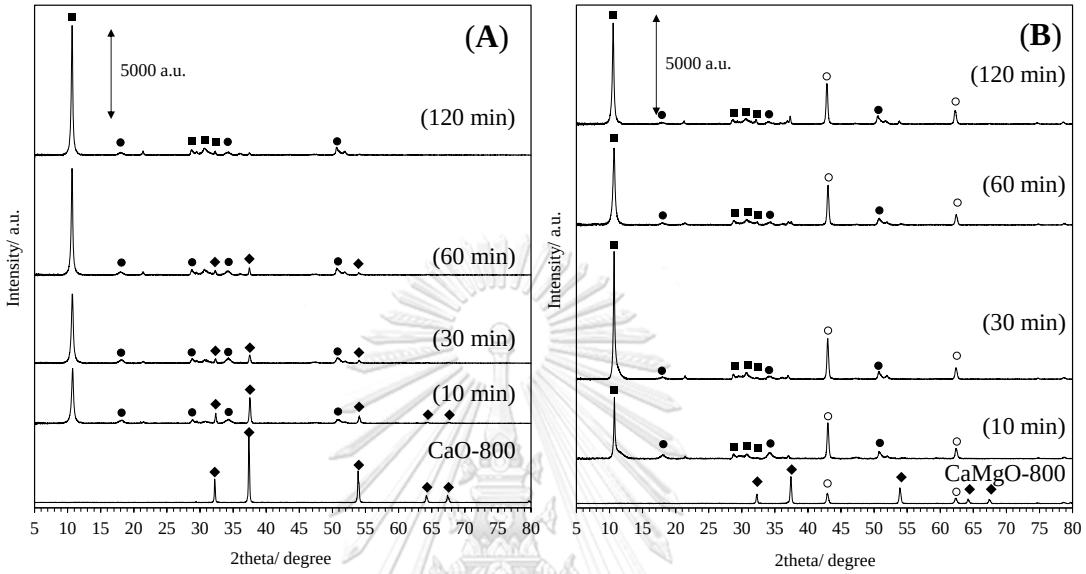


**Figure 4.10** Direct reaction of (A) CaO-800 and (B) CaMgO-800 with methanol at different reaction times. Reaction condition: catalyst amount, 1.5 g; methanol, 17.1 g; temperature, 60 °C. (Symbols: ◆ = CaO, ● = $Ca(OH)_2$, ○ = MgO and ■ = $Ca(OCH_3)_2$.

Glycerol is by-product in transesterification, which the reaction between CaO and glycerol in refluxing methanol creates calcium glyceroxides ($Ca(C_3H_7O_3)_2$) as a new catalytically active phase [81]. However, the $Ca(C_3H_7O_3)_2$ had high solubility in methanol (6216 mg $L^{-1}$) [56], which compared with CaO (28 mg $L^{-1}$) [8] and $Ca(OCH_3)_2$ (200 mg $L^{-1}$) [16]. The $Ca(C_3H_7O_3)_2$ formation contributed to homogeneous catalysis, resulting in calcium leaching into product contaminated. The structural change to $Ca(C_3H_7O_3)_2$ from CaO-800 and CaMgO-800 with glycerol in methanol solution at different reaction time was analyzed by the XRD technique (Figure 4.11). The CaO phase was changed to $Ca(C_3H_7O_3)_2$ according to Eq. (4.6)). Probably, $Ca(OH)_2$ generated by CaO reacted with $H_2O$ as a by-product (Eq. (4.5)).

$$CaO + 2C_3H_8O_3 \longleftrightarrow Ca(C_3H_7O_3)_2 + H_2O \quad (4.6)$$

$$Ca(OH)_2 + 2C_3H_8O_3 \longleftrightarrow Ca(C_3H_7O_3)_2 + 2H_2O \quad (4.7)$$

When increased the reaction time, the $Ca(C_3H_7O_3)_2$ phase was gradually increased. After direct reaction of 120 min, $Ca(OH)_2$ was disappeared, which it reacted with glycerol to $Ca(C_3H_7O_3)_2$ form (Eq. (4.7)). To confirm this reaction, pure $Ca(OH)_2$ was mixed with glycerol at 60 °C for 1h. The formation of $Ca(C_3H_7O_3)_2$ can be obtained (Figure 4.12). Due to large cluster size of CaO in CaO-800, the glycerol gradually diffused and gradually generated of $Ca(C_3H_7O_3)_2$. In the case of CaMgO-800 (Figure 4.11 (B)), $Ca(C_3H_7O_3)_2$ was not appeared at initial reaction (10–30 min). It should be because $Ca(C_3H_7O_3)_2$ has large volume, which the formation favors on large crystals. According to Blamey *et al.* [82] the formation of $CaCO_3$ *via* direct carbonation of $Ca(OH)_2$ preferred on large crystals.

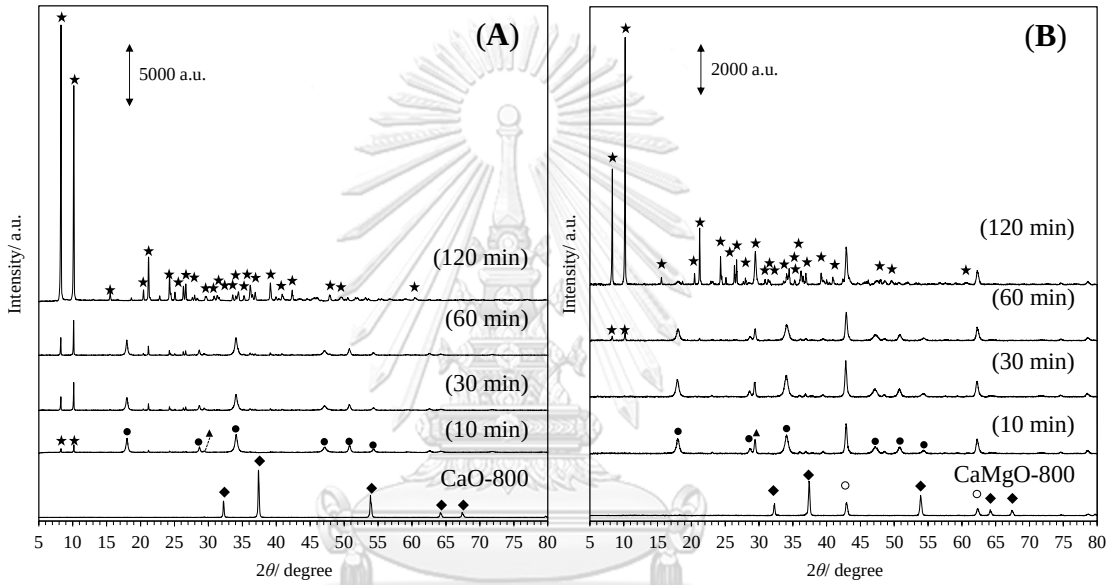


**Figure 4.11** Direct reaction of (A) CaO-800 and (B) CaMgO-800 with glycerol at different reaction times. Reaction condition: catalyst amount, 1.5 g; glycerol, 5 g; methanol, 22 g; temperature, 60 °C. (Symbols: ● = $Ca(OH)_2$, ▲ = $CaCO_3$, ♦ = CaO, ○ = MgO and ★ = $Ca(C_3H_7O_3)_2$).

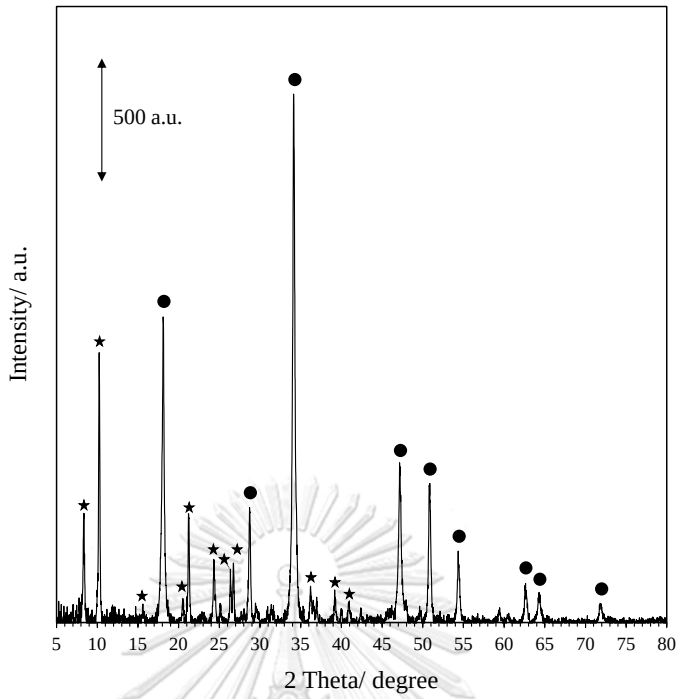


**Figure 4.12** XRD patterns of $Ca(OH)_2$ reacted with glycerol (1: 0.6 by weight) at 60 °C (Symbols: ● = $Ca(OH)_2$ and ★ = $Ca(C_3H_7O_3)_2$).

# CHAPTER V
# Calcium-based Compounds Derived from Calcite and Dolomite as Solid Base Catalysts in Transesterification of Palm Oil with Methanol

In this Chapter, different Ca-based compounds were prepared from calcite and dolomite calcined at 800 °C (CaO-800 and CaMgO-800, respectively). The Ca-based methoxides and glyceroxides were synthesized by the reaction of CaO-800 and CaMgO-800 with methanol and glycerol, respectively, as described in Section 3.3.2. The Ca-based methoxides derived from CaO-800 and CaMgO-800 were denoted as CaMet and MgO·CaMet, respectively. On the other hand, the Ca-based glyceroxides were designated as CaGly (from CaO-800) and MgO·CaGly (from CaMgO-800). All Ca-based catalysts obtained were characterized for their physicochemical properties using various techniques. The reusability of Ca-based oxide, methoxide and glyceroxide catalysts in the transesterification of palm oil with methanol was studied. Moreover, the Ca-based compounds freshly prepared were exposed to ambient air (RH ≈ 73%) under different conditions in order to reveal their structural and catalytic stability towards chemisorption of atmospheric moisture and $CO_2$. The structural change of the spent Ca-based catalysts after the repetitive uses and the air exposure was investigated using the XRD technique.

## 5.1 Physicochemical properties of different Ca-based compound catalysts

The XRD patterns of Ca-based oxide, methoxide and glyceroxide catalysts are shown in Figure 5.1 and the cluster size calculated by Sherrer's equation are summarized in Table 5.1. The CaO-800 shows a pure CaO phase (Figure 5.1(a)), whereas the CaMgO-800 obtained from dolomite was consisted of mixed CaO and MgO phases (Figure 5.11(b)). The cluster size of CaO (38.1 nm) presenting in CaMgO was smaller than that of CaO (45.2 nm) derived from calcite (Table 5.1). This result indicates that the presence of MgO as the mixed oxide form reduced the CaO agglomeration [53]. In the preparation of Ca-based methoxides, the CaO presenting in both the calcined calcite and dolomite was fully transformed to $Ca(OCH_3)_2$, while the MgO phase was not reacted (Figure 5.1 (c) and (d)). Similarly, the MgO was inactive with glycerol (Figure 5.1(f)). The cluster size of $Ca(C_3H_7O_3)_2$ in CaGly (130.2 nm) was larger than that in MgO·CaGly (67.7 nm) (Table 5.1). According to Phromprasit *et al.*, the unreacted MgO covered on CaO particles, which could reduce the carbonation of CaO to $CaCO_3$ and prevented sintering phenomena of the CaO particles [83]. This result suggests that the unreacted MgO prevented the cluster

growth of $Ca(OCH_3)_2$ and $Ca(C_3H_7O_3)_2$ in the MgO·CaMet and MgO·CaGly prepared from the calcined dolomite.

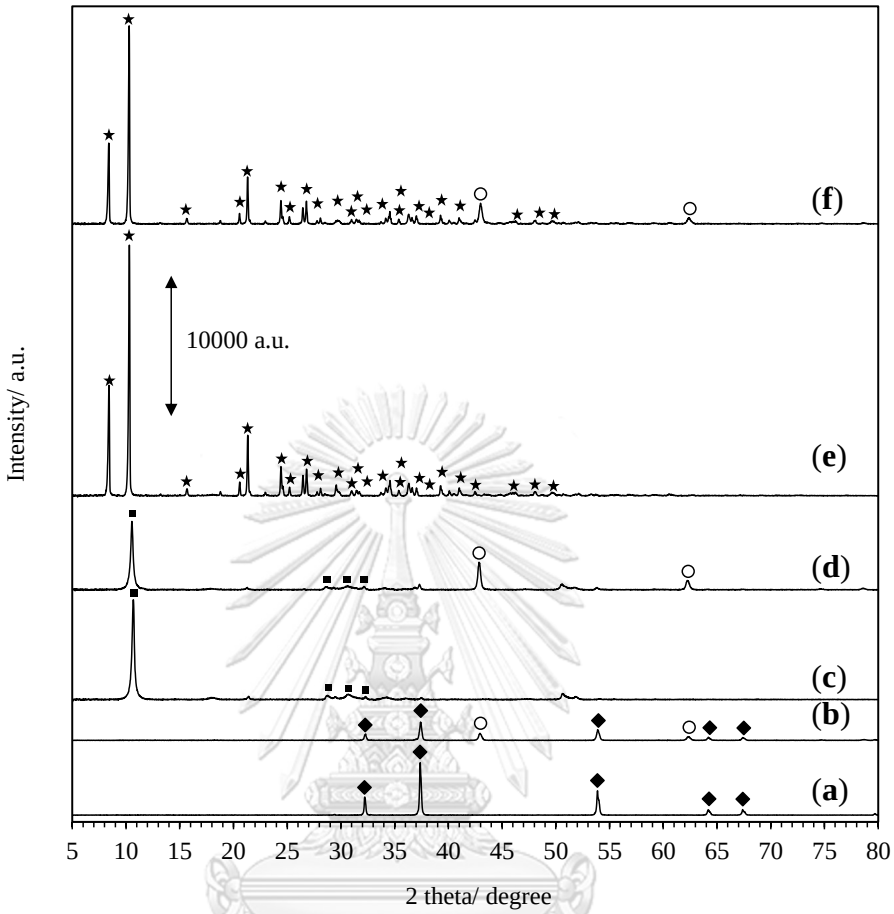


**Figure 5.1** XRD patterns of (a) CaO-800, (b) CaMgO-800, (c) CaMet, (d) MgO·CaMet, (e) CaGly, and (f) MgO·CaGly. (Symbols: ◆ = CaO, ○ = MgO, ■ = $Ca(OCH_3)_2$ and ★ = $Ca(C_3H_7O_3)_2$).

**Table 5.1** Physicochemical properties of the Ca-based compounds and FAME yield obtained from transesterification of palm oil with methanol over different Ca-based catalysts

| Catalyst | Cluster size[a] (nm) | | $S_{BET}$[b] | $Vp$[c] | $Dp$[d] | Basicity[e] | Initial rate[f] | FAME yield[g] |
|---|---|---|---|---|---|---|---|---|
| | Ca- | MgO | ($m^2\ g^{-1}$) | ($cm^3\ g^{-1}$) | (Å) | (μmol $g^{-1}$) | ($g_{FAME}\ g^{-1}_{cat}.\ h^{-1}$) | (wt%) |
| CaO | 45.2[h] | - | 17.5 | 0.029 | 75.0 | 96.3 | 61.4 | 99.9 |
| CaMgO | 38.1[h] | 29.1 | 14.7 | 0.024 | 116.4 | 108.0 | 32.9 | 99.9 |
| CaMet | 36.6[i] | - | 34.0 | 0.057 | 61.0 | 90.7 | 22.6 | 67.8 |
| MgO·CaMet | 34.2[i] | 34.8 | 54.8 | 0.084 | 82.9 | 49.5 | 19.0 | 53.4 |
| CaGly | 130.2[j] | - | 4.0 | 0.001 | 14.3 | 0 | 53.2 | 93.9 |
| MgO·CaGly | 67.7[j] | 37.6 | 9.9 | 0.009 | 44.2 | 0 | 31.4 | 86.4 |

[a] Determined from the XRD patterns using Sherrer's equation.
[b] BET surface area
[c] Total pore volume
[d] Average pore size
[e] Determined by the $CO_2$ pulse chemisorption. (*See* Figure 5.5)
[f] Determined at 5 min of reaction.
[g] Reaction conditions: catalyst amount, 10 wt%; RBD palm oil amount, 10 g; methanol: oil molar ratio, 30: 1; temperature, 60 °C; time, 60 min.
[h] Cluster size of CaO

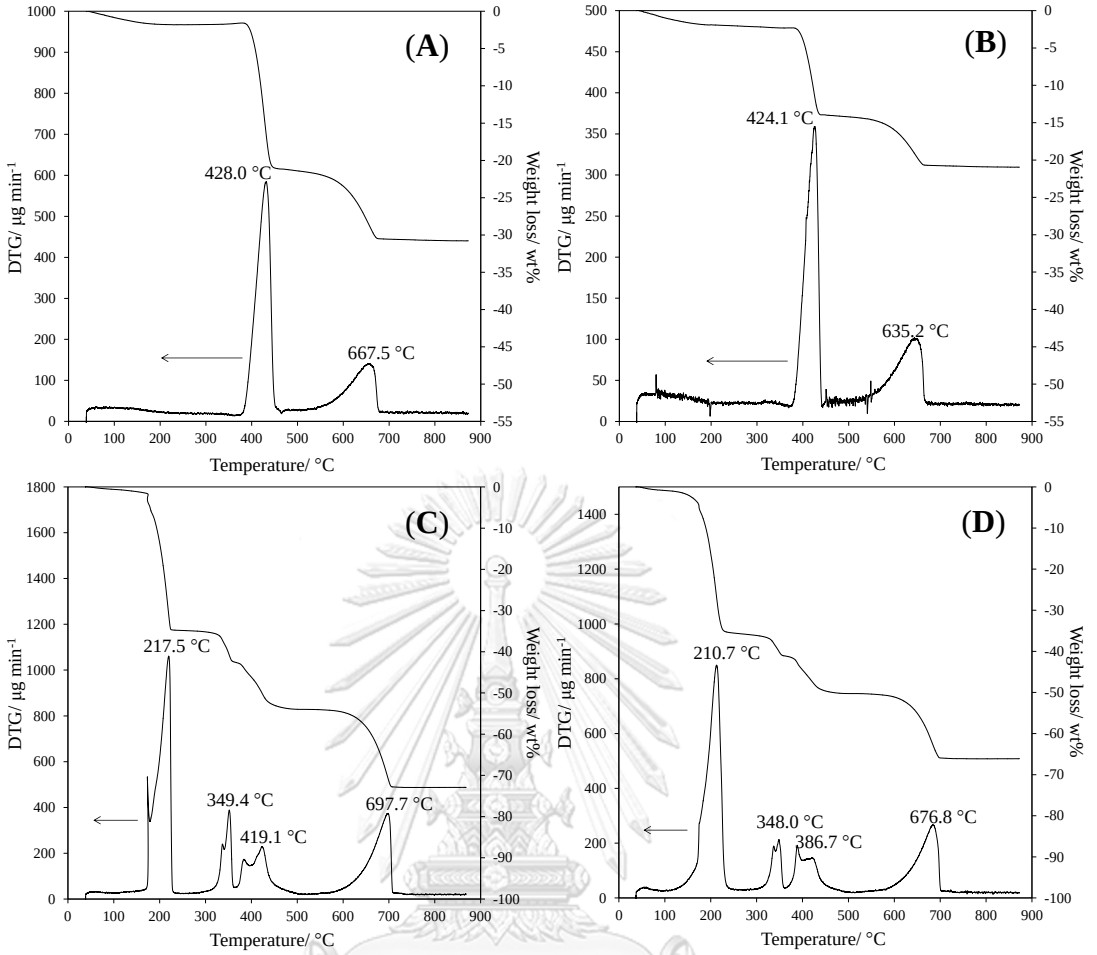


**Figure 5.2** Weight loss and DTG curves of (A) CaMet, (B) MgO·CaMet, (C) CaGly and (D) MgO·CaGly.



The weight loss and DTG curves of the methoxide and glyceroxide catalysts are shown in Figure 5.2, and the corresponding phase composition are summarized in Table 5.2. The weight loss in the first stage (1–2 g) was due to evaporation of moisture in the temperature range of 60–120 °C, and the final weight loss (500–800 °C) corresponded to decarbonation of $CaCO_3$ to CaO. The CaMet exhibited a similar weight loss curve to the MgO·CaMet (Figure 5.2 (A) and (B)), showing the decomposition of $Ca(OCH_3)_2$ around 425 °C [11, 62]. Since MgO remained intact in the presence of methanol, the total weight loss of MgO·CaMet (21.0 wt%) was lower than that of CaMet (30.9 wt%).

In the case of glyceroxide catalysts (Figure 5.2 (C) and (D)), the weight loss profiles were complicated. At the temperatures around 120–250 °C, the weight loss was attributed to releasing of one glycerol molecule to form calcium glycerolate ($Ca(C_3H_6O_3)$), which was confirmed by the XRD result obtained from CaGly and MgO·CaGly calcined at 200 °C for 2 h (Figure 5.3). Reyero and co-workers [58]

assigned the main peak of $Ca(C_3H_7O_3)_2$ at 2theta = 10.2 degree. The weight loss in this step was 34.0 wt% and 34.6 wt% for CaGly and MgO·CaGly, respectively, which were close to the theoretical weight loss (37.8 wt%) of glycerol from $Ca(C_3H_7O_3)_2$ to produce $Ca(C_3H_6O_3)$. The weight loss at 350 °C should be due to dehydration of $Ca(C_3H_6O_3)$, releasing $H_2O$. The weight loss around 360–500 °C was probably corresponded to decomposition of $Ca(C_3H_4O_2)$ to $CaCO_3$. When compared with the theoretical weight loss of $Ca(C_3H_7O_3)_2$ (74.7 wt%), the total weight loss of CaGly (73.0 wt%) was lower than that of MgO·Gly (66.1 wt%) due to the presence of unreacted MgO. It should be noted that thermally treating $Ca(C_3H_7O_3)_2$ at 200 °C for 2 h produced $Ca(C_3H_6O_3)$, which is probably in a new catalytic compound.

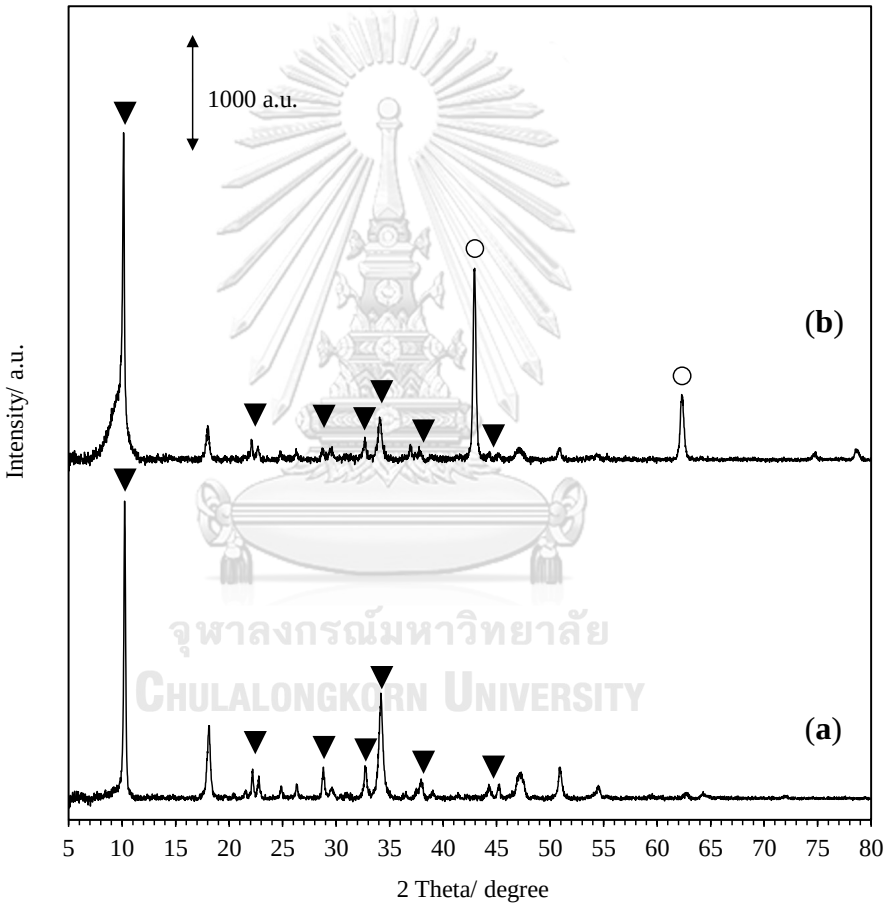




**Figure 5.3** XRD patterns of (a) CaGly and (b) MgO·CaGly calcined at 200 °C for 2 h. (Symbols: ▼ = $Ca(C_3H_6O_3)$ and ○ = MgO).

**Table 5.2** Phase composition of Ca-based methoxides or glyceroxides, derived from the calcined calcite and dolomite, as identified using TGA

| Sample | Temperature range (°C) | Weight loss (wt%) | Assignment |
|---|---|---|---|
| CaMet | 60–120 | 1.7 | Moisture |
| | 120–500 | 19.7 | Decomposition of $Ca(OCH_3)_2$ |
| | 500–700 | 9.5 | Decarbonation of $CaCO_3$ |
| | Total | 30.9 | |
| MgO·CaMet | 60–120 | 2.0 | Moisture |
| | 120–500 | 12.1 | Decomposition of $Ca(OCH_3)_2$ |
| | 500–700 | 6.9 | Decarbonation of $CaCO_3$ |
| | Total | 21.0 | |
| CaGly | 60–120 | 1.0 | Moisture |
| | 120–250 | 34.0 | Glycerol from $Ca(C_3H_7O_3)_2$ |
| | 250–360 | 7.8 | $H_2O$ from $Ca(C_3H_6O_3)$ |
| | 360–500 | 10.2 | Decarbonation of $Ca(C_3H_4O_2)$ |
| | 500–800 | 20.0 | Decarbonation of $CaCO_3$ |
| | Total | 73.0 | |
| MgO·CaGly | 60–120 | 1.3 | Moisture |
| | 120–250 | 34.6 | Glycerol from $Ca(C_3H_7O_3)_2$ |
| | 250–357 | 5.3 | $H_2O$ from $Ca(C_3H_6O_3)$ |
| | 357–500 | 9.0 | Decarbonation of $Ca(C_3H_4O_2)$ |
| | 500–800 | 15.9 | Decarbonation of $CaCO_3$ |
| | Total | 66.1 | |

The morphology of Ca-based oxide, methoxide and glyceroxide catalysts was observed by using SEM, as shown in Figure 5.4. The CaO-800 particles exhibited sintered irregular shape, whereas the small spheres were found on the surface of CaMgO-800 (Figure 5.4 (A) and (B), respectively). This result indicates that the MgO in the mixed oxide reduced the agglomeration of CaO particles. This observation was similar to that observed for the Ca and Zn mixed oxides [53]. The methoxide catalysts derived from calcite and dolomite possessed thin platelet particles (Figure 5.4 (C) and (D)), which is in accord with the previous works [11, 62]. Nevertheless, the platelet particles of CaMet were smaller in size than those of MgO·CaMet. In the case of glyceroxide catalysts, the particles were merged to large sizes (Figure 5.4 (E) and (F)).

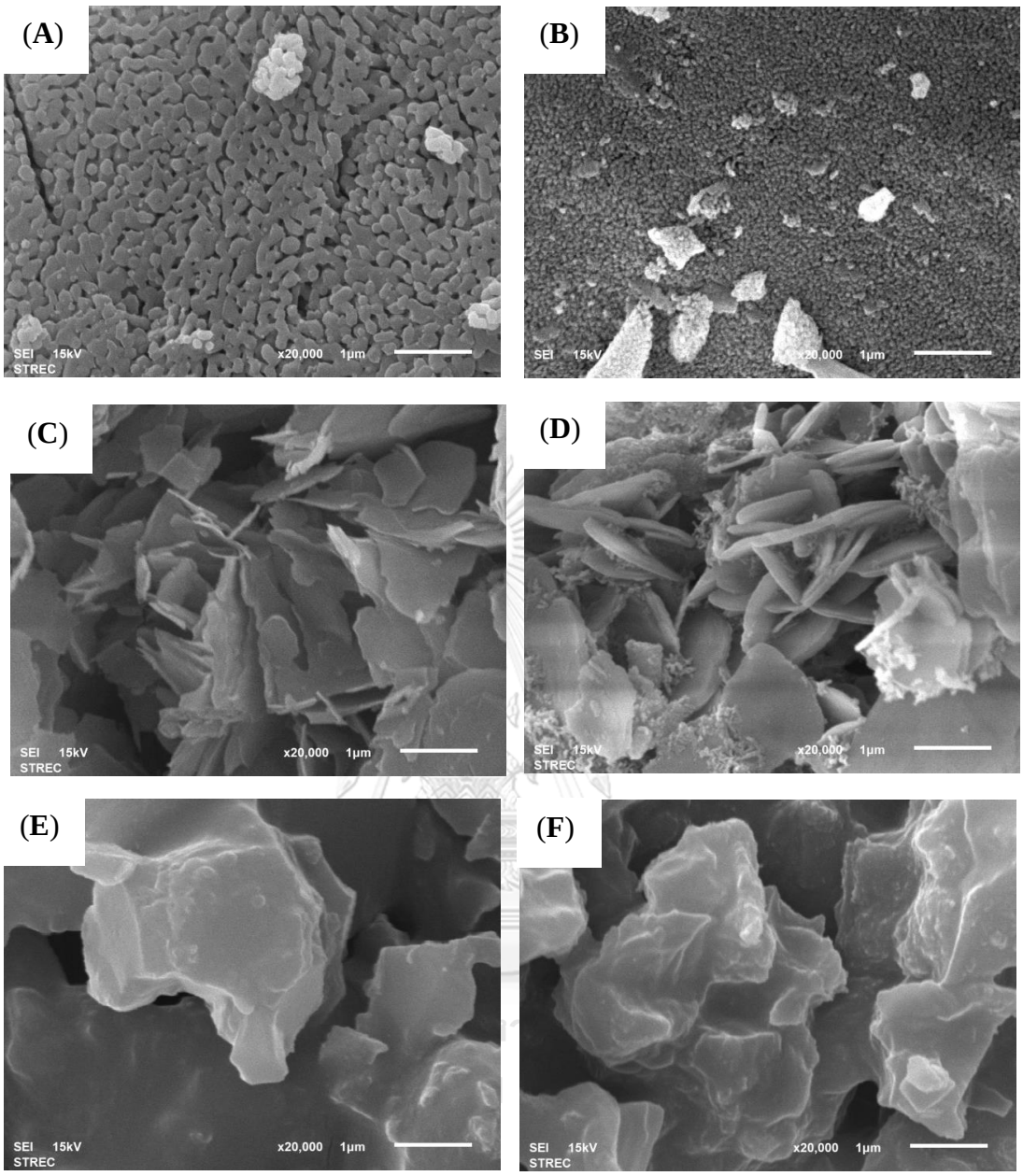


**Figure 5.4** SEM images of (A) CaO-800, (B) CaMgO-800, (C) CaMet, (D) MgO·CaMet, (E) CaGly, and (F) MgO·CaGly at magnification of 2000×.

The physicochemical properties of Ca-based oxide, methoxide and glyceroxide catalysts obtained are summarized in Table 5.1. The surface area of CaO-800 (17.5 $m^2$ $g^{-1}$) was higher than that of CaMgO-800 (14.7 $m^2$ $g^{-1}$). Although the particles of CaO-800 on surface were agglomerated as shown in Figure 5.4 (A), the surface area increased should be due to secondary pores formed in between the primary particles. CaMet and MgO·CaMet had high surface area because both particles were transformed into the thin platelets of which the secondary pore formation was promoted (Figure 5.4 (C) and (D)). Due to the formation of large

particles, the surface area of CaGly and MgO·CaGly was decreased. The unreacted MgO particles dispersed in MgO·CaMet and MgO·CaGly should contribute an increase in the surface area when compared to the pure Ca methoxide and glyceroxide prepared from CaO-800.

Figure 5.5 shows the $CO_2$ pulse chemisorption of Ca-based compound catalysts. This technique allowed us to determine the total basicity of the catalysts at low temperatures. As summarized in Table 5.1, the basicity was ranked in the descending order: CaMgO-800 > CaO-800 > CaMet > MgO·CaMet. At 60 min of reaction, the Ca-based oxide catalysts promoted the reaction to nearly completion (99.9% FAME yield). However, the basicity trend was not well correlated with either the initial rate (CaMgO-800 > CaO-800 > CaMet > MgO·CaMet > CaGly = MgO·CaGly) or the FAME yield (CaO-800 = CaMgO-800 > CaGly > MgO·CaGly > CaMet = MgO·CaMet). Since small probe molecule ($CO_2$) was used in the chemisorption measurement, the unclear trend between the basicity and activity of the catalysts could be expected [84]. It is worth noting that both CaGly and MgO·CaGly could not adsorbed $CO_2$ under the studied conditions although a high activity of metal glyceroxides was reported previously [81]. The $Ca(C_3H_7O_3)_2$ formation was believed to contribute homogeneous catalysis in the transesterification [8, 14] since it has a high solubility in methanol (6216 mg $L^{-1}$ [14]). Therefore, the $Ca(C_3H_7O_3)_2$ phase of CaGly and MgO·CaGly required a solvent in order to generate the $Ca^{2+}$ ions and glyceroxide anion for the catalytic transesterification. Regarding the role of MgO in the reaction, it can be figured out that the MgO presenting in MgO·CaMet and MgO·CaGly did not straightforwardly promote the FAME formation.

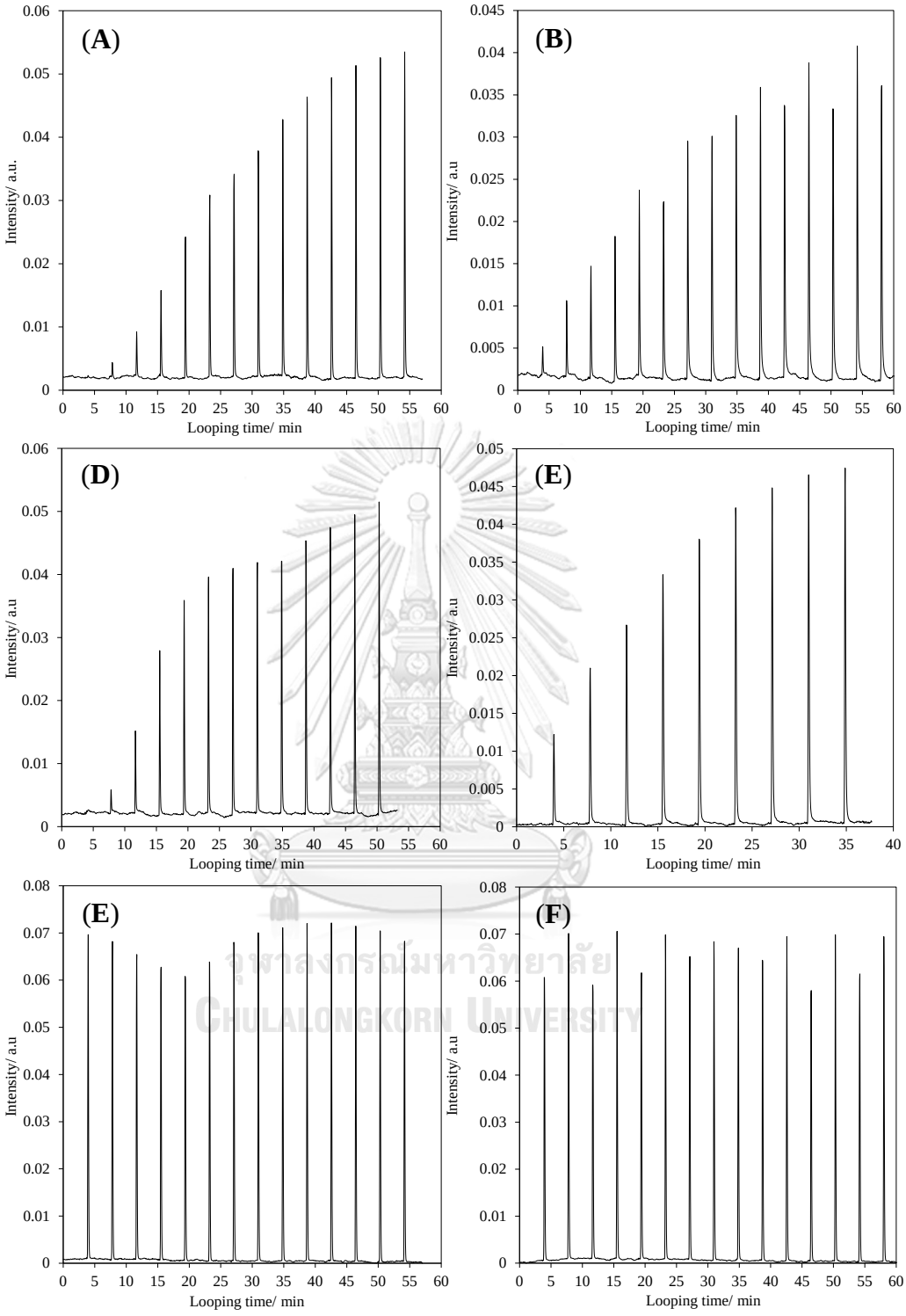


**Figure 5.5** $CO_2$-Pulse chemisorption of (A) CaO-800, (B) CaMgO-800, (C) CaMet, (D) MgO·CaMet, (E) CaGly, and (F) MgO·CaGly.

### 5.2 Transesterification over different Ca-based compound catalysts

Figure 5.6 shows the dependence of FAME yield on time in the transesterification of RBD palm oil with methanol over Ca-based oxide, methoxide and glyceroxide catalysts. The CaO-800 and CaMgO-800 gave the FAME yield of 99.9 wt% after 30 min of reaction, while other catalysts required 120 min to drive the reaction to a comparable FAME yield. The FAME yield obtained over CaO-800 and CaMgO-800 was not significantly different. The Ca content of CaO-800 was about 1.7-fold higher than that of CaMgO-800. Therefore, the MgO presented in the mixed oxides was key factor in the catalytic properties. The activity of CaGly was faster than that of CaMet although the Ca content of CaMet was higher than that of CaGly. As evidenced by $CO_2$-pulse chemisorption (Table 5.1), CaGly and MgO·CaGly did not chemisorb CO2. Therefore, the reaction catalyzed by $Ca(C_3H_7O_3)_2$ occurred as a homogeneous system [15, 56].

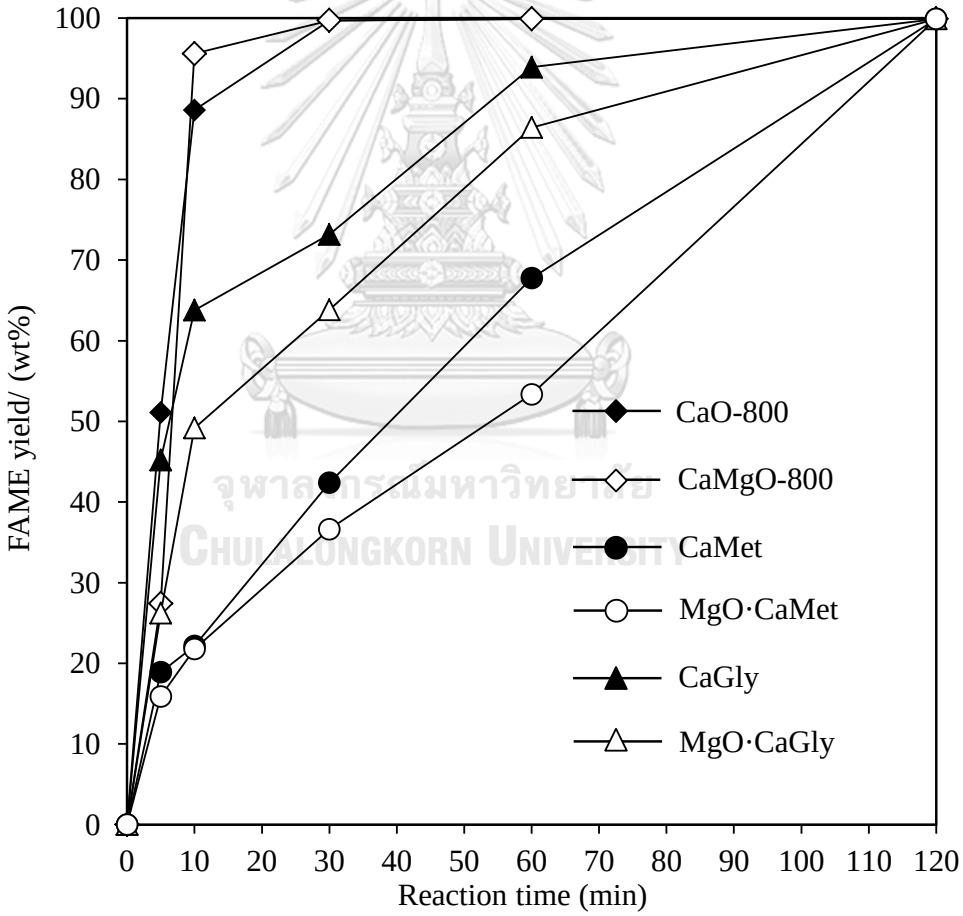


**Figure 5.6** Catalytic activity of CaO-800, CaMgO-800, CaMet, MgO·CaMet, CaGly and MgO·CaGly in the transesterification of RBD palm oil with methanol. Reaction conditions: catalyst amount, 10 wt%; methanol: oil molar ratio, 30: 1; temperature, 60 °C.

### 5.3 Reusability of different Ca-based compound catalysts

Figure 5.7 shows the reusability of Ca-based oxide, methoxide or glyceroxide catalysts in the transesterification of RBD palm oil with methanol. The CaO-800, CaMet, MgO·CaMet and CaGly catalysts could be repeatedly used for five runs. A severe decrease in the FAME yield was found in the reaction using CaMgO-800 and MgO·CaGly as catalysts. The small CaO crystallites promoted by the Ca and Mg mixed oxide formation had high catalytic activity but they showed faster deactivation. It is worth noting that the FAME yield obtained over MgO·CaMet was more stable. This result implied that the methoxide form improved the catalytic stability of CaMgO-800. To reveal the structural change of the spent catalysts, the fresh and spent forms of Ca-based oxides, methoxides and glyceroxides were analyzed by the XRD technique as shown in Figures 5.8–5.10.

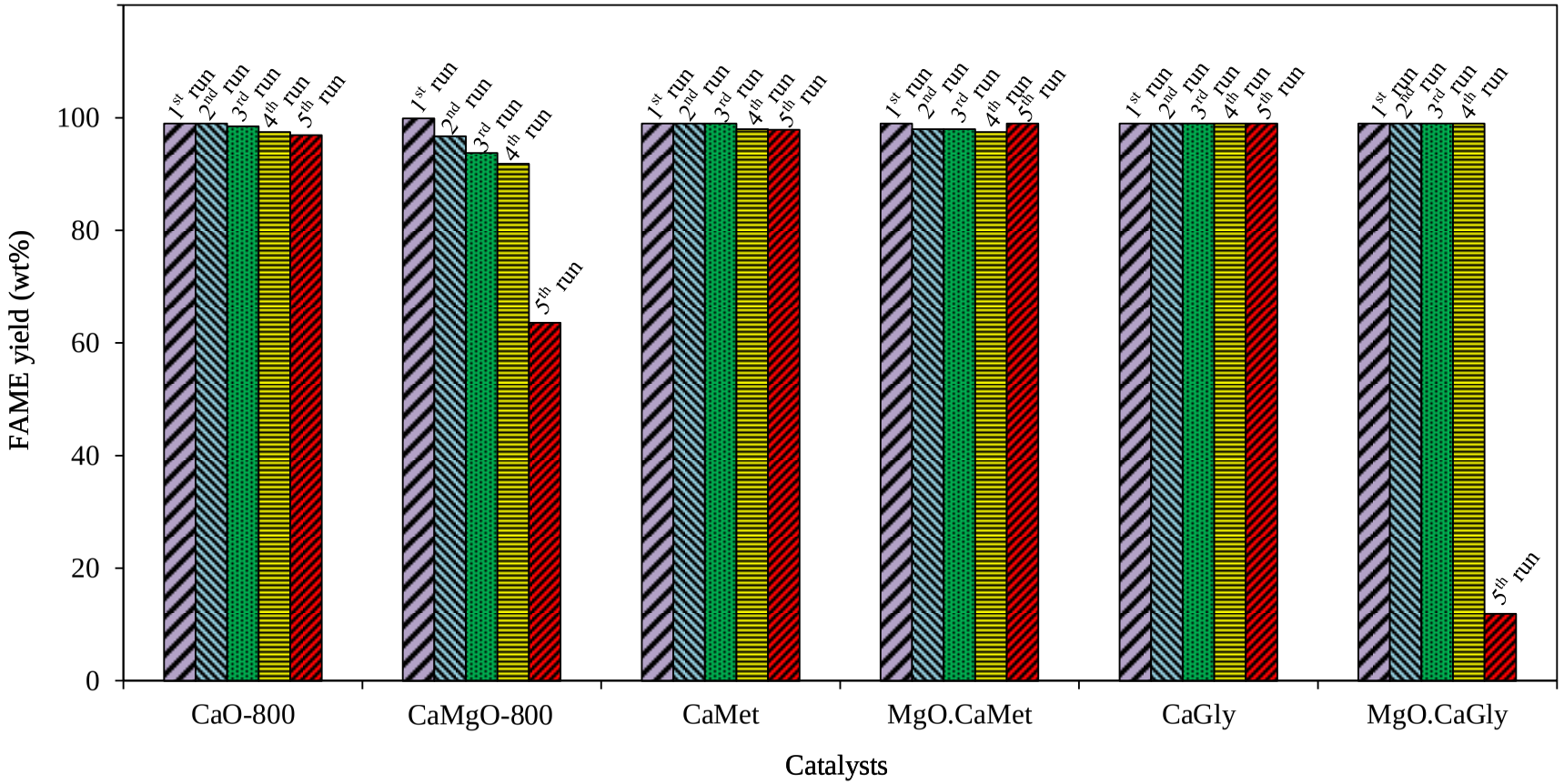


**Figure 5.7** Reusability of different Ca-based compound catalysts. Reaction conditions: catalyst amount, 10 wt%; methanol: oil molar ratio, 30: 1; reaction time, 2 h; temperature, 60 °C.

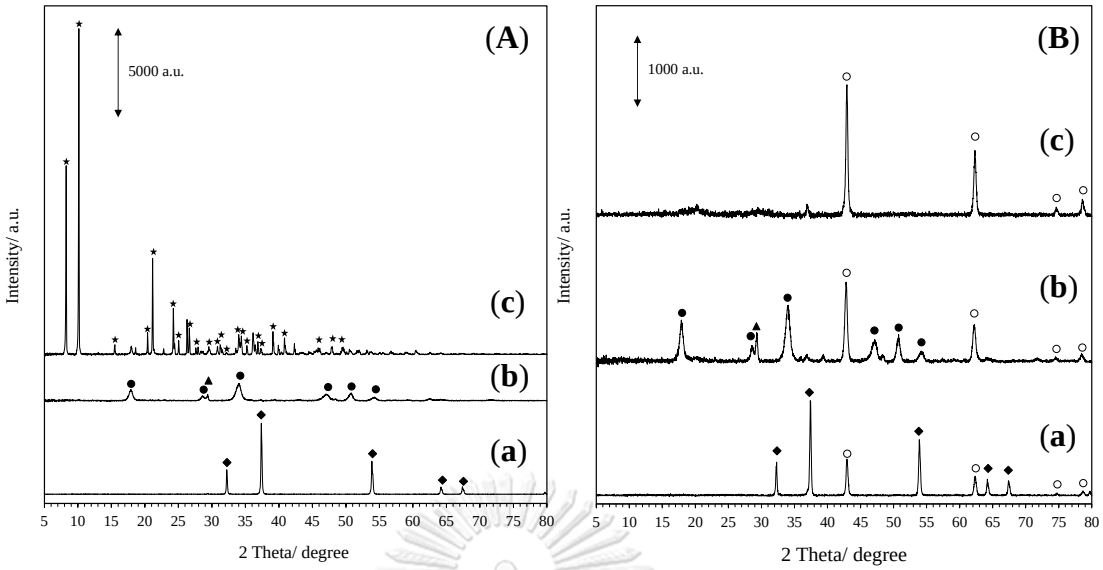


**Figure 5.8** XRD patterns of (A) CaO-800 and (B) CaMgO-800 as (a) fresh and spent catalysts recovered after (b) 1st and (c) 5th repetitive uses. (Symbols: ◆ = CaO, ● = $Ca(OH)_2$, ○ = MgO, ▲ = $CaCO_3$ and ★ = $Ca(C_3H_7O_3)_2$).

Figure 5.8 shows the structure change of Ca-based oxide catalysts after the first and fifth repetitive uses. According to the reaction between triglycerides and methanol on the catalyst surface, CaO was converted to $Ca(OCH_3)_2$ and $H_2O$ was produced as a by-product (Eq. (5.1)). Since the $Ca(OCH_3)_2$ generated on the CaO surface participated in tetrahedral intermediate formation, the main peak of $Ca(OCH_3)_2$ (2theta = 11.6 degree) was not found. The $H_2O$ by-product chemically adsorbed on the CaO surface, resulting in the formation of $Ca(OH)_2$ (Eq. (5.2)). CaO-800 was completely changed to $Ca(C_3H_7O_3)_2$ after the fifth repetition (Figure 5.8 (A)), which the $Ca(C_3H_7O_3)_2$ phase catalyzed the transesterification of vegetable oil with methanol [81]. In the case of CaMgO-800 (Figure 5.8 (B)), the small crystal size of CaO in CaMgO-800 created slightly larger crystal size of $Ca(OH)_2$ (12.9 nm) than that in CaO-800 (10.7 nm). However, the glyceroxide phase was not found. There are two explanations for this result, relating to the lower Ca content of CaMgO-800. The $Ca(C_3H_7O_3)_2$ formed might be completely leached during the successive reaction tests. Other explanation is that, the reaction between glycerol and CaO onto the CaMgO-800 surface yielded amorphous product.

$$CaO + CH_3OH \leftrightarrow Ca(OCH_3)_2 + H_2O \quad (5.1)$$

$$CaO + H_2O \rightarrow Ca(OH)_2 \quad (5.2)$$

The $Ca(OCH_3)_2$ form was active and both CaMet and MgO·CaMet stably gave a high FAME yield throughout the five repetitions. The methoxide phase was not

changed after the fifth repetitive use (Figure 5.9 (A) and Figure 5.9 (B)). Moreover, the main peak of $Ca(OCH_3)_2$ (2theta = 10.6 degree) was increased in its intensity in the case of CaMet. It should be because $Ca(OCH_3)_2$ was agglomerated to large particles. According to Liu *et al.* [13], the activity of $Ca(OCH_3)_2$ catalyst sustained even after being used for 20 repetitions and the FAME yield was slightly reduced. Although the solubility of $Ca(OCH_3)_2$ in methanol (200 mg $L^{-1}$ [16]) was higher than that of CaO (28 mg $L^{-1}$ [15]), it is about 30-fold lower than that of $Ca(C_3H_7O_3)_2$ (6216 mg $L^{-1}$ [14]).

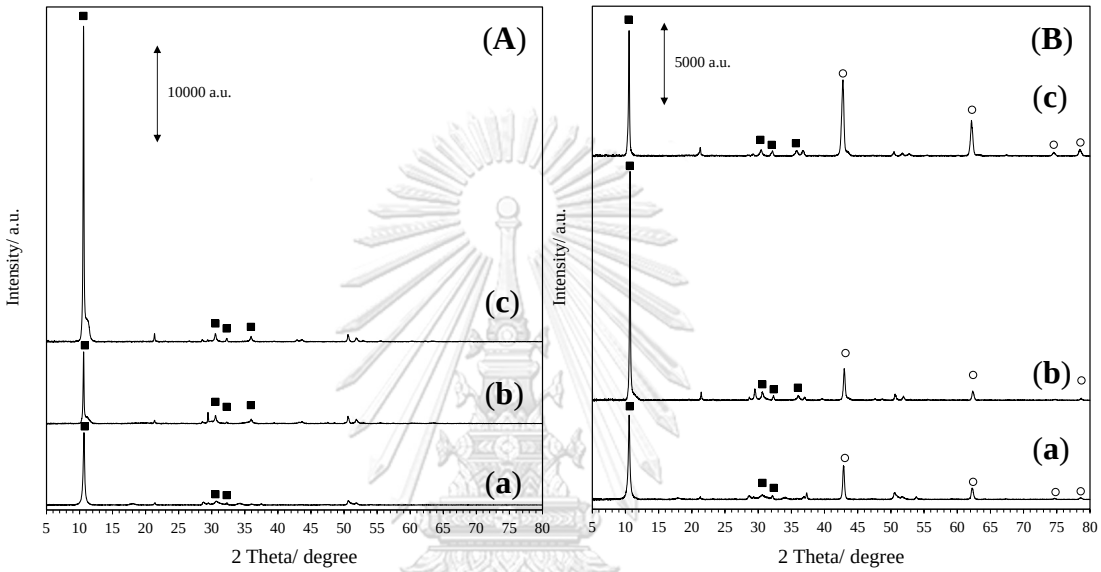


**Figure 5.9** XRD patterns of (A) CaMet and (B) MgO·CaMet as (a) fresh and spent catalysts recovered after (b) 1st and (c) 5th repetitive uses. (Symbols: ○ = MgO and ■ = $Ca(OCH_3)_2$).



In the case of glyceroxide catalysts with $Ca(C_3H_7O_3)_2$ as an active phase, the spent CaGly exhibited a gradual decrease in the $Ca(C_3H_7O_3)_2$ intensity when increasing the number of repetition (Figure 5.10 (A)), while the glyceroxide phase of MgO·CaGly disappeared after the fifth repetition (Figure 5.10 (B)). $Ca(C_3H_7O_3)_2$ was highly soluble in methanol and the resulting dissolved ions contributed the homogeneous catalysis [15, 56]. It can be seen that the MgO·CaGly spent for four times showed a sudden decrease in the FAME yield at the fifth repetitive use concomitantly with the presence of amorphous phase at 2theta ≈ 14–24 degree. It might be related to soap formation during reaction.

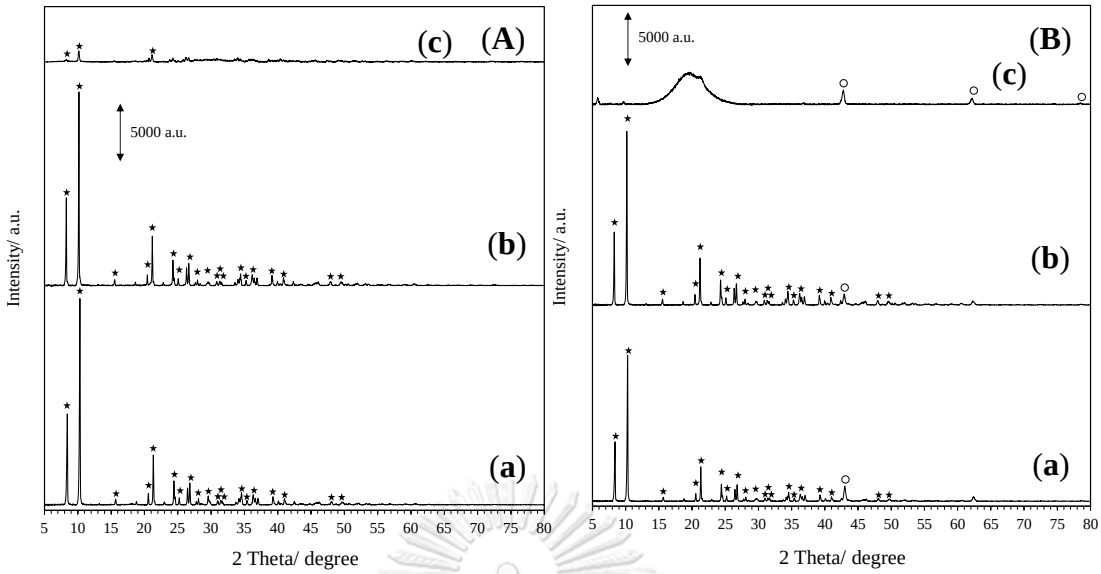


**Figure 5.10** XRD patterns of (A) CaGly and (B) MgO·CaGly as (a) fresh and spent catalysts recovered after (b) 1st and (c) 5th repetitive uses. (Symbols: ○ = MgO and ★ = $Ca(C_3H_7O_3)_2$).

## 5.4 Study on structural and catalytic stability of different Ca-based compound catalysts after exposed to ambient air

After the Ca-based oxide, methoxide and glyceroxide catalysts were exposed to ambient air under different conditions, including at 60 °C for 2 h and at room temperature for 2 h, 10 d and 42 d, the catalysts were investigated for the structural change by using XRD technique. The XRD results are shown in Figures 5.11–5.13. The CaO phase was transformed to $CaCO_3$ and $Ca(OH)_2$ *via* chemisorption of $CO_2$ and $H_2O$, respectively. According to the activation energy ($E_a$) determined by previous studies, the CaO hydration to $Ca(OH)_2$ (Eq. (5.3); $E_a$ = 11.0–20.3 kJ $mol^{-1}$) [85] occurs more readily than the CaO carbonation to $CaCO_3$ (Eq. (5.4); $E_a$ = 24–33 kJ $mol^{-1}$) [86]. Besides, the formation of $CaCO_3$ relatively favors the $Ca(OH)_2$ carbonation route (Eq. (5.5)) when compared to the direct carbonation of CaO (Eq. (5.4)). The $Ca(OCH_3)_2$ phase presenting in CaMet and MgO·CaMet was probably transformed to $Ca(OH)_2$ and $CaCO_3$ according to Eqs. (5.6) and (5.7), respectively, in the presence of $H_2O$. In the case of CaGly and MgO·CaGly, $Ca(C_3H_7O_3)_2$ possibly reacted with $H_2O$ and $CO_2$, yielding $Ca(OH)_2$ and $CaCO_3$, as shown in Eqs. (5.8) and (5.9), respectively.

$$CaO_{(s)} + H_2O_{(g)} \leftrightarrow Ca(OH)_{2(s)} \quad (5.3)$$

$$CaO_{(s)} + CO_{2(g)} \leftrightarrow CaCO_{3(s)} \quad (5.4)$$

$$Ca(OH)_{2(s)} + CO_{2(g)} \leftrightarrow CaCO_{3(s)} + H_2O_{(g)} \quad (5.5)$$

$$Ca(OCH_3)_{2(s)} + 2H_2O_{(g)} \leftrightarrow Ca(OH)_{2(s)} + 2CH_3OH_{(g)} \quad (5.6)$$

$$Ca(OCH_3)_{2(s)} + CO_{2(g)} + 2H_2O_{(g)} \leftrightarrow CaCO_{3(s)} + 2CH_3OH_{(g)} \quad (5.7)$$

$$Ca(C_3H_7O_3)_{2(s)} + 2H_2O_{(g)} \leftrightarrow Ca(OH)_{2(s)} + 2C_3H_8O_{3(l)} \quad (5.8)$$

$$Ca(C_3H_7O_3)_{2(s)} + CO_{2(g)} + H_2O_{(g)} \leftrightarrow CaCO_{3(s)} + 2C_3H_8O_{3(l)} \quad (5.9)$$

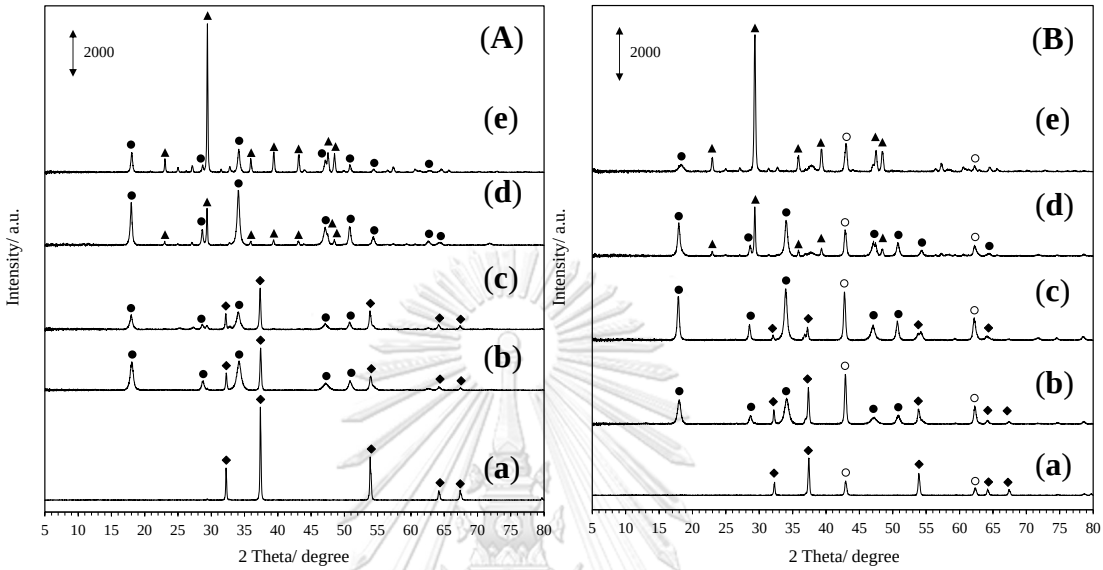


**Figure 5.11** Effect of air exposure on the structure change of (A) CaO-800 and (B) CaMgO-800: (a) fresh catalysts and (b-e) the catalysts after exposed to ambient air at (b) 60 °C for 2 h, and at room temperature for (c) 2 h, (d) 10 d and (e) 42 d. (Symbols: ◆ = CaO, ● = $Ca(OH)_2$, ○ = MgO and ▲ = $CaCO_3$).

For the CaO-800 and CaMgO-800 catalysts, CaO as main active site was transformed to $CaCO_3$ *via* the generation of $Ca(OH)_2$ in ambient atmosphere because the carbonation at low temperature requires $H_2O$ for $CO_2$ dissolution on the solid surface [87]. When compared the main CaO peak (2 theta = 37.5 degree) of CaO-800 exposed at 60 °C for 2 h and that at room temperature for 2 h, decreasing of the CaO peaks was not significantly different due to its large particle (Figure 5.11 (A) (b) and (c)). After the air exposure of CaO-800 at room temperature for 10 d, the mixed phases of $CaCO_3$ and $Ca(OH)_2$ were found concomitantly with the disappearing of CaO (Figure 5.11 (A) (d)). When the exposure time was increased to 42 d, $CaCO_3$ was increased while $Ca(OH)_2$ was decreased (Figure 5.11 (A) (e)).

Since the hydration of CaO is exothermic reaction, the CaO presenting in the mixed oxides was relatively stable when the air exposure was carried out at 60 °C for 2 h, compared to at room temperature for 2 h (Figure 5.11 (B) (b) and (c)). Under the same experimental conditions, the crystal size of $Ca(OH)_2$ on the exposed CaMgO-800 was larger than that on the exposed CaO-800. The result indicates that the CaO in the mixed oxides was more sensitive, and so higher activity, than that in the pure

oxide form. Moreover, the generation of $CaCO_3$ *via* the $Ca(OH)_2$ carbonation was faster for CaMgO-800 than for CaO-800. It was explained by the fact that the carbonation of $Ca(OH)_2$ favors on large crystals [82], because $CaCO_3$ (36.9 $cm^3$ $g^{-1}$) has larger volume than $Ca(OH)_2$ (33.6 $cm^3$ $g^{-1}$) and CaO (16.9 $cm^3$ $g^{-1}$) [88].

The structure change of CaMet and MgO·CaMet after exposing to air is shown in Figure 5.12. The $Ca(OCH_3)_2$ phase was not significantly changed at the exposure temperature of 60 °C for 2 h (Figure 5.12 (A) (b) and Figure 5.12 (B) (b)). The main peak of $Ca(OCH_3)_2$ was extremely decreased concomitantly with the small main peal of $Ca(OH)_2$ when exposed to ambient air at room temperature for 2 h. According to Eq. (5.6), the methanol formed as a hydrolysis product covered on the surface and reduced the crystalline growth of $Ca(OH)_2$. After the air exposure at room temperature for 10 d, $CaCO_3$ was only found for CaMet, while the exposed MgO·CaMet still had $Ca(OH)_2$ (Figure 5.12 (A) (d) and Figure 5.12 (B) (d)). The complete carbonation of $Ca(OH)_2$ to generate $CaCO_3$ in MgO·CaMet required the prolonged exposure time to 42 d (Figure 5.12 (B) (e)).

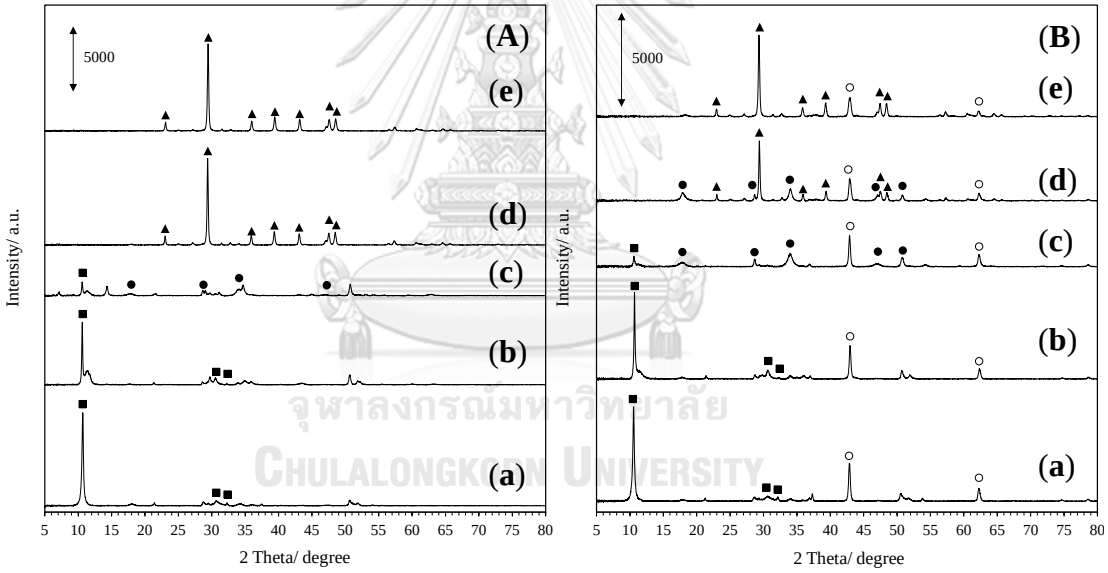


**Figure 5.12** Effect of air exposure on the structure change of (A) CaMet and (B) MgO·CaMet: (a) fresh catalysts and (b-e) the catalysts after exposed to ambient air at (b) 60 °C for 2 h, and at room temperature for (c) 2 h, (d) 10 d and (e) 42 d. (Symbols: ■ = $Ca(OCH_3)_2$, ● = $Ca(OH)_2$, ○ = MgO and ▲ = $CaCO_3$)**.**

The $Ca(C_3H_7O_3)_2$ phase in both CaGly and MgO·CaGly was stable after the air exposure at 60 °C for 2 h or at room temperature for 2 h (Figure 5.13 (A) (b) and (c), and Figure 5.13 (B) (b) and (c)). After the air exposure at room temperature for 10 d (Figure 5.13 (A) (d) and Figure 5.13 (B) (d)), the separate phases between white solid powder as top layer and viscous liquid as bottom layer were found. According to $CO_2$-pulse chemisorption, $Ca(C_3H_7O_3)_2$ did not adsorb $CO_2$. Therefore, the $CaCO_3$

generated was resulted from reaction of $Ca(C_3H_7O_3)_2$ with moisture, followed by the $Ca(OH)_2$ carbonation (Eq. (5.9)).

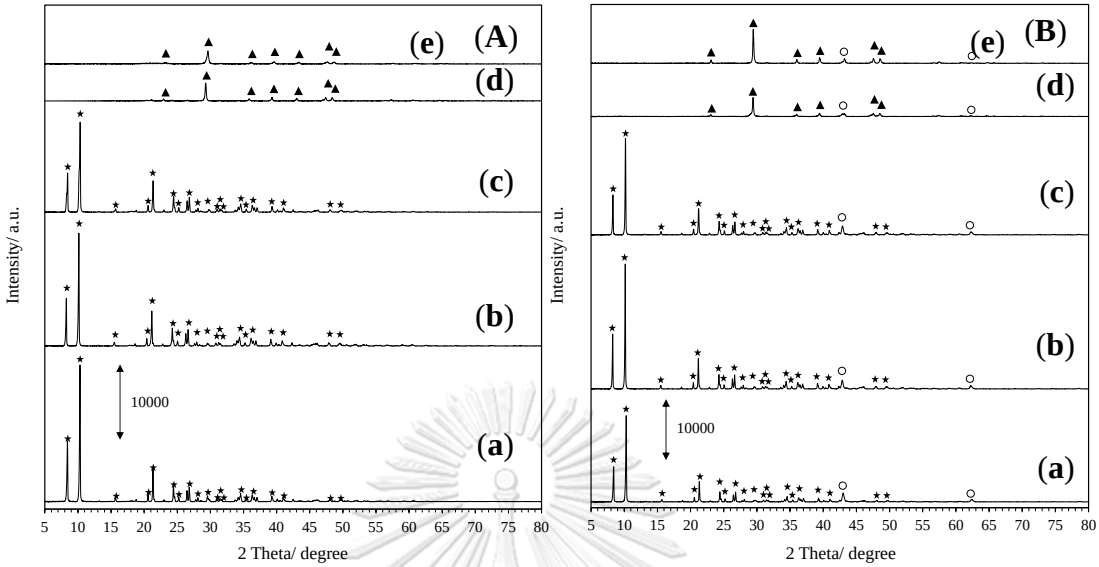


**Figure 5.13** Effect of air exposure on the structure change of (A) CaGly and (B) MgO·CaGly: (a) fresh catalysts and (b-e) the catalysts after exposed to ambient air at (b) 60 °C for 2 h, and at room temperature for (c) 2 h, (d) 10 d and (e) 42 d. (Symbols: ★ = $Ca(C_3H_7O_3)_2$, ○ = MgO and ▲ = $CaCO_3$).

Figure 5.14 shows the FAME yield obtained from the transesterification of RBD palm oil with methanol over the Ca-based oxide, methoxide and glyceroxide catalysts exposed to ambient air under different exposure conditions. After the exposure to ambient air at 60 °C for 2 h, the FAME yield obtained over MgO·CaMet, CaGly and MgO·CaGly was not significantly altered since their crystalline phases were not changed (Figure 5.12 (B) and Figure 5.13). In the case of CaMet, the main peak of $Ca(OCH_3)_2$ as active phase was decreased (Figure 5.12 (A) (a) and (b)), resulting in a decrease in the FAME yield. A severe activity loss was observed for the Ca-based oxides due to the transformation of CaO to $Ca(OH)_2$ *via* hydration with moisture.

In the case of air exposure at room temperature for 2 h, the Ca-based glyceroxides showed a superior structural and catalytic stability to other Ca-based compounds. The FAME yield obtained over CaMgO-800 was higher than that over CaO-800 due to a larger proportion of CaO phase remaining in the exposed CaO-800. Decreasing of $Ca(OCH_3)_2$ as active phase severely deactivated the CaMet and MgO·CaMet catalysts. Surprisingly, the CaO-800 exposed to air at room temperature for 10 d gave a high FAME yield (80.4 wt%). In the case of the CaMgO-800 exposed to ambient air under the same conditions, the FAME yield was decreased to 22.2 wt% since $CaCO_3$ was found as main phase mixed with $Ca(OH)_2$. The $Ca(OH)_2$ generated

in the exposed MgO·CaMet promoted the reaction to lesser extent, (the FAME yield = 13.8 wt%). When the pristine Ca phases were completely converted to $CaCO_3$, the resulting Ca-based catalysts completely lost their activity in the transesterification.

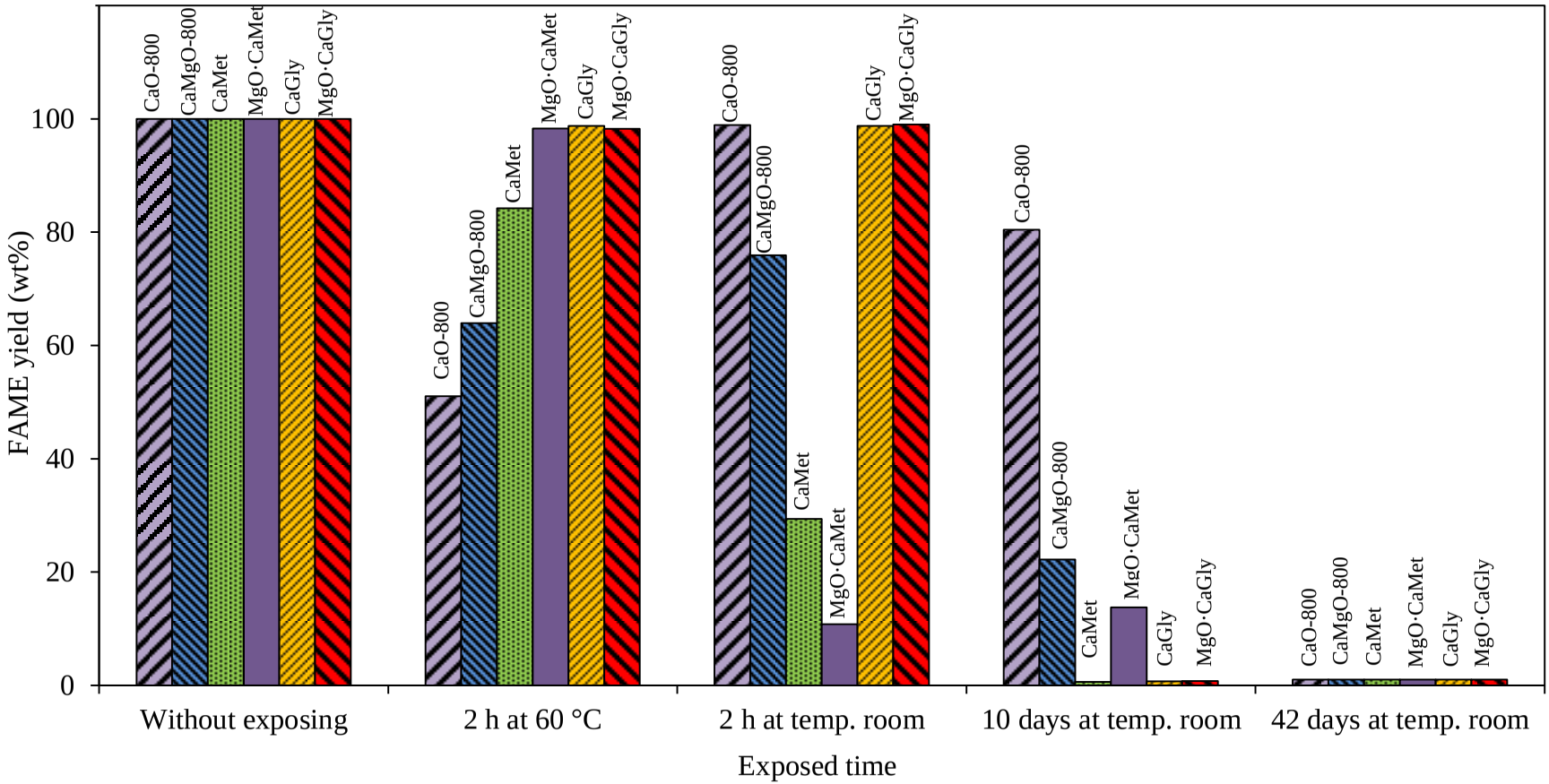


**Figure 5.14** The FAME yield obtained from transesterification of RBD palm oil with methanol over the Ca-based compound catalysts exposed to ambient air under different conditions . Reaction conditions: catalyst amount, 10 wt%; methanol: oil molar ratio, 30: 1; reaction time, 2 h; temperature, 60 °C.

# CHAPTER VI
# ZSAH Extrudates and Their Application as Catalysts in Transesterification of Palm Oil with Methanol in Fixed-Bed Reactor

In this chapter, heterogeneous base catalysts in form of extrudates were characterized and used in the transesterification of palm oil with methanol in a continuous-flow fixed-bed reactor at 65 °C and ambient pressure. As described in Section 3.3.3, the catalyst extrudates were prepared *via* a dissolution–precipitation method, using waste enamel venus shell as a renewable Ca source. Zinc nitrate and alumina were used as binder precursors; these were partly converted to spinel $ZnAl_2O_4$ after calcination. The catalyst paste was shaped using either manual extruder or single-screw extruder. The effects of adding HEC as a plasticizer on extrusion and the characteristics of the resulting extrudates, designated as ZSAH catalysts, were studied. The effect of premixing the ZSAH extrudates with methanol, vegetable oil or commercial methyl esters (CMEs) with different fatty acid chain lengths on the catalytic transesterification was also investigated.

## 6.1 Formulation of ZSAH catalyst extrudates

**Table 6.1** Effect of extruder types and HEC amount on the extrudate characteristics

| Extruder | HEC amount (wt%) | Extrusion | Extrudate characteristics | |
|---|---|---|---|---|
| | | | Drying at 100 °C | Calcining at 400 °C |
| Manual | 0 | Failed [a] | *n.d.* | *n.d.* |
| | 3 | Easy | Hard | Very brittle |
| | 5 | Easy | Hard | Broken [b] |
| Single screw | 0 | Difficult | Dense and hard | Hard |
| | 3 | Easy | Dense and hard | Hard |
| | 5 | Easy | Hard | Very brittle |

[a] *See* the Figure 6.1 (A) and (B).
[b] *See* the Figure 6.1 (C) and (D).
*n.d.* means not determined.

The effects of the type of extruder and the HEC amount used in the extrudate forming on the extrudate characteristics are summarized in Table 6.1. The HEC addition was required in the extrudate forming when using a manual extruder due to the separation between solid and liquid phase (Figure 6.1 (A) and (B)). The HEC added increased the plasticity of the catalyst paste due to hydrogen bonding with water as a liquid media, which then facilitated the extrusion process [24]. When the

extrudates were calcined at 400 °C, the mechanical strength of catalyst obtained was lower than that of the dried extrudates. Moreover, the extrudates prepared with a high HEC amount (5 wt%) were broken after calcination (Figure 6.1 (C) and (D)). Ketcong *et al.* found that the HEC burned off by calcination in air flow increased the porosity of the resulting extrudates, which adversely affected the mechanical strength [22]. In the case of using single-screw extruder, the extrudates obtained were dense and hard because the catalyst paste was pressed under high pressure and high-shear mixing. Moreover, the agglomerate particles were broken down to small particles coated with layer of liquid [4]. Although the HEC addition was not of necessity for the single-screw extrusion, the presence of HEC prevented the phase separation during the extrusion and reduced heat generated. After calcination, the extrudates obtained exhibited shape and size retention better than those formulated using the manual extruder. Forming of the ZSAH catalyst extrudate was, therefore, prepared by using 3 wt% HEC and the single-screw extruder. The extrudate obtained after calcination at 400 C was denoted as ZSAH-400.

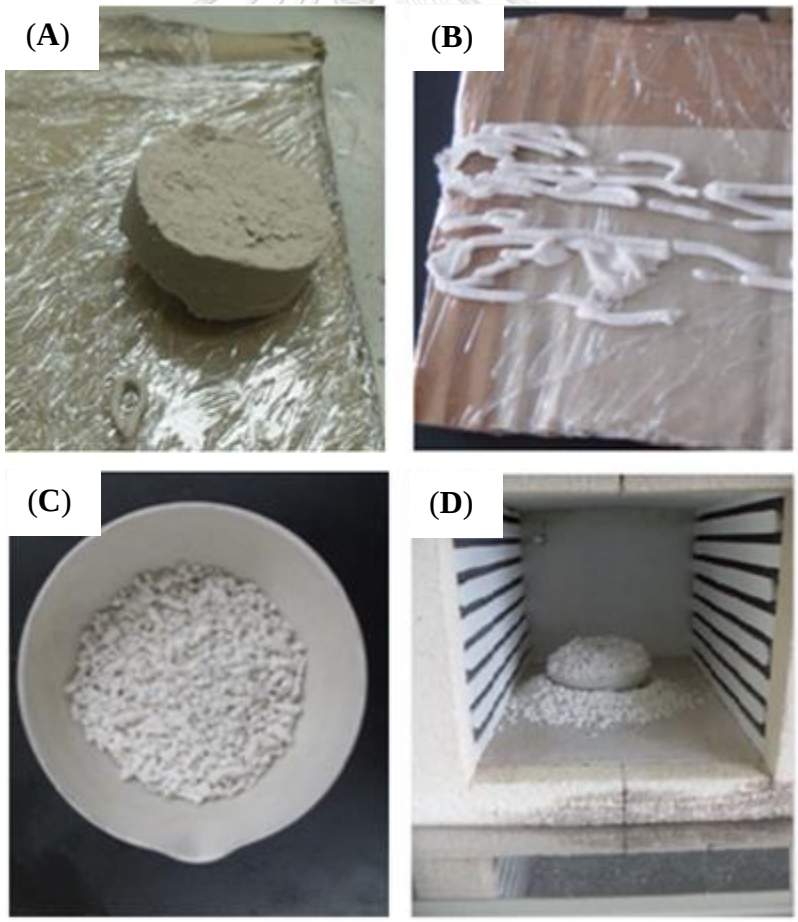


**Figure 6.1** Characteristics of extrudates formulated by the manual extrusion: (A) and (B) are extruded without the HEC addition, whereas (C) and (D) are the extrudates broken when prepared by using 5 wt% HEC, followed by calcination at 400 °C.

### 6.2 Characterization of ZSAH extrudate catalyst

The as-received seashell was composed of $CaCO_3$ and $Ca(OH)_2$ as crystalline phases (Figure 6.2 (a)). After calcined at 800 °C, these Ca compounds were completely transformed to CaO (Figure 6.2 (b)). From XRF spectroscopy, the enamel venus shell calcined at 800 °C for 2 h was composed of CaO (68.6 wt%) with a trace amount of MgO (0.5 wt%), $SiO_2$ (0.8 wt%), and $Fe_2O_3$ (0.1 wt%). Combining the results with TGA, the amount of $Ca(OH)_2$ and $CaCO_3$ was 62.1 wt% and 37.8 wt%, which were decomposed at 445 and 767 °C, respectively (Figure 6.3). From the XRF, XRD and TGA results, the seashell calcined at 800 °C could be used as an active phase precursor in the preparation of ZSAH extrudate catalyst.

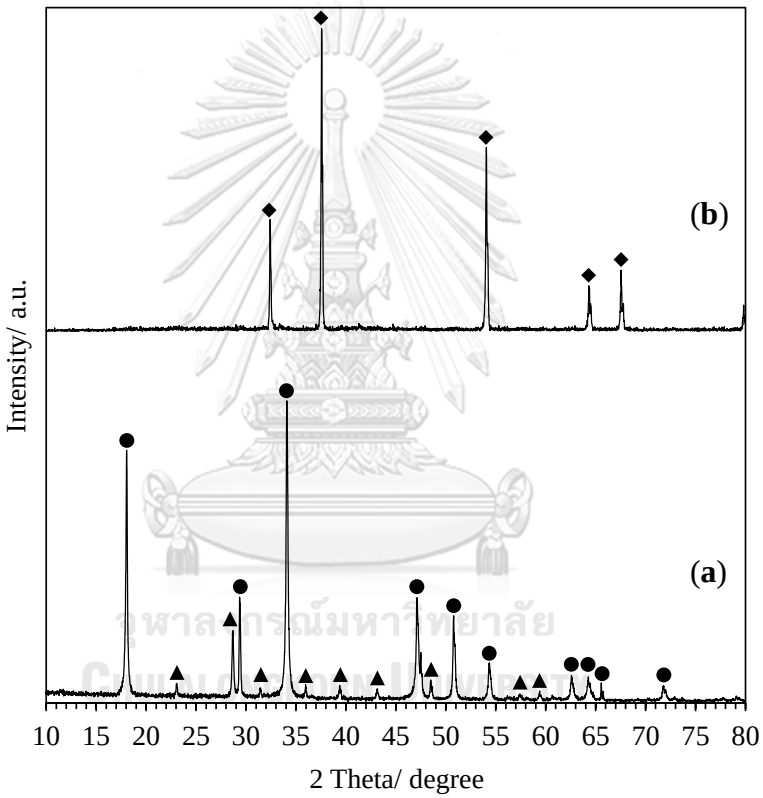


**Figure 6.2** XRD patterns of (a) as-received enamel venus shell and (b) after calcination at 800 °C. (Symbols: ▲ = $CaCO_3$, ● = $Ca(OH)_2$, ◆ = CaO).

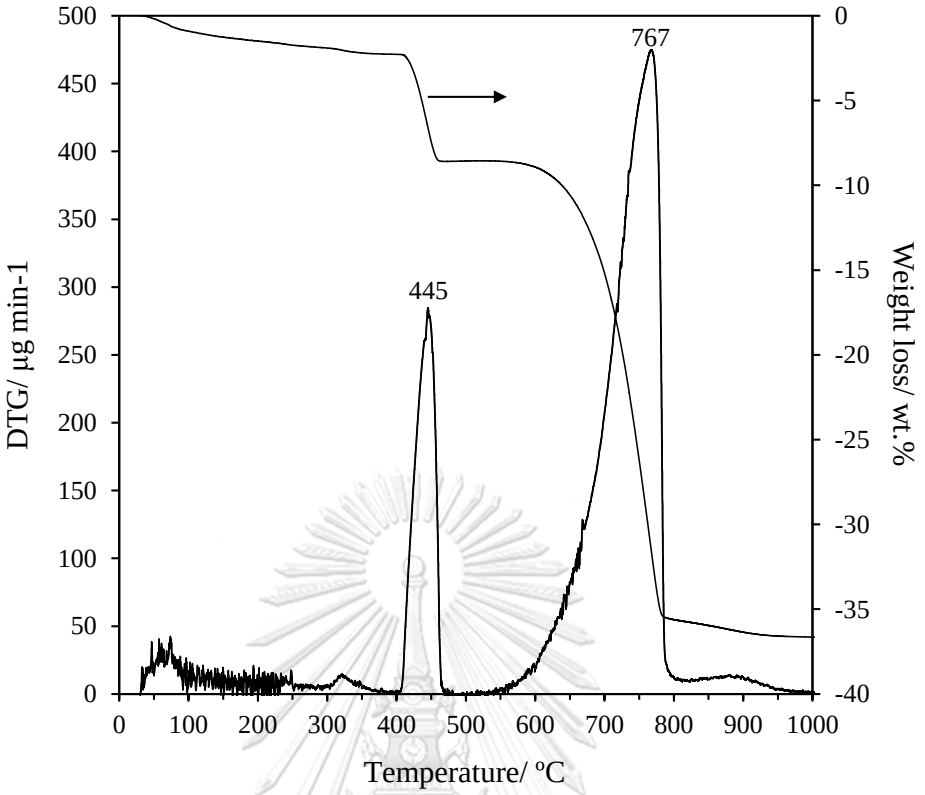


**Figure 6.3** Thermal decomposition pattern of as-received enamel venus shell.

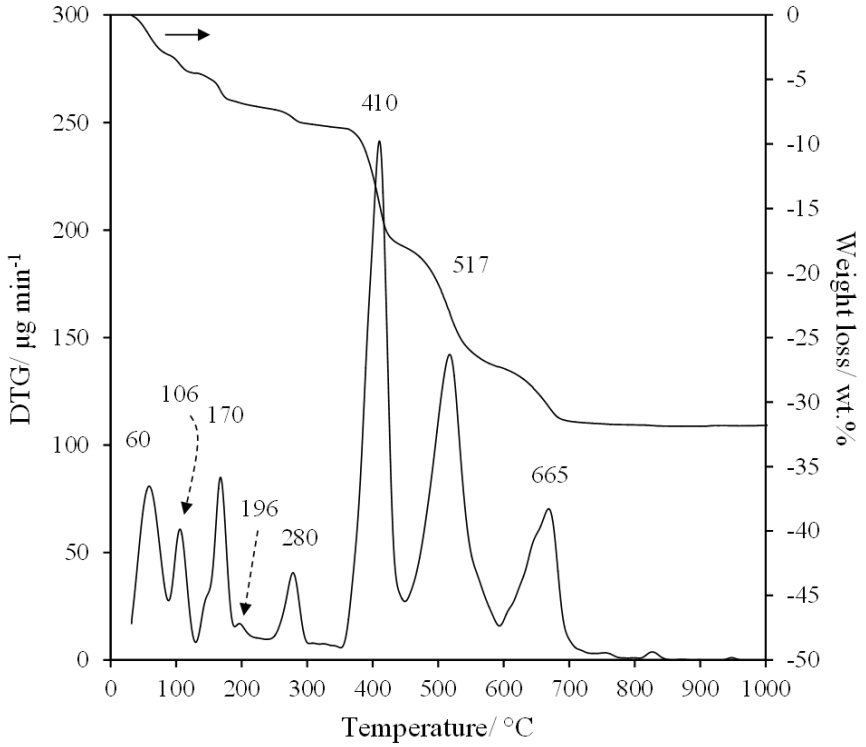


**Figure 6.4** Thermal decomposition pattern of as-prepared ZSAH extrudate (without HEC addition).

**Table 6.2** Phase composition of uncalcined ZSAH and ZSAH-400 prepared without adding HEC as determined by TGA technique

| Weight loss temperature (ºC) | Phase in ZSAH | Composition (wt%) | Phase in ZSAH-400 | Composition (wt%) |
|---|---|---|---|---|
| 0–100 | $H_2O$ (moisture) | 3.5 | - | - |
| 100–160 | $Zn_5(OH)_8(NO_3)_2.2H_2O$ | 5.1 | ZnO | 0.9 |
| 160–220 | $CaZn_2(OH)_6.2H_2O$ | 7.8 | CaO/ 2ZnO | 7.0 |
| 220–340 | $Al(OH)_3$ | 4.8 | $Al_2O_3$ | 25.6 |
| - | $Al_2O_3$ [a] | 16.8 | | |
| 340–450 | $Ca(OH)_2$ | 36.4 | CaO | 34.5 |
| 450–590 | $Ca(NO_3)_2$ | 14.0 | $Ca(NO_3)_2$ | 18.2 |
| 590–760 | $CaCO_3$ | 10.1 | $CaCO_3$ | 13.2 |
| | Total | 98.5 | | 100 |

[a] Corresponding to the quantity added in the synthesis mixture.

Figure 6.4 shows the weight loss and DTG curve of uncalcined ZSAH prepared without HEC addition, and their phase composition is summarized in Table 6.2. The weight loss of the as-prepared ZSAH occurred in multiple steps. The assignment of each decomposition step was compared with authentic compounds and the data related in the relating literature [89-95]. The as-prepared ZSAH was mainly composed of $Ca(OH)_2$ (36.4 wt%). $Zn_5(OH)_8(NO_3)_2 \cdot 2H_2O$ (5.1 wt%), $Al(OH)_3$ (4.8 wt%), $CaZn_2(OH)_6 \cdot 2H_2O$ (7.8 wt%) and $Ca(NO_3)_2$ (14.0 wt%) were generated from dissolution of $Zn(NO_3)_2$, $Al_2O_3$ and CaO precursors under acidic solution, followed by precipitation when the mixture pH was changed and water was removed during drying. The presence of $CaZn_2(OH)_6 \cdot 2H_2O$ and $Ca(NO_3)_2$ confirmed that $Ca^{2+}$ was dissolved from CaO. After calcination at 400 °C, $Ca(OH)_2$ and $CaZn_2(OH)_6 \cdot 2H_2O$ were converted to CaO. The CaO generated was considered an active phase in the transesterification of triglycerides with refluxed methanol [13, 14, 16, 25, 29, 81, 89, 96]. ZnO was generated from the decomposition of $Zn_5(OH)_8(NO_3)_2 \cdot 2H_2O$ and $CaZn_2(OH)_6 \cdot 2H_2O$, which was not active in the transesterification under the reaction conditions used in this study [91, 93]. $Al(OH)_3$ was dehydrated at 280 °C to form $Al_2O_3$ [92]. The $Ca(NO_3)_2$ and $CaCO_3$ remained were not active in the transesterification [29]. Since the HEC decomposition occurred at 200–400 °C (Figure 6.5), which interfered the quantification of phase composition, the ZSAH prepared with adding HEC was not analyzed by TGA technique.

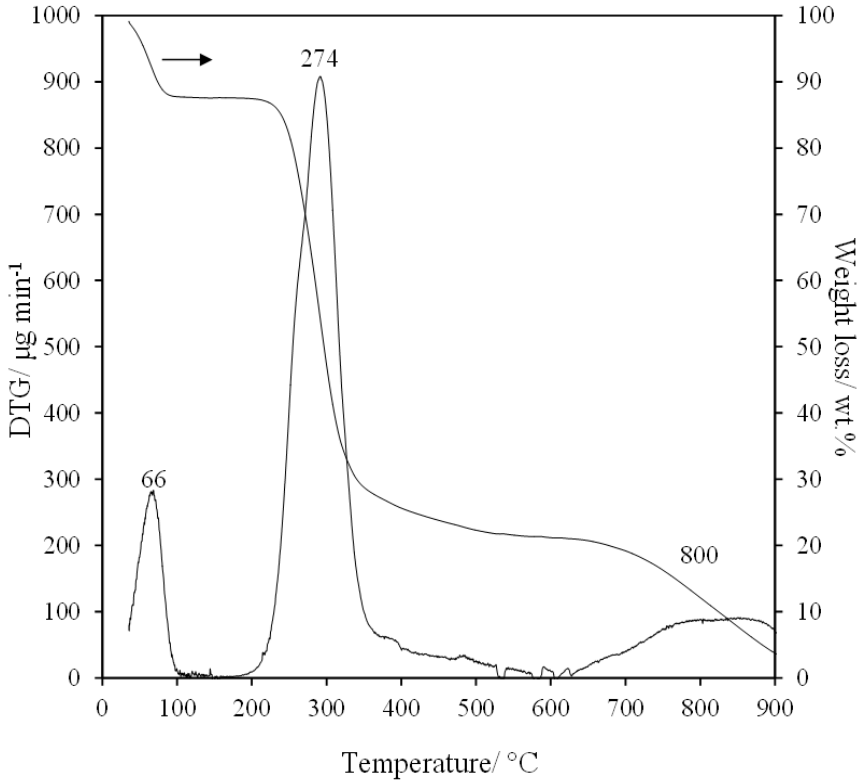


**Figure 6.5** Thermal decomposition pattern of HEC.

The XRD patterns of the as-prepared ZSAH and ZSAH-400 extrudates are shown in Figure 6.6. The as-prepared ZSAH was composed of $Ca(OH)_2$, $CaZn_2(OH)_6 \cdot 2H_2O$, and $CaCO_3$ phases. $Zn_5(OH)_8(NO_3)_2 \cdot 2H_2O$, $Ca(NO_3)_2$, $Al(OH)_3$, and $Al_2O_3$ were not found by XRD technique due to its low crystallinity. In the case of ZSAH-400, $CaZn_2(OH)_6 \cdot 2H_2O$ was decomposed concomitantly with the formation of CaO and ZnO as new phases. CaO was also obtained from the $Ca(OH)_2$ decomposition. Due to highly active nature of CaO, it was reacted with atmospheric moisture to obtain $Ca(OH)_2$ during the XRD analysis. Since the $Zn^{2+}$ dissolved was deposited on $Al_2O_3$, the solid-state reaction to $ZnAl_2O_4$ form can be generated at moderate temperatures. The atmospheric $CO_2$ chemically adsorbed onto CaO during catalyst preparation, which resulted in an increased intensity of $CaCO_3$ phase ($2\theta$ = 29.4°).

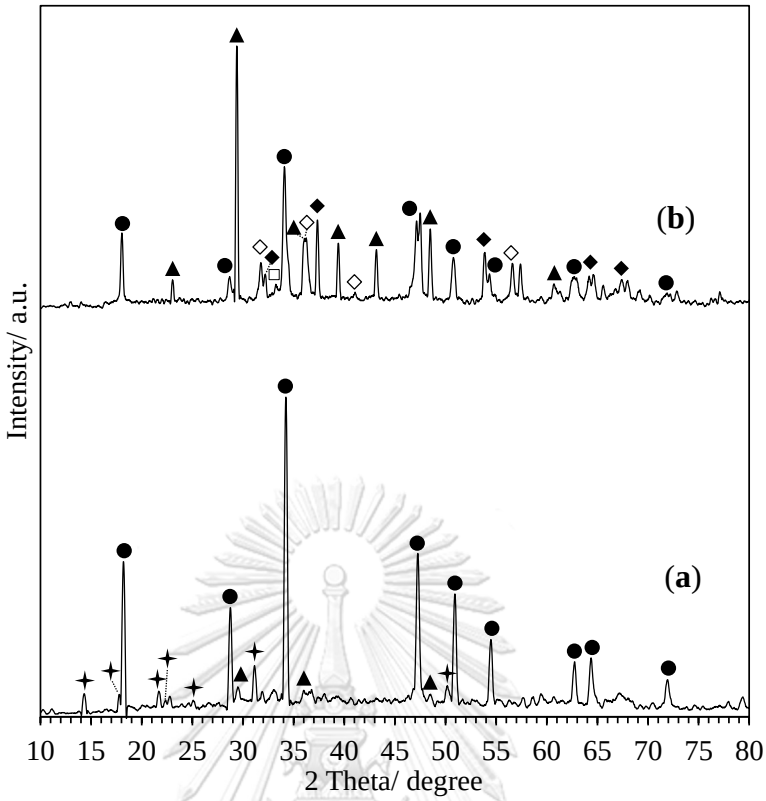


**Figure 6.6** XRD patterns of (a) uncalcined ZSAH and (b) ZSAH-400 prepared using single screw extruder. (Symbols: ▲ = $CaCO_3$, ◆ = CaO, ◇ = ZnO, ● = $Ca(OH)_2$, □ = $ZnAl_2O_4$ and ✦ = $CaZn_2(OH)_6.2H_2O$)

Optical microscopy (OM) images of side view and cross sections of as-prepared ZSAH and ZSAH-400 are shown in Figure 6.7. The as-prepared ZSAH had rough surfaces in both of side view and cross sections. The side-view and cross-section of ZSAH-400 remained similar. The SEM images of as-prepared ZSAH and ZSAH-400 are shown in Figure 6.8. The small particles with an average diameter of 0.50 μm were found in the as-prepared ZSAH, which were randomly packed along the length and on the cross-sectional area. Secondary pores (average size 20 nm) dispersed on the extrudate were generated by water released during the drying step. In the case of ZSAH-400, the small particles were together agglomerated to large particles and uniformly distributed in the calcined extrudate.

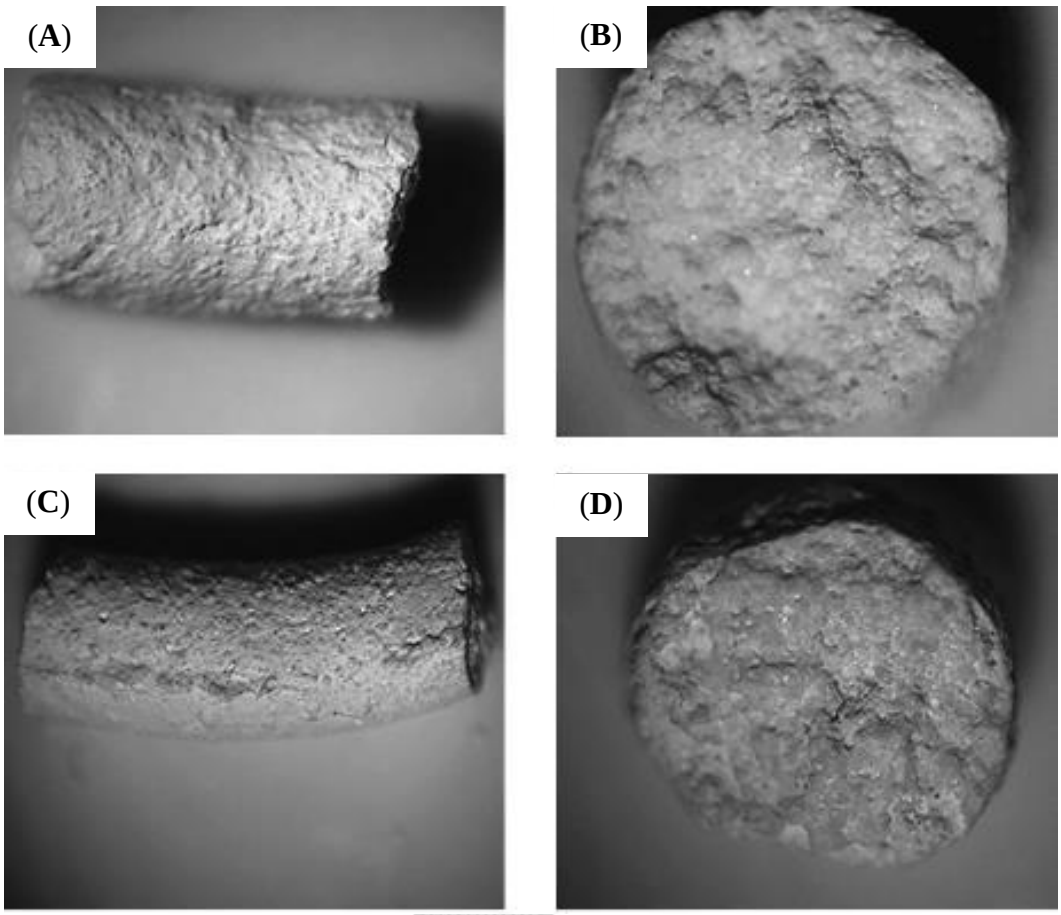


**Figure 6.7** OM images of as-prepared ZSAH (A) side view and (B) cross section, and (C) ZSAH-400 side view and (D) cross section.

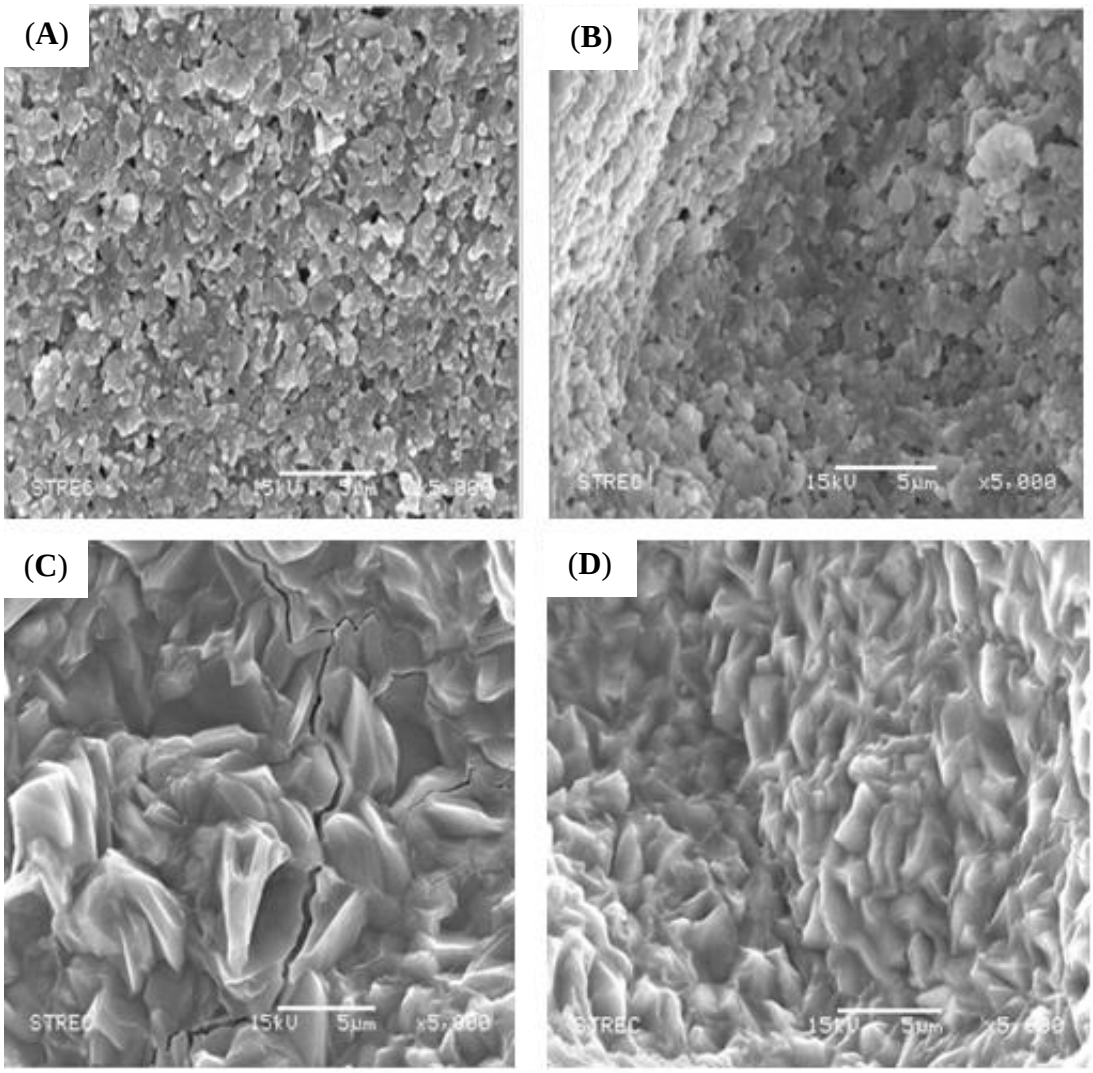


**Figure 6.8** SEM images of as-prepared ZSAH ((A) side view and (B) cross section) and ZSAH-400 ((C) side view and cross (D) section).



To compare the elemental composition on the surface with the bulk composition of ZSAH-400, EDX technique was used. The atomic ratio of Ca: Zn: Al on the surface was found to be 24.2: 6.1: 1, while the bulk composition (Ca: Zn: Al =5.4: 1: 1.6), calculated from the amount of metal precursors used in the catalyst preparation, was lower in Ca and Zn than that of the surface composition. These results confirm that the $Ca^{2+}$ and $Zn^{2+}$ dissolved in the synthesis mixture were precipitated as different types of Ca, Zn, and Al mixed compounds on the $Al_2O_3$ support.

The physicochemical properties of as-prepared ZSAH and calcined ZSAH-400 are summarized in Table 6.3. After the catalyst was calcined at 400 °C, the bulk density of extrudate obtained was not significantly changed, while the BET surface area of ZSAH-400 was increased from 4.23 to 6.40 $m^2\ g^{-1}$. It should be due to the

porosity as small surface fractures generated from the HEC decomposition. However, the crushing strength of ZSAH-400 was much lower than that of as-prepared ZSAH. The SEM images indicated that the microscale fractures observed on both sides of the ZSAH-400 surface (Figure 6.8 (C) and (D)). The fractures are probably related to HEC decomposition during calcination, which liberated water and $CO_2$ from the catalyst extrudates. Moreover, the crushing strength of the catalyst extrudate calcined at 800 °C was further decreased to 0.02 MPa. It is worth noting that, after ZSAH-400 was used in the fixed-bed reactor, the shape and size of the extrudate were not significantly changed although it had a low crushing strength (Figure 6.9). The fractures generated probably promoted the diffusion of triglycerides and methanol into interior active sites. When the catalyst was formulated, the basicity of the ZSAH-400 extrudate (9.3 μmol $g^{-1}$) was reduced from that of the ZSAH-400 powder (27.0 μmol $g^{-1}$). However, from preliminary reaction tests under batch conditions, the FAME yield obtained over the ZSAH-400 extrudate (97.9 wt%) and powdery ZSAH-400 (99.9 wt%) was slightly different because the extrudates were broken to small pieces by vigorous magnetic stirring.

**Table 6.3** Physicochemical properties of the ZSAH extrudates

| Catalyst | Bulk density (g $cm^{-3}$) | Crushing strength[a] (MPa) | $S_{BET}$[b] | $V_p$[c] | $D_p$[d] | Total basicity[e] | FAME yield[f] |
|---|---|---|---|---|---|---|---|
| ZSAH | 1.01 | 1.15 | 4.23 | 6.5 | 52.8 | *n.d.* | 49.9 |
| ZSAH-400 | 0.96 | 0.13 | 6.40 | 9.0 | 42.7 | 9.3 | 97.9 |
| ZSAH-400[g] | *n.d.* | *n.d.* | 3.82 | 11.1 | 118.2 | 27.0 | 99.9 |
| ZSAH-800 | 0.99 | 0.02 | *n.d.* | *n.d.* | *n.d.* | *n.d.* | 85.9 |

[a] Determined by ASTM D-4179-82.
[b] BET surface area ($m^2$ $g^{-1}$)
[c] Total pore volume ($mm^3$ $g^{-1}$)
[d] Average pore size (Å)
[e] Determined by $CO_2$ pulse chemisorption. (μmol $g^{-1}$)
[f] Reaction conditions: methanol: oil molar ratio, 30: 1; catalyst amount, 10 wt%; temperature, 65 °C; time, 3 h. (wt%)
[g] The ZSAH-400 powder
*n.d.* means not determined.

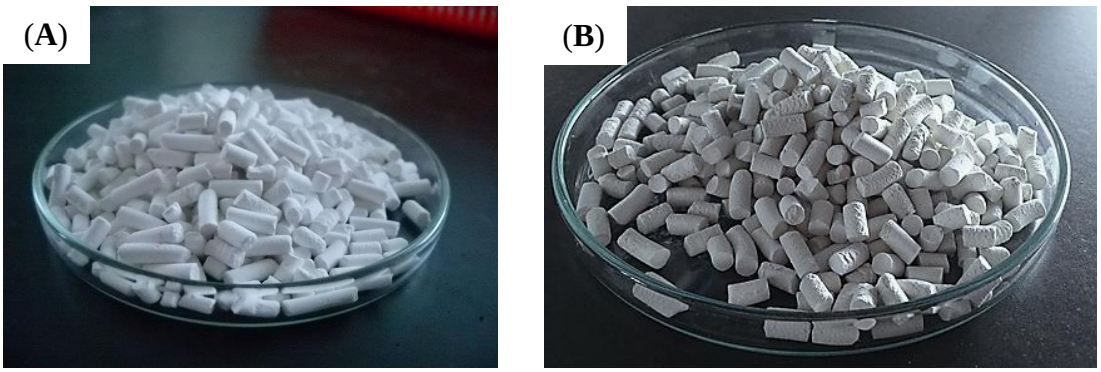


**Figure 6.9** Photographs of the ZSAH-400 extrudates (A) before and (B) after being used in the transesterification of palm oil with methanol in the fixed-bed reactor.

## 6.3 Effect of premixing of methanol, palm kernel oil, and CMEs with ZSAH catalyst extrudates

### 6.3.1 Miscibility of methanol–oil–CME system

In this work, the miscibility of the methanol–oil–CME system was investigated because the FAME as a co-solvent was added in order to improve the mass transfer of the reaction system [14]. Figure 6.10 shows a three phase diagram for methanol, palm kernel oil, and $C_{12}$–$C_{14}$ CMEs. The separate phases were found in all proportions of methanol and palm oil, but the $C_{12}$–$C_{14}$ CMEs were miscible with either methanol or palm oil. A large amount of the CMEs added into a mixture of methanol and oil induced a miscible phase in the system. It was explained by molecular structure of methyl esters consisting of the ester group as hydrophilic head and long hydrocarbon chains as hydrophobic tails, which enables them to dissolve well in both triglycerides and methanol. It was reported that FAME can behave like a surfactant [97], which promotes the formation of microemulsions in triglycerides-in-methanol and methanol-in-triglycerides systems [25]. Therefore, the CME addition enhanced the solubility of oil in methanol or that of methanol in oil.

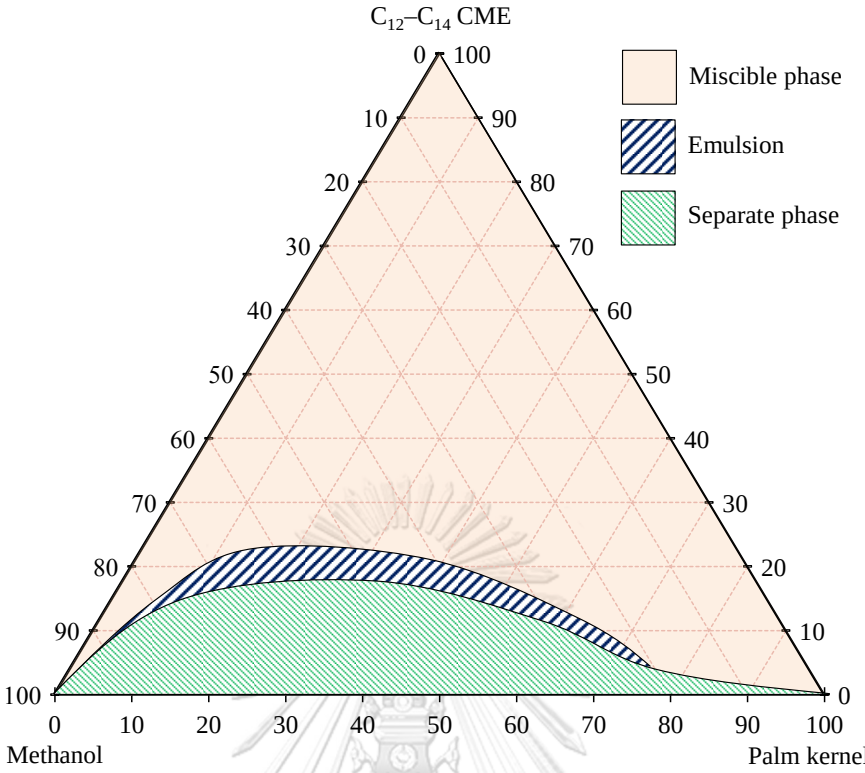


**Figure 6.10** Ternary diagram of methanol, palm kernel oil and the $C_{12}$–$C_{14}$ CMEs based on volume fraction.

### 6.3.2 Transesterification over ZSAH-400 extrudates premixed with methanol, palm kernel oil, and $C_{12}$–$C_{14}$ CMEs

Figure 6.11 shows dependence of FAME yield on time on stream in the continuous transesterification of palm oil with methanol over the ZSAH-400 extrudates in the fixed-bed reactor. The feed flow rate of methanol and oil was maintained at a constant molar ratio of 30: 1 (50 vol%) in which the oil and methanol mixture exhibited a separate phase. The effluent was collected and analyzed to determine the FAME yield after a time-on-stream of 120 min. During the increasing of FAME yield from 39% to 65% within 240 min, the separate phase of methanol and oil was transformed to miscible phase, which was visually observed inside the column reactor. This result indicates that the FAME generated from the reaction enhanced the methanol–oil solubility, and probably promoted contact between the reactant molecules and the catalyst surface.

The ZSAH-400 extrudate premixed with methanol gave an initial FAME yield of 40.1 wt%, which was similar to the reaction performed on the extrudates without premixing. It should be because the reaction in the pristine case was started up in the presence of methanol (*See* Section 3.10). However, the FAME yield obtained from premixing with methanol was enhanced to 96.8% at 360 min. It was explained by an

enhanced formation of methoxide species on the surface since the extrudate catalyst was premixed with methanol overnight. According to Kouzu *et al*., the methoxide species can be easily generated on the CaO surface at room temperature [26]. Although the catalyst surface was largely covered by methoxide species, the initial stage of the reaction was essentially controlled by diffusion of bulky triglyceride molecules to the hydrophilic catalyst surface through the adsorbed methanol layer. This result was similar to the case without premixing, which the FAME yield was increased when the FAME generated from the reaction reduced the mass transfer limitation of the reaction system.

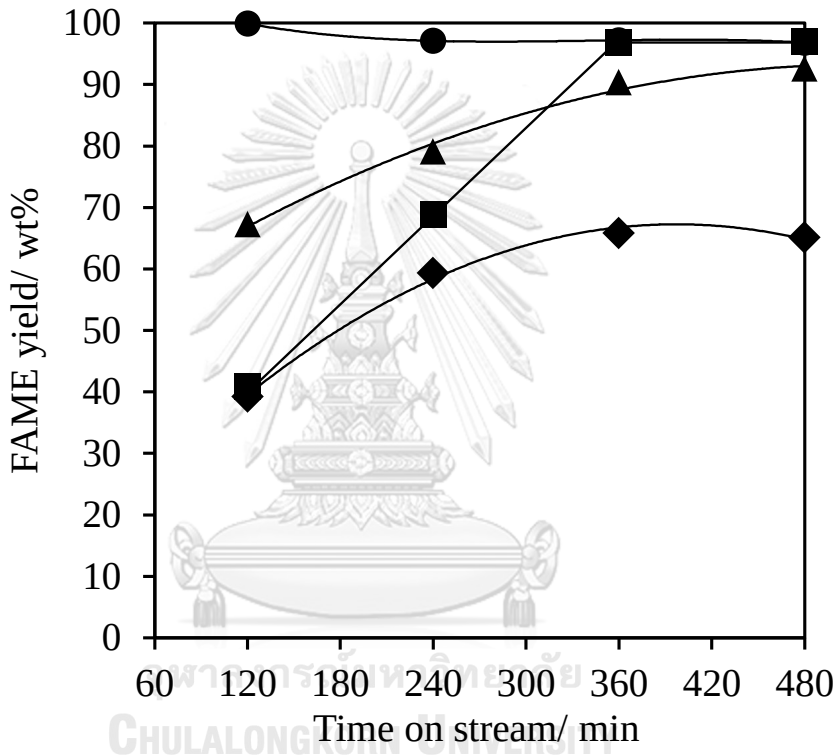


**Figure 6.11** Dependence of FAME yield on time on stream in the continuous transesterification of palm oil with methanol over the ZSAH-400 extrudates (♦) without premixing and (■) premixed with methanol, (▲) palm kernel oil and (●) the $C_{12}$–$C_{14}$ CMEs. Reaction conditions: methanol: oil molar ratio, 30: 1; LHSV, 1.43 $h^{-1}$; temperature, 65 °C.

The ZSAH-400 extrudate premixed with palm kernel oil gave an initial FAME yield of 67.3% at 120 min. The FAME yield obtained in this case was higher than that of premixing the extrudate with methanol. The result suggests that diffusion of methanol into the catalyst surface through the adsorbed triglyceride layer was faster than that of triglyceride through the adsorbed methanol layer due to a favorable interaction between methanol and the catalyst surface both of which had hydrophilic

properties. The FAME yield was increased to 92.6% within 480 min due to a high initial concentration of triglyceride reactants. Besides, the formation of FAME products promoted the methanol–oil miscibility.

### 6.3.3 Replacement of methanol and triglycerides onto ZSAH-400 extrudates premixed with $C_{12}$–$C_{14}$ CMEs and solubility parameter

The TGA technique was used to reveal the advantages of the ZSAH-400 extrudates premixed $C_{12}$–$C_{14}$ CMEs. Figure 6.12 shows the thermal decomposition patterns of the ZSAH-400 extrudates premixed with different organic substances. The methanol adsorbed in ZSAH-400 extrudates was evaporated at temperatures below 100 °C (Figure 6.12 (A)). The multistep weight losses (>400 °C) observed were inorganic species, such as rehydrated $Ca(OH)_2$, $Ca(NO_3)_2$, and $CaCO_3$ remaining, as shown in Figure 6.4. Figure 6.12 (B) shows multiple steps of weight losses in the range of 200–400 °C for the extrudate premixed with palm kernel oil. The ZSAH-400 extrudates premixed with $C_{12}$–$C_{14}$ CMEs showed a main weight loss at 174 °C (Figure 6.12 (C)). In a subsequent experiment, the ZSAH-400 extrudates were previously mixed with $C_{12}$–$C_{14}$ CMEs overnight, followed by immersion in methanol or palm kernel oil as shown in Figure 6.12 (D) and (E), respectively. The main weight loss observed at 174 °C, corresponding to $C_{12}$–$C_{14}$ CMEs, disappeared concomitantly with the appearance of patterns derived from methanol or palm kernel oil. The results indicated that methanol and triglycerides replaced the layer of $C_{12}$–$C_{14}$ CMEs adsorbed onto the ZSAH-400 extrudates due to a high solubility of these reactants in methyl esters (Figure 6.9). According to the composition of reaction products obtained over the ZSAH extrudate premixed with $C_{12}$–$C_{14}$ CMEs, it should be noted that the CMEs used in the premixing was completely replaced at the early stage of the operation (120 min). Subsequently, the FAME generated from the reaction was, therefore, a main contribution to promote contact between the reactant molecules and the catalyst surface by reducing the mass transfer limitation in the reaction system.

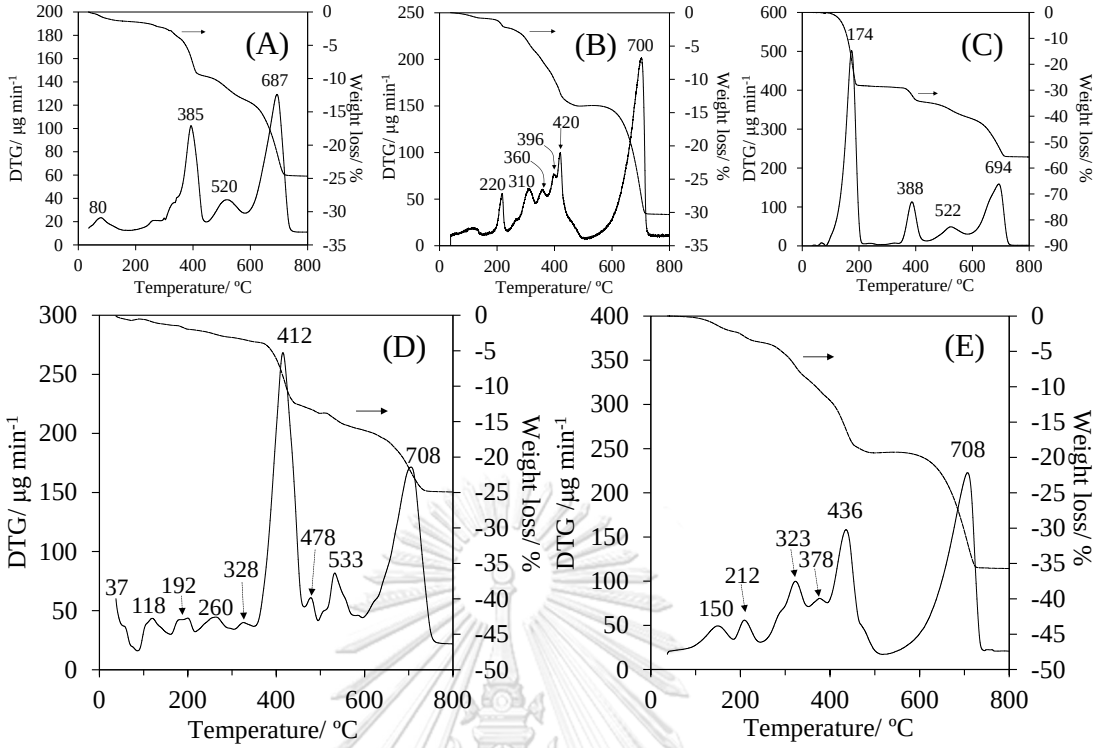


**Figure 6.12** Thermal decomposition patterns of the ZSAH-400 extrudates premixed with (A) methanol, (B) palm kernel oil, (C) the $C_{12}$–$C_{14}$ CMEs and the extrudates premixed with the $C_{12}$–$C_{14}$ CMEs, followed by (E) immersing in methanol or (F) palm kernel oil.

The solubility parameter (δ; (cal $cm^{-3}$)$^{1/2}$) was used to consider the compatibility of methanol and palm oil as reactants with the CME layer coated on the catalyst extrudate. The parameter can be calculated using Eq. (6.1) [98]:

$$\delta = \frac{\rho \sum G}{M} \qquad (6.1)$$

where ρ is the density (g $mL^{-1}$), G is the group molar attraction constant ((cal $cm^3$)$^{1/2}$ $mol^{-1}$), and M is the molecular weight (g $mol^{-1}$). The solubility of two liquid components is related to the heat of mixing ($\Delta H_M$; kJ $mol^{-1}$), which is determined by the difference between their solubility parameters, as shown in Eq. (6.2):

$$\Delta H_M = V_M[(\delta_1 - \delta_2)^2 v_1 v_2] \qquad (6.2)$$

where $V_M$ is the molar volume of the mixture ($cm^3$ $mol^{-1}$), while $v_1$ and $v_2$ are respectively the volume fraction of component 1 and 2 in the mixture. Based on

thermodynamic consideration, a change in Gibbs free energy on mixing ($\Delta G_M$; kJ $mol^{-1}$) depends on the magnitude of $\Delta H_M$ as follows:

$$\Delta G_M = \Delta H_M - T\Delta S_M \quad (6.3)$$

where T is the absolute temperature (K) and $\Delta S_M$ is the entropy of mixing (kJ $mol^{-1}$ $K^{-1}$). If the liquid components have similar solubility parameters, $\Delta H_M$ becomes small. A spontaneous dissolution of two liquid components occurs when the calculated $\Delta G_M$ has negative value.

According to Eq. (6.1), the solubility parameter of $C_{12}$–$C_{14}$ CMEs was calculated to be 8.31 $(cal\ cm^{-3})^{1/2}$. This value was in between those of methanol (9.47 $(cal\ cm^{-3})^{1/2}$) and palm kernel oil (7.88 $(cal\ cm^{-3})^{1/2}$). It confirmed that methanol or oil was readily dissolved in the CME phase, while the mixing of methanol and oil together was less spontaneous. Nevertheless, the solubility parameter calculated for methanol might be underestimated since methanol has a strong intermolecular interaction via hydrogen bonding, which was not considered in Eq. (6.1). Alternatively, the solubility parameter was calculated by Hansen equation in which various interactions between molecules are taken into account (Eq. (6.4)) [99].

$$\delta_t^2 = \delta_d^2 + \delta_p^2 + \delta_h^2 \quad (6.4)$$

where $\delta_t$ is the total solubility parameter, $\delta_d$ is the non-polar (dispersion) interactions, $\delta_p$ is the polar (dipole–dipole and dipole–induced dipole) interactions, and $\delta_h$ is the hydrogen bonding. The calculation indicates that the total solubility parameter of methanol was 14.5 $(cal\ cm^{-3})^{1/2}$ [100], which was 1.7-fold higher than the solubility parameter of $C_{12}$–$C_{14}$ CMEs. As revealed in the three-phase diagram (Figure 6.9), a high miscibility of methanol and CMEs in all proportions should be attributed to hydrogen bonding between the hydroxyl group of methanol and the ester group of CMEs.

### 6.3.4 Effect of premixing of ZSAH catalyst extrudate with different types of CMEs

**Table 6.4** Calculated solubility parameters of CMEs with different fatty acid chain lengths and related group molar attraction constants (*G*)

| CME type | Solubility parameter (cal $cm^{-3}$)$^{1/2}$ |
|---|---|
| Methyl octanoate ($C_9H_{18}O_2$) | 8.51 |
| Methyl decanoate ($C_{11}H_{22}O_2$) | 8.43 |
| Methyl laurate ($C_{13}H_{26}O_2$) | 8.39 |
| Methyl myristate ($C_{15}H_{30}O_2$) | 8.23 |
| Methyl palmitate ($C_{17}H_{34}O_2$) | 8.19 |
| Methyl stearate ($C_{19}H_{38}O_2$) | 8.16 |
| Methyl oleate ($C_{19}H_{36}O_2$) | 8.09 |
| Methyl linoleate ($C_{19}H_{34}O_2$) | 7.96 |

Group molar attraction constants at 25 °C [98]

| Group | *G* (cal $cm^3$)$^{1/2}$ $mol^{-1}$ |
|---|---|
| $–CH_3$ (single bonded) | 214 |
| $–CH_2–$ (single bonded) | 133 |
| –CH= (double bonded) | 111 |
| –OOC– (ester) | 310 |

According to Eq. (6.1), the solubility parameters of $C_8$–$C_{18}$ CMEs were calculated and summarized in Table 6.4. It can be seen that the solubility parameters of these methyl esters were similar in the range 7.96–8.51 (cal $cm^{-3}$)$^{1/2}$. Figure 6.13 shows the dependence of FAME yield on time on stream in the continuous transesterification of palm oil with methanol over the ZSAH-400 extrudates premixed with CMEs with different fatty acid chain lengths. The premixed extrudates gave a stable FAME yield of 96.5% since the early stage of the operation, regardless of the type of CMEs used for premixing. Based on the overall results, it can be concluded that the advantage of premixing the catalyst extrudates with different CMEs in the transesterification of triglycerides with methanol was a physical effect dominated by the high solubility of methanol and oil in the CME phase.

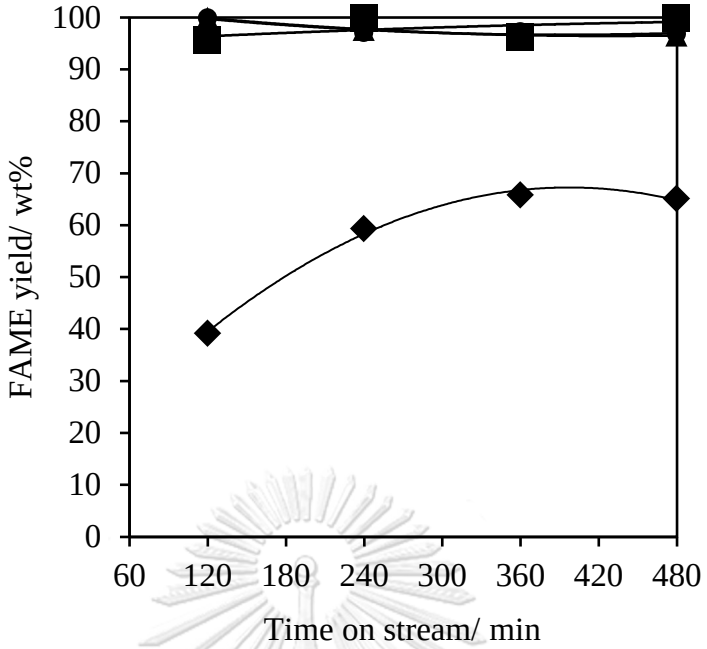


**Figure 6.13** Dependence of FAME yield on time on stream in the continuous transesterification of palm oil with methanol over the ZSAH-400 extrudates (♦) without premixing and premixed with the (▲) $C_8$–$C_{10}$, (●) $C_{12}$–$C_{14}$ and (■) $C_{16}$–$C_{18}$ CMEs. Reaction conditions: *see* Figure 6.11.

### 6.3.5 Proposed model for the diffusion of triglycerides and methanol to the surface of catalyst extrudates premixing with CME

Figure 6.14 shows a simplified model for beneficial effects of premixing the catalyst extrudates with CMEs on the transesterification**.** The reaction mechanism of triglycerides with methanol on the catalyst surface occurred through the Eley–Rideal mechanism [14]. At the start-up period of ZSAH-400 extrudate without premixing, the surface of the fresh catalyst was covered with methanol. The methoxide species were formed on the basic sites of the catalyst. Transesterification of triglyceride with surface methoxide should be determined by diffusion of bulky triglyceride molecules passing through the methanol-rich layer. In the case of ZSAH-400 extrudate premixed with CMEs, the diffusion of methanol and triglycerides to the catalyst surface was facilitated by the CME-rich layer, as suggested by the TGA results (Figure 6.12). At the early stage of the fixed-bed operation, the mass transfer limitation was therefore reduced by premixing the ZSAH-400 extrudate with different CMEs. Subsequently, the FAME generated from the reaction increased the methanol–oil solubility, which promoted contact between the reactant molecules and the catalyst surface. As a result, the FAME yield (96.5%) was stably obtained throughout the operation.

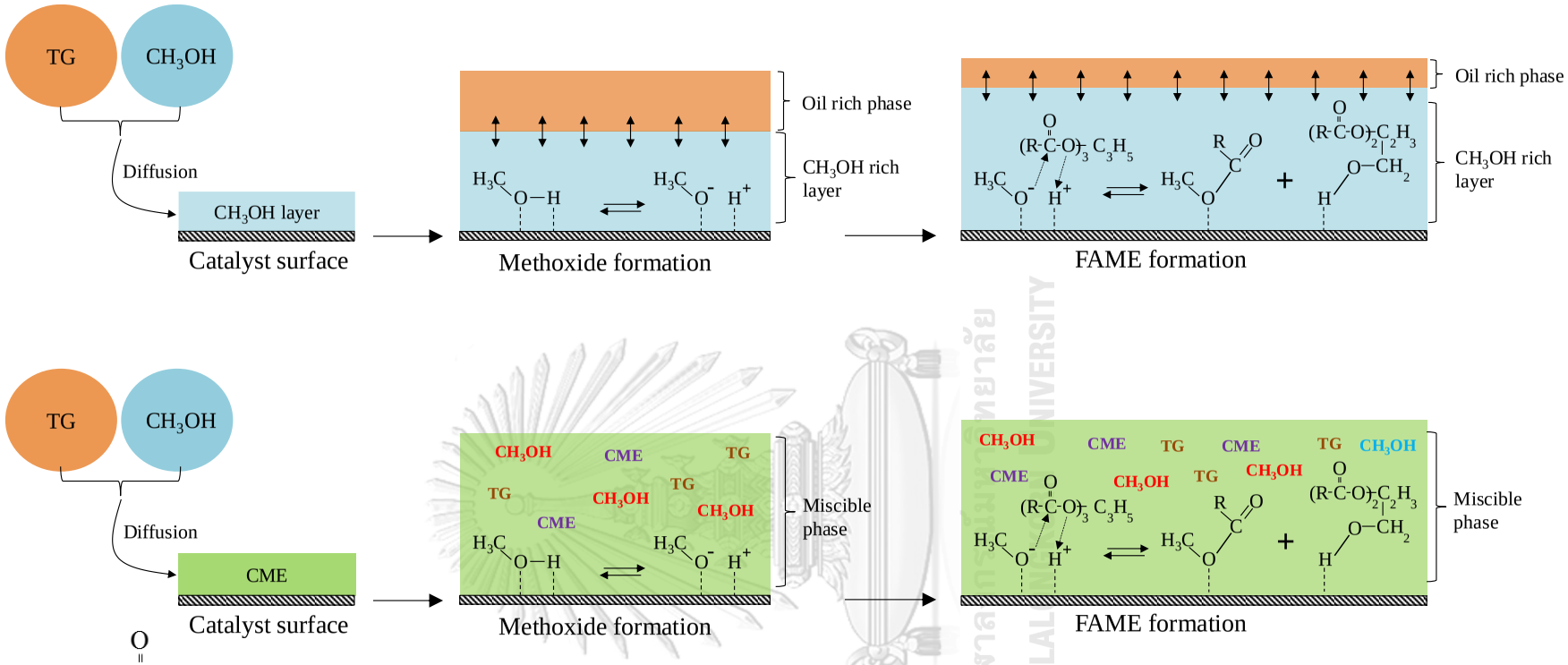


TG and $(R\text{-}\overset{O}{\overset{\|}{C}}\text{-}O)_3\ C_3H_5$ represent triglycerides as reactants.

CME represents the commercial fatty acid methyl esters used in the premixing of catalyst extrudates.

**Figure 6.14** Simplified model for the diffusion of triglycerides and methanol to the surface of catalyst extrudates (A) without premixing and (B) premixing with CME.

# CHAPTER VII
# Conclusions and recommendations

## 7.1 Conclusions

CaO was real active phase in CaO-800 and CaMgO-800 gave high FAME yield (≈90 wt%) in the transesterification after 10 min of reaction, whereas pure MgO obtained from $MgCO_3$ was not active. Although calcium content of the CaMgO-800 was less than that of the CaO-800, MgO presenting can reduced agglomeration and increased basic amount and strength in the catalyst. The cluster size and phase change were depended on calcination temperature and heating rate. The $MgO{\cdot}CaCO_3$ obtained from dolomite was generated when calcined at 750 °C using heating rate of 3 °C $min^{-1}$. The MgO was diffused on surface of mixed oxide, whereas the bulk was abundant of CaO. After direct reaction with methanol, the growth of $Ca(OCH_3)_2$ over CaMgO-800 was higher than that over CaO-800 because small cluster size of CaO was maintained by MgO presenting in calcined dolomite. In the case of direct reaction with glycerol, MgO presenting delayed the $Ca(C_3H_7O_3)_2$ formation because the MgO was not interacted with glycerol in this condition.

The crystallites of CaO obtained from mixed oxides were smaller than that of pure CaO. MgO presenting can reduced agglomeration of CaO particles and increased the surface area of MgO·CaMet and MgO·CaGly. The $Ca(C_3H_7O_3)_2$ as an active phase of CaGly and MgO·CaGly cannot be chemisorbed by $CO_2$ as a molecular probes. Therefore, the $Ca(C_3H_7O_3)_2$ must be required with methanol in order to change to an anion form before being used. The CaO and $Ca(OCH_3)_2$ can be reacted with $CO_2$ on surface. $CaCO_3$ and gradually transformed to $Ca(C_3H_7O_3)_2$ that can leach out. During the reaction, the CaO was rapidly changed to $Ca(OH)_2$ and stable and gave high FAME yield after fifth repetition. The $Ca(OCH_3)_2$ and $Ca(C_3H_7O_3)_2$ were completely changed to $CaCO_3$ phase after 10 days of exposing time, whereas CaO was firstly changed to $Ca(OH)_2$ and followed by carbonation. The $Ca(OH)_2$ generated by moisture can be reactive, but $CaCO_3$ was not reacted. The large crystallites of CaO obtained from CaO-800 were slowly reacted with moisture and $CO_2$ compared to small crystallites obtained from CaMgO-800.

The Ca-based catalysts in extrudate form were successfully prepared by dissolution–precipitation method. Although the addition of HEC enhanced the plasticity of the catalyst paste and facilitated extrusion, its decomposition generated microscale fractures, which decreased the crushing strength of the resulting extrudate. However, the mechanical strength, textural properties, and basicity of the catalyst extrudate were sufficient for biodiesel production *via* transesterification of palm oil

with methanol in a fixed-bed reactor under mild conditions. Since triglycerides and methanol are immiscible, the reaction on the catalyst extrudate premixed with either methanol or oil suffered from mass transfer problems. Premixing the catalyst extrudate with different types of CMEs resulted in a stable FAME yield of ≈96.5% throughout the operation. This beneficial effect arises from the high solubilities of both reactants in the CME layer covering the catalyst extrudate.

### 7.2 Recommendations for future works

- To confirm the MgO increased the activity of CaO, CaO mixed with other metals, such as ZnO, $Al_2O_3$ and $TiO_2$ was also investigated.
- To deeply study the effect of the crystal size on the activity in transesterification, the CaO at different crystal sizes should be prepared and catalyzed to produce FAME.
- To confirm the Ca-based glyceroxide catalysts catalyzed in homogeneous system, the leaching of $Ca^{2+}$ ion in the products over Ca-based catalysts should be tested.
- Since the Ca-based methoxide prepared had high stability, the Ca-based methoxide in extrudate form should be prepared and used to produce FAME in continuous reactor.
- To improve the crushing strength of the catalyst extrudates, the formulation process should be done by using a twin screw extruder or using of new binder.

## REFERENCES


[1] PERP (The ChemSystems Process Evaluation/Research Planning), Oleochemical, Report Abstract, April, 2012.

[2] F. Ma, M.A. Hanna, Biodiesel production: a review, Bioresource technology, 70 (1999) 1–15.

[3] L. Bournay, D. Casanave, B. Delfort, G. Hillion, J.A. Chodorge, New heterogeneous process for biodiesel production: A way to improve the quality and the value of the crude glycerin produced by biodiesel plants, Catalysis Today, 106 (2005) 190–192.

[4] C.H. Bartholomew, R.J. Farrauto, Fundamentals of Industrial Catalytic Processes, John Wiley & Sons, New Jersey, 2006.

[5] J. Benbow, J. Bridgwater, Paste Flow and Extrusion, Oxford University Press, Inc., New York, 1993.

[6] S. Jaiyen, T. Naree, C. Ngamcharussrivichai, Comparative study of natural dolomitic rock and waste mixed seashells as heterogeneous catalysts for the methanolysis of palm oil to biodiesel, Renewable Energy, 74 (2015) 433–440.

[7] M. Kouzu, T. Kasuno, M. Tajika, S. Yamanaka, J. Hidaka, Active phase of calcium oxide used as solid base catalyst for transesterification of soybean oil with refluxing methanol, Applied Catalysis A: General, 334 (2008) 357–365.

[8] M.L. Granados, M.D.Z. Poves, D.M. Alonso, R. Mariscal, F.C. Galisteo, R. Moreno-Tost, J. Santamaría, J.L.G. Fierro, Biodiesel from sunflower oil by using activated calcium oxide, Applied Catalysis B: Environmental, 73 (2007) 317–326.

[9] W. Jindapon, S. Jaiyen, C. Ngamcharussrivichai, Seashell-derived mixed compounds of Ca, Zn and Al as active and stable catalysts for the transesterification of palm oil with methanol to biodiesel, Energy Conversion and Management, 122 (2016) 535–543.

[10] A.A. Refaat, Biodiesel production using solid metal oxide catalysts, International Journal of Environmental Science & Technology, 8 (2011) 203–221.

[11] X. Liu, X. Piao, Y. Wang, S. Zhu, H. He, Calcium methoxide as a solid base catalyst for the transesterification of soybean oil to biodiesel with methanol, Fuel, 87 (2008) 1076–1082.

[12] M. Sánchez-Cantú, L.M. Pérez-Díaz, I. Pala-Rosas, E. Cadena-Torres, L. Juárez-Amador, E. Rubio-Rosas, M. Rodríguez-Acosta, J.S. Valente, Hydrated lime as an effective heterogeneous catalyst for the transesterification of castor oil and methanol, Fuel, 110 (2013) 54–62.

[13] X. Liu, H. He, Y. Wang, S. Zhu, X. Piao, Transesterification of soybean oil to biodiesel using CaO as a solid base catalyst, Fuel, 87 (2008) 216–221.

[14] M. Kouzu, T. Kasuno, M. Tajika, Y. Sugimoto, S. Yamanaka, J. Hidaka, Calcium oxide as a solid base catalyst for transesterification of soybean oil and its application to biodiesel production, Fuel, 87 (2008) 2798–2806.

[15] M.L. Granados, D.M. Alonso, I. Sádaba, R. Mariscal, P. Ocón, Leaching and homogeneous contribution in liquid phase reaction catalysed by solids: The case of triglycerides methanolysis using CaO, Applied Catalysis B: Environmental, 89 (2009) 265–272.

[16] S. Gryglewicz, Rapeseed oil methyl esters preparation using heterogeneous catalysts, Bioresource Technology, 70 (1999) 249–253.

[17] D. Bradley, E. Levin, C. Rodriguez, P.G. Williard, A. Stanton, A.M. Socha, Equilibrium studies of canola oil transesterification using a sodium glyceroxide catalyst prepared from a biodiesel waste stream, Fuel Processing Technology, 146 (2016) 70–75.
[18] S. Pradhan, J. Shen, S. Emami, P. Mohanty, S.N. Naik, A.K. Dalai, M.J.T. Reaney, Synthesis of potassium glyceroxide catalyst for sustainable green fuel (biodiesel) production, Journal of Industrial and Engineering Chemistry, 46 (2017) 266–272.
[19] E. Wang, J. Shen, Y. Wang, S. Tang, S. Emami, M.J.T. Reaney, Production of biodiesel with lithium glyceroxide, Fuel, 160 (2015) 621–628.
[20] D.M. Reinoso, D.E. Damiani, G.M. Tonetto, Zinc glycerolate as a novel heterogeneous catalyst for the synthesis of fatty acid methyl esters, Applied Catalysis B: Environmental, 144 (2014) 308–316.
[21] J. Lanas, J.I. Alvarez, Dolomitic limes: evolution of the slaking process under different conditions, Thermochimica Acta, 423 (2004) 1–12.
[22] A. Ketcong, W. Meechan, T. Naree, I. Seneevong, A. Winitsorn, S. Butnark, C. Ngamcharussrivichai, Production of fatty acid methyl esters over a limestone-derived heterogeneous catalyst in a fixed-bed reactor, Journal of Industrial and Engineering Chemistry, 20 (2014) 1665–1671.
[23] C. Ngamcharussrivichai, W. Meechan, A. Ketcong, K. Kangwansaichon, S. Butnark, Preparation of heterogeneous catalysts from limestone for transesterification of vegetable oils—Effects of binder addition, Journal of Industrial and Engineering Chemistry, 17 (2011) 587–595.
[24] J. Freiding, F.-C. Patcas, B. Kraushaar-Czarnetzki, Extrusion of zeolites: Properties of catalysts with a novel aluminium phosphate sintermatrix, Applied Catalysis A: General, 328 (2007) 210–218.
[25] M.L. Granados, D.M. Alonso, A.C. Alba-Rubio, R. Mariscal, M. Ojeda, P. Brettes, Transesterification of triglycerides by CaO: Increase of the reaction rate by biodiesel addition, Energy & Fuels 23 (2009) 2259–2263.
[26] M. Kouzu, J.-s. Hidaka, Transesterification of vegetable oil into biodiesel catalyzed by CaO: A review, Fuel, 93 (2012) 1–12.
[27] D.M. Marinković, M.V. Stanković, A.V. Veličković, J.M. Avramović, M.R. Miladinović, O.O. Stamenković, V.B. Veljković, D.M. Jovanović, Calcium oxide as a promising heterogeneous catalyst for biodiesel production: Current state and perspectives, Renewable and Sustainable Energy Reviews, 56 (2016) 1387–1408.
[28] W. Jindapon, S. Jaiyen, C. Ngamcharussrivichai, $Al_2O_3$-supported mixed Ca and Zn compounds prepared from waste seashells for synthesis of palm fatty acid methyl esters, Chemical Engineering Communications, 202 (2014) 1591–1599.
[29] C. Ngamcharussrivichai, P. Nunthasanti, S. Tanachai, K. Bunyakiat, Biodiesel production through transesterification over natural calciums, Fuel Processing Technology, 91 (2010) 1409–1415.
[30] N. Viriya-Empikul, P. Krasae, B. Puttasawat, B. Yoosuk, N. Chollacoop, K. Faungnawakij, Waste shells of mollusk and egg as biodiesel production catalysts, Bioresource Technology, 101 (2010) 3765–3767.
[31] Y.B. Cho, G. Seo, D.R. Chang, Transesterification of tributyrin with methanol over calcium oxide catalysts prepared from various precursors, Fuel Processing Technology, 90 (2009) 1252–1258.

[32] G.-Y. Chen, R. Shan, B.-B. Yan, J.-F. Shi, S.-Y. Li, C.-Y. Liu, Remarkably enhancing the biodiesel yield from palm oil upon abalone shell-derived CaO catalysts treated by ethanol, Fuel Processing Technology, 143 (2016) 110–117.
[33] X. Yin, X. Duan, Q. You, C. Dai, Z. Tan, X. Zhu, Biodiesel production from soybean oil deodorizer distillate usingcalcined duck eggshell as catalyst, Energy Conversion and Management, 112 (2016) 199–207.
[34] B. Yoosuk, P. Udomsap, B. Puttasawat, P. Krasae, Modification of calcite by hydration–dehydration method for heterogeneous biodiesel production process: The effects of water on properties and activity, Chemical Engineering Journal, 162 (2010) 135–141.
[35] R.S. Watkins, A.F. Lee, K. Wilson, Li–CaO catalysed tri-glyceride transesterification for biodiesel applications, Green Chemistry, 6 (2004) 335–340.
[36] C.S. MacLeod, A.P. Harvey, A.F. Lee, K. Wilson, Evaluation of the activity and stability of alkali-doped metal oxide catalysts for application to an intensified method of biodiesel production, Chemical Engineering Journal, 135 (2008) 63–70.
[37] M. Zabeti, W.M.A.W. Daud, M.K. Aroua, Optimization of the activity of $CaO/Al_2O_3$ catalyst for biodiesel production using response surface methodology, Applied Catalysis A: General, 366 (2009) 154–159.
[38] S. Benjapornkulaphong, C. Ngamcharussrivichai, K. Bunyakiat, $Al_2O_3$-supported alkali and alkali earth metal oxides for transesterification of palm kernel oil and coconut oil, Chemical Engineering Journal, 145 (2009) 468–474.
[39] C. Samart, C. Chaiya, P. Reubroycharoen, Biodiesel production by methanolysis of soybean oil using calcium supported on mesoporous silica catalyst, Energy Conversion and Management, 51 (2010) 1428–1431.
[40] M.C.G. Albuquerque, I. Jiménez-Urbistondo, J. Santamaría-González, J.M. Mérida-Robles, R. Moreno-Tost, E. Rodríguez-Castellón, A. Jiménez-López, D.C.S. Azevedo, C.L. Cavalcante Jr, P. Maireles-Torres, CaO supported on mesoporous silicas as basic catalysts for transesterification reactions, Applied Catalysis A: General, 334 (2008) 35–43.
[41] S. Yan, H. Lu, B. Liang, Supported CaO catalysts used in the transesterification of rapeseed oil for the purpose of biodiesel production, Energy & Fuels, 22 (2008) 646–651.
[42] W. Xie, L. Zhao, Production of biodiesel by transesterification of soybean oil using calcium supported tin oxides as heterogeneous catalysts, Energy Conversion and Management, 76 (2013) 55–62.
[43] C. Rodriguez-Navarro, K. Kudlacz, E. Ruiz-Agudo, The mechanism of thermal decomposition of dolomite: New insights from 2D-XRD and TEM analyses, American Mineralogist, 97 (2012) 38–51.
[44] K. Sasaki, X. Qiu, Y. Hosomomi, S. Moriyama, T. Hirajima, Effect of natural dolomite calcination temperature on sorption of borate onto calcined products, Microporous and Mesoporous Materials, 171 (2013) 1–8.
[45] C. Xu, D.I. Enache, R. Lloyd, D.W. Knight, J.K. Bartley, G.J. Hutchings, MgO catalysed triglyceride transesterification for biodiesel synthesis, Catalysis Letters, 138 (2010) 1–7.
[46] M. Verziu, B. Cojocaru, J. Hu, R. Richards, C. Ciuculescu, P. Filip, V.I. Parvulescu, Sunflower and rapeseed oil transesterification to biodiesel over different nanocrystalline MgO catalysts, Green Chemistry, 10 (2008) 373–381.

[47] K. Wilson, C. Hardacre, A.F. Lee, J.M. Montero, L. Shellard, The application of calcined natural dolomitic rock as a solid base catalyst in triglyceride transesterification for biodiesel synthesis, Green Chemistry, 10 (2008) 654–659.
[48] S.L. Niu, M.J. Huo, C.M. Lu, M.Q. Liu, H. Li, An investigation on the catalytic capacity of dolomite in transesterification and the calculation of kinetic parameters, Bioresource Technology, 158 (2014) 74–80.
[49] S.H. Teo, U. Rashid, S.Y. Thomas Choong, Y.H. Taufiq-Yap, Heterogeneous calcium-based bimetallic oxide catalyzed transesterification of *Elaeis guineensis* derived triglycerides for biodiesel production, Energy Conversion and Management, 141 (2017) 20–27.
[50] Y.L. Meng, B.Y. Wang, S.F. Li, S.J. Tian, M.H. Zhang, Effect of calcination temperature on the activity of solid Ca/Al composite oxide-based alkaline catalyst for biodiesel production, Bioresource Technology, 128 (2013) 305–309.
[51] S. Yan, M. Kim, S.O. Salley, K.Y.S. Ng, Oil transesterification over calcium oxides modified with lanthanum, Applied Catalysis A: General, 360 (2009) 163–170.
[52] X. Yu, Z. Wen, H. Li, S.-T. Tu, J. Yan, Transesterification of *Pistacia chinensis* oil for biodiesel catalyzed by $CaO–CeO_2$ mixed oxides, Fuel, 90 (2011) 1868–1874.
[53] C. Ngamcharussrivichai, P. Totarat, K. Bunyakiat, Ca and Zn mixed oxide as a heterogeneous base catalyst for transesterification of palm kernel oil, Applied Catalysis A: General, 341 (2008) 77–85.
[54] D. Molaei Asghar, M. Ghasemi, Transesterification of waste cooking oil to biodiesel using Ca and Zr mixed oxides as heterogeneous base catalysts, Fuel Processing Technology, 97 (2012) 45–51.
[55] S. Limmanee, T. Naree, K. Bunyakiat, C. Ngamcharussrivichai, Mixed oxides of Ca, Mg and Zn as heterogeneous base catalysts for the synthesis of palm kernel oil methyl esters, Chemical Engineering Journal, 225 (2013) 616–624.
[56] M. Kouzu, J.-s. Hidaka, K. Wakabayashi, M. Tsunomori, Solid base catalysis of calcium glyceroxide for a reaction to convert vegetable oil into its methyl esters, Applied Catalysis A: General, 390 (2010) 11–18.
[57] I. Lukić, Ž. Kesić, M. Zdujić, D. Skala, Calcium diglyceroxide synthesized by mechanochemical treatment, its characterization and application as catalyst for fatty acid methyl esters production, Fuel, 165 (2016) 159–165.
[58] I. Reyero, G. Arzamendi, L.M. Gandía, Heterogenization of the biodiesel synthesis catalysis: CaO and novel calcium compounds as transesterification catalysts, Chemical Engineering Research and Design, 92 (2014) 1519–1530.
[59] D. Soares Ana Paula, J. Puna, J. Gomes, C. Neiva Maria Joana, J. Bordado, Biodiesel production over lime. Catalytic contributions of bulk phases and surface Ca species formed during reaction, Renewable Energy, 99 (2016) 622–630.
[60] S.N. Csernica, J.T. Hsu, The phase behavior effect on the kinetics of transesterification reactions for biodiesel production, Industrial & Engineering Chemistry Research, 51 (2012) 6340–6349.
[61] O.S. Stamenkovic, V.B. Veljkovic, Z.B. Todorovic, M.L. Lazic, I.B. Bankovic-Ilic, D.U. Skala, Modeling the kinetics of calcium hydroxide catalyzed methanolysis of sunflower oil, Bioresource Technology, 101 (2010) 4423–4430.
[62] V.G. Deshmane, Y.G. Adewuyi, Synthesis and kinetics of biodiesel formation via calcium methoxide base catalyzed transesterification reaction in the absence and presence of ultrasound, Fuel, 107 (2013) 474–482.

[63] N. Pasupulety, K. Gunda, Y. Liu, G.L. Rempel, F.T.T. Ng, Production of biodiesel from soybean oil on $CaO/Al_2O_3$ solid base catalysts, Applied Catalysis A: General, 452 (2013) 189–202.
[64] H. Hideshi, S. Masaomi, K. Hajime, Alcoholysis of ester and epoxide catalyzed by solid bases, Studies in Surface Science and Catalysis, 130 (2000) 3507–3512.
[65] Y.C. Sharma, B. Singh, J. Korstad, Application of an efficient nonconventional heterogeneous catalyst for biodiesel synthesis from pongamia pinnata oil, Energy & Fuels, 24 (2010) 322–3231.
[66] H. Masood, R. Yunus, T.S.Y. Choong, U. Rashid, Y.H. Taufiq Yap, Synthesis and characterization of calcium methoxide as heterogeneous catalyst for trimethylolpropane esters conversion reaction, Applied Catalysis A: General, 425–426 (2012) 184–190.
[67] S. Ulf, S. Ricardo, V. Rogério Matheus, Transesterification of vegetable oils: a Review, Journal of the Brazilian Chemical Society, 9 (1998) 199–210.
[68] M. Kouzu, J.-s. Hidaka, Y. Komichi, H. Nakano, M. Yamamoto, A process to transesterify vegetable oil with methanol in the presence of quick lime bit functioning as solid base catalyst, Fuel, 88 (2009) 1983–1990.
[69] M. Kouzu, S.-y. Yamanaka, J.-s. Hidaka, M. Tsunomori, Heterogeneous catalysis of calcium oxide used for transesterification of soybean oil with refluxing methanol, Applied Catalysis A: General, 355 (2009) 94–99.
[70] Y.H. Taufiq-Yap, H.V. Lee, R. Yunus, J.C. Juan, Transesterification of non-edible *Jatropha curcas* oil to biodiesel using binary Ca–Mg mixed oxide catalyst: Effect of stoichiometric composition, Chemical Engineering Journal, 178 (2011) 342–347.
[71] F. Demir, B. Dönmez, H. Okur, F. Sevim, Calcination kinetic of magnesite from thermogravimetric data, Chemical Engineering Research and Design, 81 (2003) 618–622.
[72] A. Palandri, P. Gilot, G. Prado, A kinetic study of the decarbonation of $CaCO_3$, Journal of Analytical and Applied Pyrolysis, 27 (1993) 119–130.
[73] A.E. Milodowski, D.J. Morgan, Thermal analysis studies of the dolomite-ferroan dolomite-ankerite series. II. Decomposition mechaism in flowing $CO_2$ atmosphere, Thermochimica Acta, 152 (1989) 279–297.
[74] J.M. Montero, M.A. Isaacs, A.F. Lee, J.M. Lynam, K. Wilson, The surface chemistry of nanocrystalline MgO catalysts for FAME production: An in situ XPS study of $H_2O$, $CH_3OH$ and $CH_3OAc$ adsorption, Surface Science, 646 (2016) 170–178.
[75] D.E. Haycock, M. Kasrai, C.J. Nicholls, D.S. Urch, The electronic structure of magnesium hydroxide (brucite) using X-ray emission, X-ray photoelectron, and auger spectroscopy, Journal of the Chemical Society, Dalton Transactions, (1987) 1791–1796.
[76] R. Jerome, P. Teyssie, J.J. Pireaux, J.J. Verbist, Surface analysis of polymers end-capped with metal carboxylates using X-ray photoelectron spectroscopy, Applied Surface Science, 27 (1986) 93–105.
[77] L. León-Reina, A. Cabeza, J. Rius, P. Maireles-Torres, A.C. Alba-Rubio, M. López Granados, Structural and surface study of calcium glyceroxide, an active phase for biodiesel production under heterogeneous catalysis, Journal of Catalysis, 300 (2013) 30–36.

[78] A.B. Christie, J. Lee, I. Sutherland, J.M. Walls, An XPS study of ion-induced compositional changes with group II and group IV compounds, Applications of Surface Science, 15 (1983) 224–237.
[79] S.L. Stipp, M.F. JR.Hochella, Structure and bonding environments at the calcite surface as observed with X-ray photoelectron spectroscopy (XPS) and low energy electron diffraction (LEED), Geochimica et Cosmochimica Acta, 55 (1991) 1723–1736.
[80] A. Demirbas, Progress and recent trends in biodiesel fuels, Energy Conversion and Management, 50 (2009) 14–34.
[81] A. Esipovich, S. Danov, A. Belousov, A. Rogozhin, Improving methods of CaO transesterification activity, Journal of Molecular Catalysis A: Chemical, 395 (2014) 225–233.
[82] J. Blamey, D.Y. Lu, P.S. Fennell, E.J. Anthony, Reactivation of CaO-Based Sorbents for $CO_2$ Capture: Mechanism for the Carbonation of $Ca(OH)_2$, Industrial & Engineering Chemistry Research, 50 (2011) 10329–10334.
[83] J. Phromprasit, J. Powell, S. Assabumrungrat, Metals (Mg, Sr and Al) modified CaO based sorbent for $CO_2$ sorption/desorption stability in fixed bed reactor for high temperature application, Chemical Engineering Journal, 284 (2016) 1212–1223.
[84] J. Ryczkowski, IR spectroscopy in catalysis, Catalysis Today 68 (2001) 263–381.
[85] Y. Wang, S. Lin, Y. Suzuki, Effect of CaO content on hydration rates of Ca-based sorbents at high temperature, Fuel Processing Technology, 89 (2008) 220–226.
[86] P. Sun, J.R. Grace, C.J. Lim, E.J. Anthony, Determination of intrinsic rate constants of the CaO–$CO_2$ reaction, Chemical Engineering Science, 63 (2008) 47–56.
[87] G. Montes-Hernandez, A. Pommerol, F. Renard, P. Beck, E. Quirico, O. Brissaud, In situ kinetic measurements of gas–solid carbonation of $Ca(OH)_2$ by using an infrared microscope coupled to a reaction cell, Chemical Engineering Journal, 161 (2010) 250–256.
[88] R.H. Perry, D.W. Green, Perry's chemical engineers's handbook. 7th ed. New York, McGraw-Hill, 1997.
[89] D.M. Alonso, F. Vila, R. Mariscal, M. Ojeda, M.L. Granados, J. Santamaría-González, Relevance of the physicochemical properties of CaO catalysts for the methanolysis of triglycerides to obtain biodiesel, Catalysis Today, 158 (2010) 114–120.
[90] J.M. Rubio-Caballero, J. Santamaría-González, J. Mérida-Robles, R. Moreno-Tost, A. Jiménez-López, P. Maireles-Torres, Calcium zincate as precursor of active catalysts for biodiesel production under mild conditions, Applied Catalysis B: Environmental, 91 (2009) 339–346.
[91] T. Biswick, W. Jones, A. Pacuła, E. Serwicka, J. Podobinski, The role of anhydrous zinc nitrate in the thermal decomposition of the zinc hydroxy nitrates $Zn_5(OH)_8(NO_3)_2 \cdot 2H_2O$ and $ZnOHNO_3 \cdot H_2O$, Journal of Solid State Chemistry, 180 (2007) 1171–1179.
[92] A.D.V. Souza, C.C. Arruda, L. Fernandes, M.L.P. Antunes, P.K. Kiyohara, R. Salomão, Characterization of aluminum hydroxide ($Al(OH)_3$) for use as a porogenic agent in castable ceramics, Journal of the European Ceramic Society, 35 (2015) 803–812.

[93] A. Zięba, A. Pacuła, E.M. Serwicka, A. Drelinkiewicz, Transesterification of triglycerides with methanol over thermally treated $Zn_5(OH)_8(NO_3)_2 \times 2H_2O$ salt, Fuel, 89 (2010) 1961–1972.
[94] C. Cordeiro, G. Arizaga, L. Ramos, F. Wypych, A new zinc hydroxide nitrate heterogeneous catalyst for the esterification of free fatty acids and the transesterification of vegetable oils, Catalysis Communications, 9 (2008) 2140–2143.
[95] F. Ziegler, C.A. Johnson, The solubility of calcium zincate ($CaZn_2(OH)_6.2H_2O$), Cement and Concrete Research, 31 (2001) 1327–1332.
[96] S.H. Teo, A. Islam, T. Yusaf, Y.H. Taufiq-Yap, Transesterification of *Nannochloropsis oculata* microalga's oil to biodiesel using calcium methoxide catalyst, Energy, 78 (2014) 63–71.
[97] I. Johansson, M. Svensson, Surfactants based on fatty acids and other natural hydrophobes, Current Opinion in Colloid & Interface Science, 6 (2001) 178–188.
[98] P.A. Small, Some factors affecting the solubility of polymers, Journal of Applied Chemistry, 3 (1953) 71–80.
[99] C.M. Hansen, Hansen Solubility Parameters: A User's Handbook, 2nd ed. CRC Press, Florida, 2007.
[100] L.H. Sperling, Introduction to Physical Polymer Science, 4th ed. Wiley-Interscience, New York, 1986.

# APPENDIX

# APPENDIX A
## Calculation of FAME and glycerides derivative

**Table A1** GC conditions for FAME and glycerides quantification

| Parameter | Value |
|---|---|
| Carrier gas (He) flow rate | 1.5 mL $min^{-1}$ |
| Make up gas (He) pressure | 28 kPa |
| Hydrogen pressure (for FID) | 30 kPa |
| Air pressure (for FID) | 300 kPa |
| Detector temperature (FID) | 380 °C |
| Split ratio | Off (on-column mode) |
| Injection port temperature | 380 °C |
| Inject volume | 0.1 µL |
| Ramp rate | 10 °C $min^{-1}$ |
| Initial column temperature | 50 °C |
| Final column temperature | 370 °C |

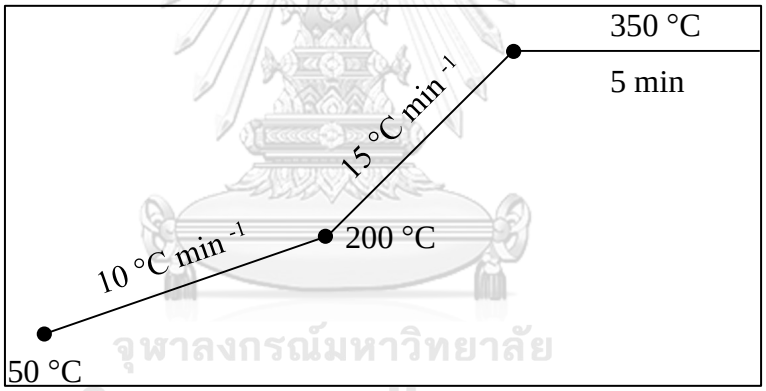


**Figure A-1** The programed-temperature column in Agilent 7890A gas chromatograph

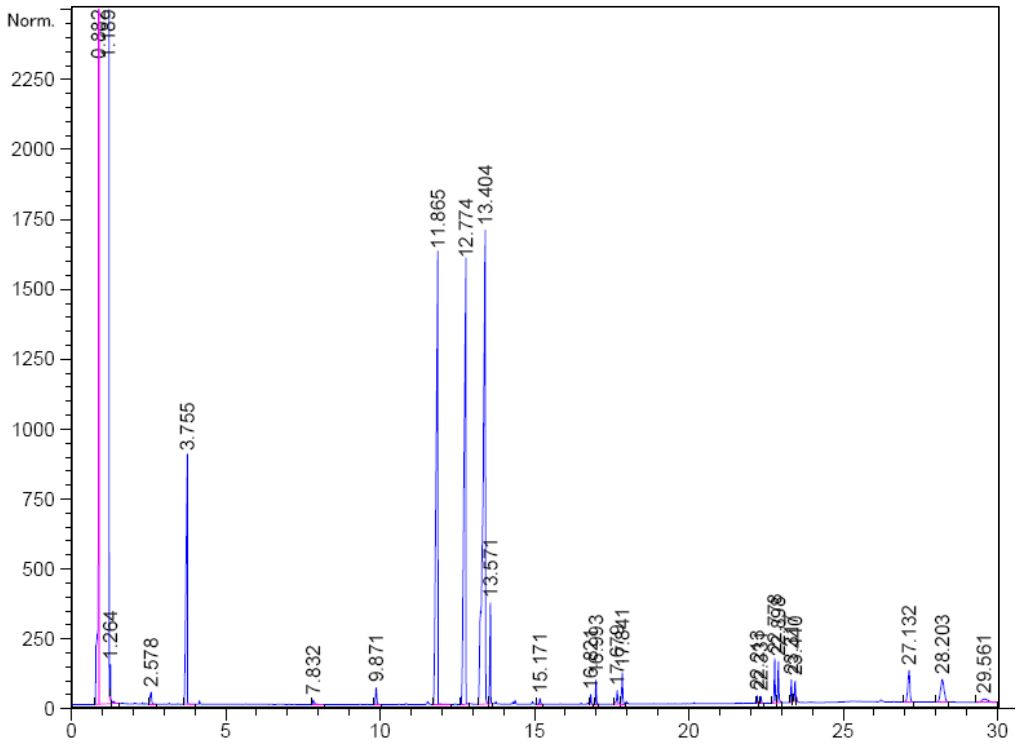


**Figure A-2** The representative chromatograms of FAME product and glycerides derivative**.**

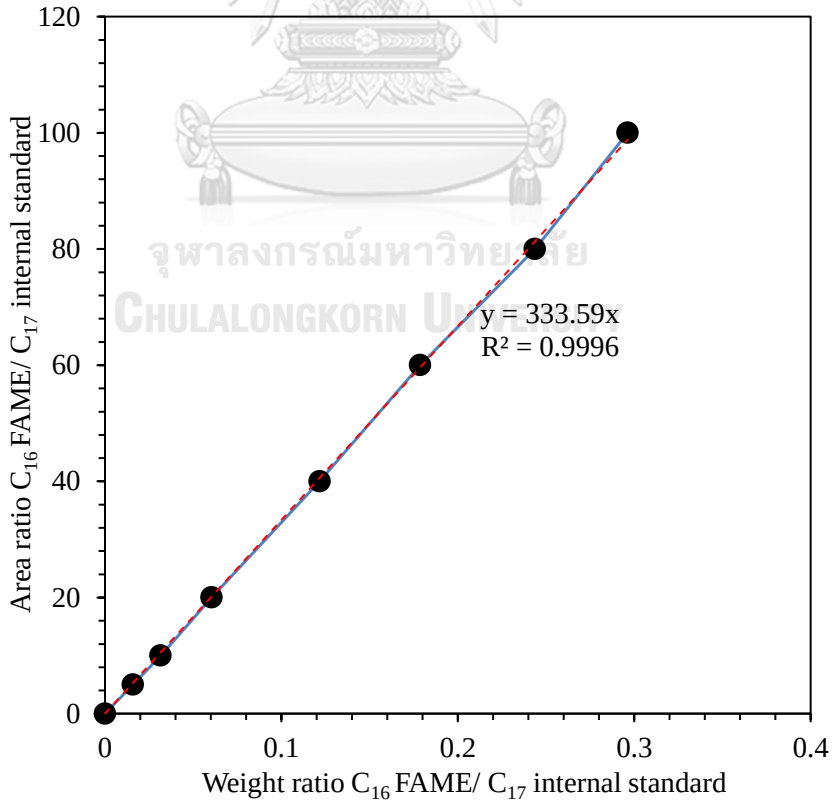


**Figure A-3** Standard curve of $C_{16}$ FAME (Methyl palmitate)

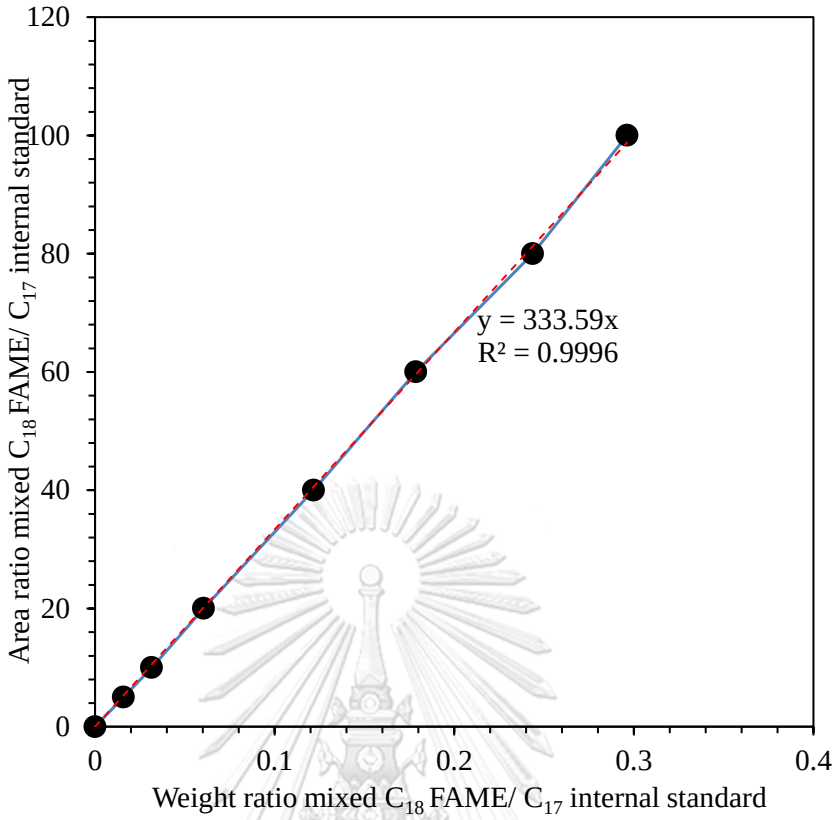


**Figure A-4** Standard curve of mixed $C_{18}$ FAME

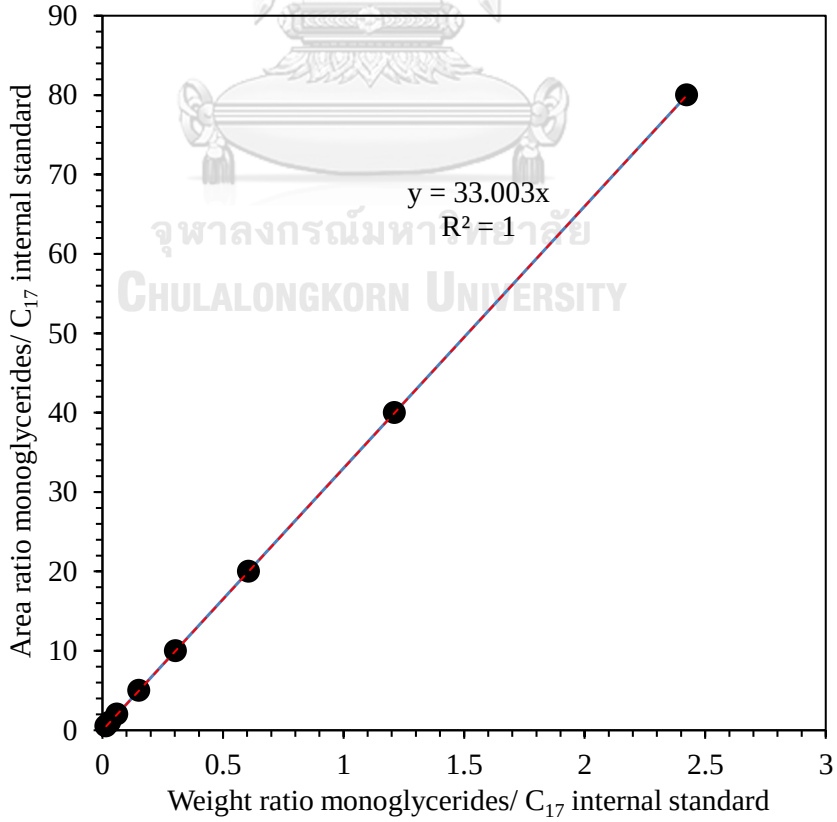


**Figure A-5** Standard curve of monoglyceride

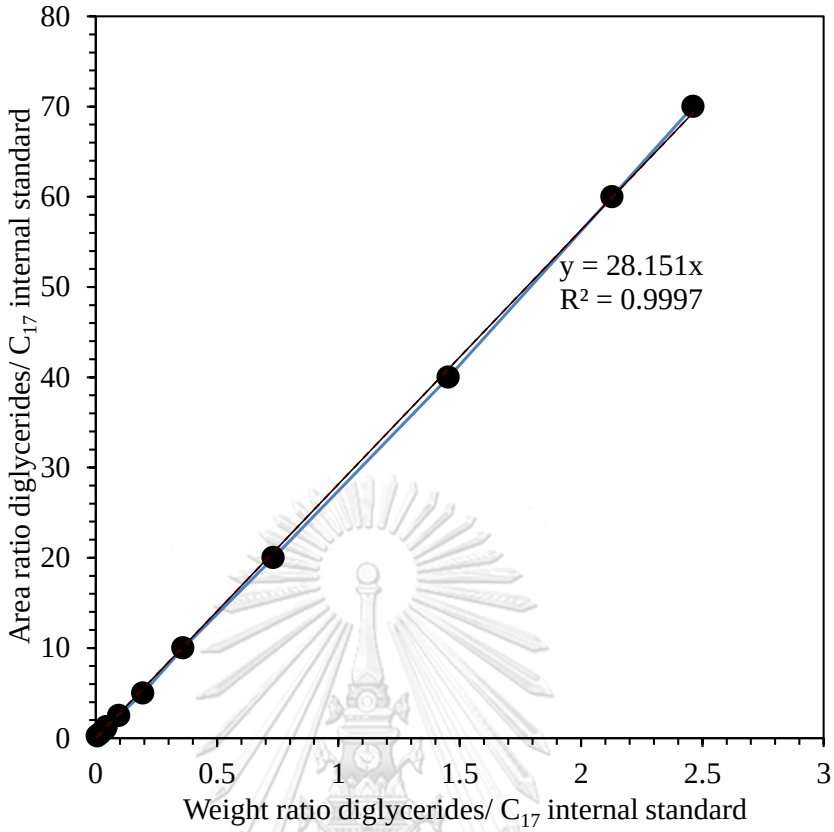


**Figure A-6** Standard curve of diglyceride

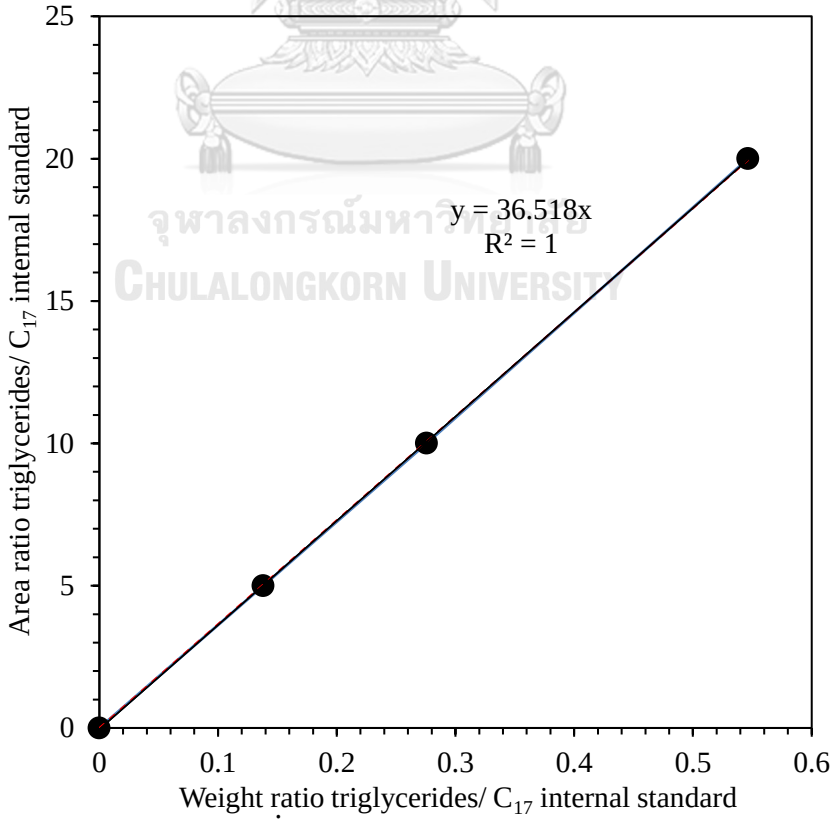


**Figure A-7** Standard curve of triglyceride

# APPENDIX B
## Calculation of FAME composition analysis

**Table B1** GC conditions for FAME composition analysis

| Parameter | Value |
|---|---|
| Carrier gas (He) flow rate | 1.0 mL $min^{-1}$ |
| Make up gas (He) pressure | 100 kPa |
| Hydrogen pressure (for FID) | 60 kPa |
| Air pressure (for FID) | 30 kPa |
| Detector temperature | 250 °C |
| Split ratio | 1: 100 |
| Injection port temperature | 250 °C |
| Inject volume | 0.1 µL |
| Initial column temperature | 180 °C |
| Ramp rate | 8 °C $min^{-1}$ |
| Final column temperature | 200 °C |

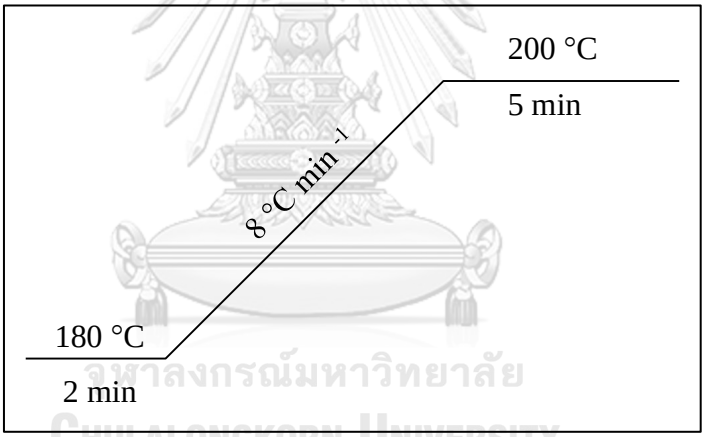




**Figure B-1** The programed-temperature column in Shimadzu 14B gas chromatograph

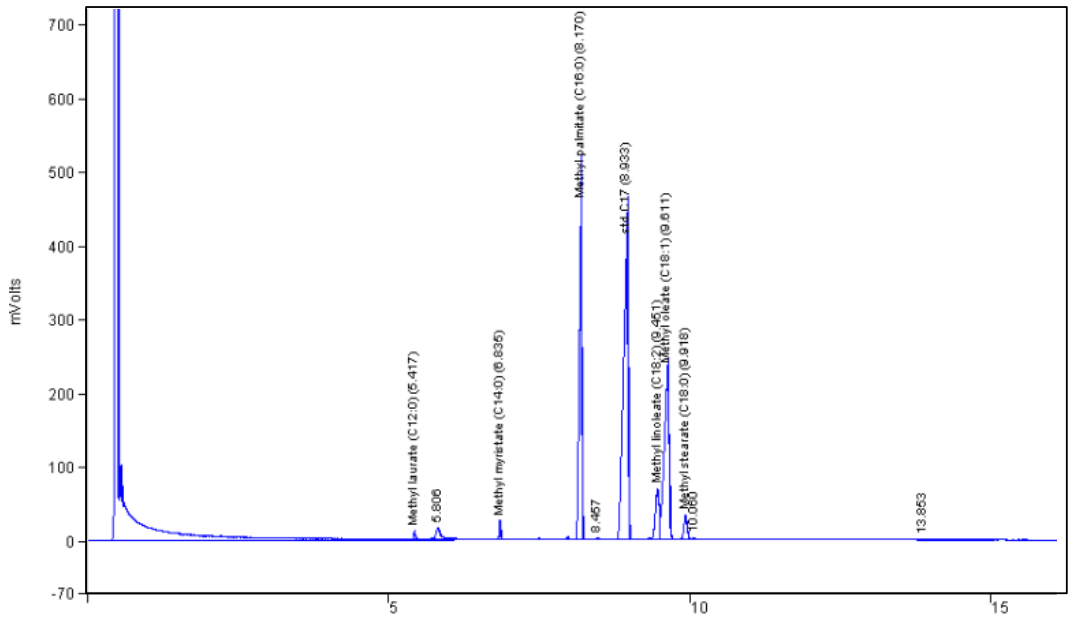


**Figure B-2** The example chromatogram of FAME product

# APPENDIX C
## Calculation of cluster size using Scherrer's equation

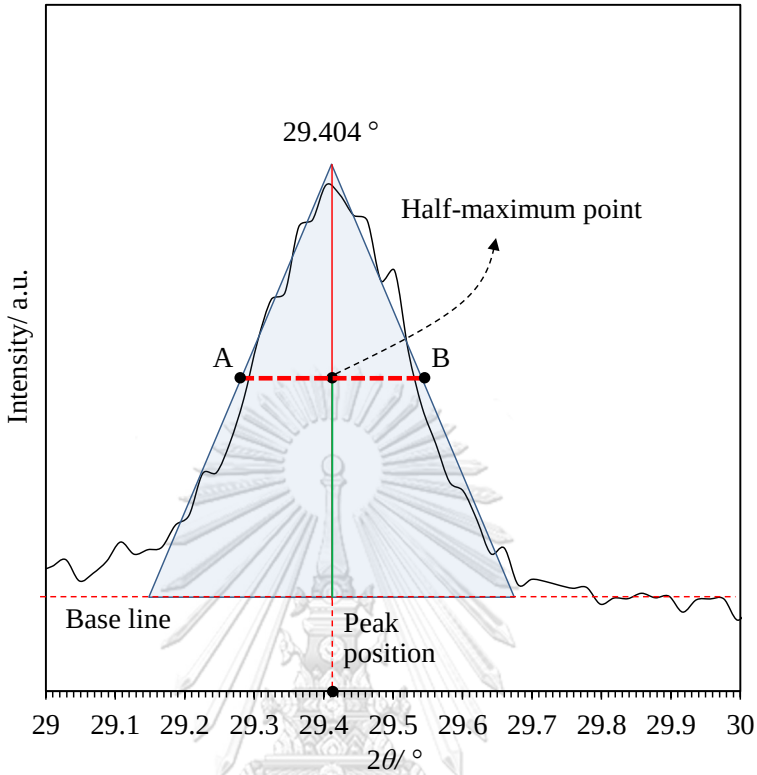


**Figure C-1** The peak of $CaCO_3$ used to calculate of cluster size using Scherrer's equation

Cluster size, which is defined in the equation below:

$$\Gamma = \frac{K\lambda}{\beta\cos\theta}$$

where

| | | | |
|---|---|---|---|
| Full width at half maximum, | $\beta$ | = | 29.543-29.281° |
| | | = | 0.262° |
| Full width at half maximum in radian, | $\beta$ | = | $0.262 \times \pi/180$ |
| | | = | 0.004572 radian |
| Angle (X-ray beam and crystal planes) | $2\theta$ | = | 29.404° |
| | $\theta$ | = | 14.702 |
| | $\cos(\theta)$ | = | 0.9672 |
| Shape factor in case of cubic, | K | = | 0.94 |
| X-ray wavelength, | $\lambda$ | = | 1.54056 Å |
| So, Crystallite size, | $\Gamma$ | = | $\frac{(0.94)(1.54056)}{(0.004572)(0.9672)}$ |
| | | = | 327.6 Å |

# VITA

Mr. Wayu Jindapon was born on September 24th, 1987 at Phang Nga, Thailand. He graduated high school from Takuapa Senanukul School, Phang Nga Province, in 2006. He graduated Bachelor in Science degree (B.Sc. Second Class Honors) in Polymer Science, Faculty of Science Prince of Songkla University in 2010 and received the Scholarship for graduate student in Young Scientist and Technologist Program (YSTP), provided by National Science and Technology Development Agency: NSTDA (2009–2010). He graduated Master of Science degree (M.Sc.) from Petrochemistry and Polymer Science program, Faculty of Science, Chulalongkorn University in 2013. During his M.Sc. study, he worked as a research assistant in the Project entitled "Pilot system for production of biodiesel through heterogeneous catalyst" funded by PTT (Public) Company Limited. He graduated Philosophy of Doctoral in Science degree (Ph.D.) from Petrochemistry program, Faculty of Science, Chulalongkorn University in 2017. During his Ph.D. study, he received the scholarships for Ph.D student from the Graduate school, Chulalongkorn University (2013–2015) and from Renewable Energy Plan (biodiesel), Energy Policy and Planning Office (EPPO), Ministry of Energy. Moreover, he worked as a research assistant in the project collaborated with SCG Chemical Company Limited.

International publication:

S. Sankaranarayanan, W. Jindapon, C. Ngamcharussrivichai, Valorization of biodiesel plant-derived products via preparation of solketal fatty esters over calcium-rich natural materials derived oxides, Journal of the Taiwan Institute of Chemical Engineers, 81 (2017) 57–64.

W. Jindapon, P. Kuchonthara, C. Ngamcharussrivichai, Biodiesel production over Ca, Zn, and Al mixed compounds in fixed-bed reactor: Effects of premixing catalyst extrudates with methanol, oil, and fatty acid methyl esters, Fuel Processing Technology, 148 (2016) 67–75.

W. Jindapon, S. Jaiyen, C. Ngamcharussrivichai, Seashell-derived mixed compounds of Ca, Zn and Al as active and stable catalysts for the transesterification of palm oil with methanol to biodiesel, Energy Conversion and Management, 122 (2016) 535–543.

W. Jindapon, S. Jaiyen, C. Ngamcharussrivichai, Al2O3-supported mixed Ca and Zn compounds prepared from waste seashells for synthesis of palm fatty acid methyl esters, Chemical Engineering Communications, 202 (2015) 1591–1599.

W. Jindapon, S. Jaiyen, A. Winitsorn, S. Butnark, C. Ngamcharussrivichai, Shell-derived heterogeneous base catalyst for transesterification of palm oil, Advanced Materials Research, 622–623 (2013) 1178–1182.